ESA CONTRACT REPORT

Contract Report to the European Space Agency

Preparatory studies for the use of observations from the Earth Radiation Mission in Numerical Weather Prediction

May 2001

Author: Marta Janisková

ESA contract No.13151/98/NL/GD

ESA Study Manager: J. Pedro V. Poiares Baptista

ECMWF
Shinfield Park
Reading
RG2 9AX
United Kingdom

For additional copies please contact: library@ecmwf.int

Series: ECMWF - ESA Contract Report

A full list of ECMWF Publications can be found on our web site under:
http://www.ecmwf.int/publications/

Contents

Abstract

The use of satellite data in cloudy conditions is an important issue of numerical weather prediction (NWP). Most operational analysis systems do not assimilate observations in the presence of clouds. The main reason lies in the difficulty to accurately describe cloud processes in atmospheric models. However, recent improvements in the representation of clouds in the models and more flexible data analysis systems such as 4D-Var (four-dimensional variational) assimilation make preliminary investigations towards the use of observations in cloudy situations possible.

Performance of the ECMWF model including various model changes related to clouds and radiation are discussed to illustrate the need for complementary datasets such as those proposed by the Earth Radiation Mission (ERM). Results underline the importance of consistent measurements of radiative fluxes, cloud fraction coverage and cloud/water ice contents within future satellite missions for more comprehensive evaluations of cloud-radiation interactions in NWP models, and hence to improvements in their parametrization.

To prepare the assimilation of cloud properties in the framework of the 4D-Var system, a proper consideration of cloud-radiation interactions in the linearized model is required. A linearized cloud scheme and a radiation scheme including cloud effects has been developed. The tangent-linear and adjoint versions of the ECMWF shortwave radiation scheme have been prepared without a priori modifications. A combination of artificial neural networks and Jacobian matrices has been defined for the linearized longwave radiation scheme. For the time being, a diagnostic cloud scheme has been linearized to be used with radiation. The accuracy of the linearization of both radiation and diagnostic cloud schemes has been examined. The inclusion of a more sophisticated radiation scheme within the existing linearized parametrizations improves the accuracy of the tangent-linear approximation. However, impact of the linearized diagnostic cloud scheme is small. Therefore the linearized model will require an improved cloud parametrization.

Some 1D-Var experiments with simulated observations have been carried out to investigate the potential of the developed radiation and cloud schemes to modify model temperature, humidity and cloud profiles to produce a better match to the observations of radiation fluxes. Results from feasibility studies in a 1D-Var framework using data from the Atmospheric Radiation Measurement (ARM) of cloud properties and radiative fluxes are also documented.

1 Introduction

Clouds are known to play a major role in the water and energy budgets of the Earth's atmosphere. Their description in General Circulation Models (GCMs) remains difficult because they encompass a broad spectrum of scales from very small ones describing microphysical processes to planetary scales describing cloud organization in large systems (frontal bands, ITCZ, easterly waves, ...). GCMs can explicitly describe atmospheric motions having horizontal scales larger than few hundreds of kilometers. Therefore, important physical processes describing the formation and dissipation of clouds cannot be explicitly resolved by global numerical models. These processes are implicitly taken into account through *parametrization* schemes. The parametrization of sub-grid scale processes is a key issue of both climate and Numerical Weather Prediction (NWP) models. They describe phenomena that are not properly sampled by conventional observations. As they are not sufficiently understood, they are not accurately modelled.

During the last decade the parametrization of clouds in climate GCMs has greatly improved (Heise and Roekner, 1990 ; Ricard and Royer, 1993; Fowler *et al.*, 1996). Such effort was stimulated by the fact that the response of GCMs to climate changes is extremely sensitive to cloud description. This has been demonstrated in various intercomparison studies (Cess *et al.*, 1990; Cess *et al.*, 1996) and recognized by the Intergovernmental Panel on Climatic Change (Houghton *et al.*, 1995). Cloud type, fractional coverage and optical properties play a role in determining feedback mechanisms that will amplify or reduce an initial external radiative forcing (Senior and Mitchell, 1993). Early descriptions of clouds using empirical dependencies with relative humidity and other quantities (Slingo, 1987) are now progressively replaced by prognostic cloud schemes. The emergence of such schemes has been made possible by the availability of new data sets from field experiments, satellite observations and also from cloud resolving models. Future satellite missions such as CloudSat (flying a lidar), PICASSO-CENA[1] (flying a single instrument - a cloud radar) and ERM[2] should provide more accurate description of the structure of clouds.

The main objective of the Earth Radiation Mission proposed by ESA[3] (Ingmann, 1997) is to document the vertical structure of cloud and aerosol fields over all climatic zones together with the components of the radiation budget at the top of the atmosphere. From ERM measurements, geophysical parameters should be derived such as vertical profiles of cloud ice water content, cloud liquid water content and aerosol optical thickness. Instruments embarked on ERM are supposed to include:

- a broadband radiometer (for measurements of the shortwave and longwave radiances at the top of the atmosphere),
- a cloud profiling radar (for detection or retrieval of cloud tops, cloud bases and vertical distribution of thick clouds),
- a backscattering lidar (for detection of cloud top and cloud base of thin clouds and aerosol layers as well as for deriving cloud optical depth),

[1] Pathfinder Instruments for Cloud and Aerosol Spaceborne Observations - Climatologie Etendue des Nuages et des Aerosols

[2] Earth Radiation Mission

[3] European Space Agency

- a visible/infrared imager (for the validation of the representativity of measured cloud fields by active instruments).

Measurements from the ERM should help to define methodologies for achieving improvements in the description of cloud-radiation interactions both for climate models and for NWP models. NWP models aim at providing a description of the atmospheric fluid over periods of time ranging from a few hours to 10 days or more, starting from the best possible knowledge of the present state of the atmosphere. The initial state of NWP models, the *analysis*, is obtained by combining in an optimal way all the possible sources of information on the atmosphere (observations of various types, climatology, atmospheric equilibriums, short-range forecasts) into a consistent picture. This complex process is achieved within a *data assimilation system* maintained and developed by the main operational weather centres such as ECMWF.

Currently, operational data assimilation systems only account for conventional and satellite observations of pressure, temperature, wind and water vapour. They do not explicitly include any quantity related to the condensed phase of water as cloud water, cloud ice or rain. The strong coupling between clouds and dynamical processes (explicitly described for the large scales by data assimilation systems) and recent improvements in the description of cloud processes in the ECMWF model (Tiedtke, 1993) have demonstrated significant skill in analysis and forecast products when compared to radar and lidar observations from field experiments (Mace *et al.*, 1998; Miller *et al.*, 1999; Morcrette, 2001). Data from ERM should provide a unique set of observations that could be used for improving the quality of operational products in various ways. A better description of cloud-radiation interactions will lead to improved forecasts in the medium-range (two-metre temperature, cloudiness, precipitation, ...) and also to a more reliable seasonal forecasting system since the ocean-atmosphere coupling in the tropics is strongly driven by the energy and water fluxes between the two systems. The inclusion of cloud observations in the ECMWF data assimilation system would lead to an improved initial state of the prognostic variables of the cloud scheme and also of the dynamical and thermodynamical variables linked to the generation and dissipation of clouds.

In this report evidence is given on the potential importance of ERM like observations for NWP, together with the development and experimentation in order to be able to assimilate these data.

The cloud and radiation parametrizations in the ECMWF model are briefly described in Section 2. Large uncertainties concern the description of optical properties for ice particles as well as the associated microphysics. Quantitative information on ice water content for various types of clouds could help to reduce the level of uncertainty on the ice phase in the ECMWF model.

The importance of data sets providing information on the vertical structure of clouds is emphasized through various field experiments (LITE[4], ARM[5],...) where the ECMWF model has shown some skill in simulating the observations but also where some weaknesses in the representation of clouds have been identified (Section 3). In this section standard evaluations of cloudiness and top of atmosphere (TOA) radiation budget using ISCCP[6] and ERBE[7] satellite climatologies are presented. The incomplete picture they provide demonstrates the necessity of a synergy between

[4] Lidar In-space Technology Experiment
[5] Atmospheric Radiation Measurement
[6] International Satellite Cloud Climatology Programme
[7] Earth Radiation Budget Experiment

instruments measuring TOA radiative fluxes and cloud properties. Currently, the vertical structure of observed global cloud distribution is only known very crudely through three main layers derived from ISCCP satellite data. Various sensitivity studies to both cloud overlap assumption and ice sedimentation on the climate simulated by the ECMWF model have demonstrated their crucial importance for physical processes (Morcrette and Jakob, 2000; Jakob and Klein, 2000).

The new data assimilation system known as 4D-Var (four-dimensional variational assimilation) and implemented at ECMWF in November 1997 (Rabier *et al.*, 2000; Mahfouf and Rabier, 2000) is described in Section 4. This data assimilation system is flexible enough to allow the inclusion of new types of observations. Some studies on assimilating rainfall data from the recently launched TRMM[8] satellite into the ECMWF analysis and forecasting system have been done by Marécal and Mahfouf (2000). A similar approach might be taken for the assimilation of cloud data from current and future satellite missions.

Section 5 explains how the assimilation of cloud properties and top of atmosphere fluxes will require the development of linearized versions of both the radiative transfer model and a cloud scheme. These linearized operators are required to get model counterparts of observations in order to solve the minimization problem within 4D-Var. A linearized version of a radiation scheme including the major cloud-radiation interactions has been developed. The shortwave radiation is based on a linearization of the operational ECMWF code. A combination of artificial neural networks and mean Jacobian matrices has been defined for the linearized longwave radiation scheme to reduce its computational cost. For the time being, the ECMWF diagnostic cloud scheme (used before the implementation of the prognostic one) has been linearized. A simplified linearized prognostic cloud scheme is under development.

The accuracy of the linearization of both radiation and diagnostic cloud schemes are examined in Section 6. The impact of including those schemes into the existing set of linearized physics has been evaluated.

To investigate the potential of radiation and cloud schemes to modify the model temperature, humidity and cloud profiles in order to better match observations of radiation fluxes, 1D-Var experiments with simulated observations have been performed (Section 7). A sensitivity of the radiation scheme to the temperature, humidity and cloud properties has been investigated. Feasibility studies in a 1D-Var framework using data from field experiments providing measurements of both cloud properties and radiative fluxes (e.g. ARM) have also been carried out.

2 Cloud and radiation processes in the ECMWF forecast model

2.1 The radiation schemes

The radiation scheme solves the radiative transfer equation in two distinct spectral regions. The computations for the longwave (LW) radiation are performed over the spectrum from 0

[8]Tropical Rainfall Measuring Mission

to 2820 cm^{-1}. The shortwave (SW) part of the scheme integrates the fluxes over the whole shortwave spectrum between 0.2 and 4.0 μm.

To save time in the rather expensive radiation computations, the full radiation part of the scheme is currently called every 3 hours (every 1 hour during the first-guess forecasts used as part of the assimilation system or during the first 12 hours of any operational forecast) in the operational ECMWF model (Morcrette, 2000). Shortwave transmissivities and longwave fluxes are computed using values of temperature, specific humidity, liquid/ice water and cloud fraction. The computations of the fluxes are not done at every-grid point. They are carried out on a reduced horizontal grid, corresponding to all points around the poles and decreasing to one point of four in the longitudinal direction in the tropics. The results are then interpolated back to the original grid using a cubic interpolation algorithm. The shortwave fluxes are updated every time-step using current values of the solar zenith angle.

2.1.1 The shortwave radiation scheme

The shortwave radiation scheme, originally developed by Fouquart and Bonnel (1980) is used in the ECMWF physical parametrization (Morcrette, 1989 and 1991). It uses the photon-path-distribution method to separate the parametrization of the scattering processes from that of molecular absorption. Upward and downward fluxes are obtained from the clear sky and cloudy reflectances and transmittances of the atmospheric layers. Solar radiation is absorbed by gases as water vapour, oxygen, carbon dioxide, methane, nitrous oxide and ozone, and scattered by molecules (Rayleigh scattering), aerosols and cloud particles. To perform the spectral integration, the solar spectral interval is discretized into subintervals in which the surface reflectance is considered as constant. Since the main cause of the important spectral variation of the surface albedo is the sharp increase in the reflectivity of the vegetation in the near infrared, and since water vapour does not absorb below 0.68 μm, the shortwave scheme considers two spectral intervals, one for the visible part (0.2 - 0.68 μm) and one for the near infrared (0.68 - 4.0 μm) part of the solar spectrum. This makes the scheme more computationally efficient since the interactions between gaseous absorption and scattering processes are accounted for only in the near-infrared interval.

Considering an atmosphere covered by clouds, the final fluxes are computed as a weighted average of the fluxes in the clear sky and in the cloudy fractions of the column (depending on cloud-overlap assumption). It is assumed that the atmosphere is divided into homogeneous layers. Upward and downward fluxes at a given layer j are obtained from the reflectance and transmittance of the atmospheric layers as

$$F^{\downarrow}_{sw}(j) = F_0 \prod_{k=j}^{N} \mathcal{T}_{bot}(k) \quad (1)$$

$$F^{\uparrow}_{sw}(j) = F^{\downarrow}_{sw}(j)\mathcal{R}_{top}(j-1) \quad (2)$$

Computations of the transmittance at the bottom of a layer $\mathcal{T}_{bot}$ start at the top of atmosphere and work downward. Those of the reflectance at the top of the same layer $\mathcal{R}_{top}$ start at the surface and work upward. In the presence of cloud in the layer, the final fluxes are computed as

a weighted average of the fluxes in the clear sky and in the cloudy fractions of the column as:

$$\mathcal{R}_{top} = C_{cloud}\mathcal{R}_{cloud} + (1 - C_{cloud})\mathcal{R}_{clear} \quad (3)$$

$$\mathcal{T}_{bot} = C_{cloud}\mathcal{T}_{cloud} + (1 - C_{cloud})\mathcal{T}_{clear} \quad (4)$$

In the previous equations, C_{cloud} is the cloud fractional coverage of the layer within the cloudy fraction of the column (depending on cloud-overlap assumption).

In the cloudy fraction of the layer, the reflectance at the top and transmittance at the bottom of a cloudy layer are calculated with the Delta-Eddington approximation. These two quantities are calculated as functions of the total optical thickness δ (related to the cloud liquid/ice water amount), the single scattering albedo ω and the total asymmetry factor g.

2.1.2 The longwave radiation scheme

The longwave radiation scheme, operational at ECMWF up to June 2000, is a band emissivity type scheme (Morcrette, 1989). The longwave spectrum from 0 to 2820 cm^{-1} is divided into six spectral regions. The transmission functions for water vapour and carbon dioxide over those spectral intervals are fitted using Padé approximations on narrow-band transmissions obtained with statistical band models (Morcrette *et al.*, 1986). Integration of the radiation transfer equation over wavenumber ν within the particular spectral regions gives the upward and downward fluxes.

The incorporation of the effects of clouds on the longwave fluxes follows the treatment discussed by Washington and Williamson (1977). The scheme calculates first upward and downward fluxes ($F_0^{\uparrow}(i)$ and $F_0^{\downarrow}(i)$) corresponding to a clear-sky atmosphere. In any cloudy layer, the scheme evaluates the fluxes assuming a unique overcast cloud of emissivity unity, i.e. $F_n^{\uparrow}(i)$ and $F_n^{\downarrow}(i)$ for a cloud present in the nth layer of the atmosphere. The fluxes for the actual atmosphere are derived from a linear combination of the fluxes calculated in the previous steps with some cloud overlap assumption in the case of clouds present in several layers. Let N be the number of model layers starting from the top of atmosphere to the bottom, C_i the fractional cloud cover in layer i, the cloudy upward $F_{lw}^{\uparrow}$ and downward $F_{lw}^{\downarrow}$ fluxes are expressed as:

$$F_{lw}^{\uparrow}(i) = (1 - CC_{N,i})F_0^{\uparrow}(i) + \sum_{k=i}^{N}(CC_{i,k+1} - CC_{i,k})F_k^{\uparrow}(i) \quad (5)$$

$$F_{lw}^{\downarrow}(i) = (1 - CC_{i-1,0})F_0^{\downarrow}(i) + \sum_{k=1}^{i-1}(CC_{i,k+1} - CC_{i,k})F_k^{\downarrow}(i) \quad (6)$$

where $CC_{i,j}$ is the cloudiness encountered between any two levels i and j in the atmosphere computed using a certain overlap assumption (see section 2.4 Cloud overlap assumptions).

In the case of semi-transparent clouds, the fractional cloudiness entering the calculations is an effective cloud cover equal to the product of the emissivity (ε_{cld}) due to condensed water and gases in the layer by the horizontal coverage of the cloud cover. This is the so called effective emissivity approach.

In June 2000, the longwave radiation scheme described above has been replaced by the Rapid Radiation Transfer Model (RRTM), which is based on a two-stream solution of the longwave radiation transfer (Morcrette *et al.*, 1998). In the previous operational scheme, the cloud emissivity used to compute the effective cloud cover is defined over the whole LW spectrum from spectrally averaged mass absorption coefficients and the relevant cloud water and/or ice paths. In RRTM, the cloud optical thickness is defined as a function of spectrally varying mass absorption coefficients and relevant cloud water and ice paths. This quantity is then used within the actual cloudy fraction of the layer.

2.2 Cloud optical properties

Considering the cloud-radiation interactions, it is not only the cloud fraction or cloud volume (cloud parametrization schemes are described in Section 2.3), but also cloud optical properties that matter. In the case of shortwave radiation, the cloud radiative properties depend on three different parameters: the optical thickness δ_c, the asymmetry factor g_c and the single scattering albedo $\overline{\omega_c}$. They are derived from Fouquart (1987) for the water clouds, and Ebert and Curry (1992) for the ice clouds. The optical thickness δ_c is related to the cloud liquid/ice water amount u_{LWP} by :

$$\delta_c = u_{LWP}\left(a_i + \frac{b_i}{r_e}\right) \tag{7}$$

where a_i and b_i are defined from Ebert and Curry (1992) for ice particles and are set to respectively 0 and 3/2 for water particles. The mean effective radius of the size distribution of the cloud water droplets is defined by r_e. For water clouds, r_e is set to 13 μm over oceans and to 10 μm over continents. When ice cloud optical properties were initially introduced in the radiation code, the effective radius was set to 40 μm. However, observations indicate that the effective radius of ice crystals increases with temperature, usually attributed to accretion from falling crystals. In the current scheme, account is taken of this by using the diagnostic formulation of Ou and Liou (1995):

$$r_e = 326.3 + 12.42 \times T_i + 0.197 \times T_i^2 + 0.0012 \times T_i^3 \tag{8}$$

where $T_i = \min(T, -23^oC)$. The effective radius is then limited within the interval 30-60 μm.

In the two spectral intervals of the shortwave scheme, the asymmetry factor g_c is fixed to 0.865 and 0.910, respectively and ω_c is given as a function of δ_c following Fouquart (1987):

$$\overline{\omega}_{c1} = 0.9999 - 5 \times 10^{-4} \exp(-0.5\delta_c) \tag{9}$$

$$\overline{\omega}_{c2} = 0.9988 - 2.5 \times 10^{-3} \exp(-0.05\delta_c) \tag{10}$$

These cloud shortwave radiative parameters have been fitted to in-situ measurements of stratocumulus clouds (Bonnel *et al.*, 1983).

The optical properties of ice clouds are expressed as:

$$\overline{\omega}_i = c_i - d_i r_e \tag{11}$$

$$g_i = e_i + f_i r_e \tag{12}$$

where the coefficients are derived from Ebert and Curry (1992).

Cloud longwave optical properties are represented by the emissivity ε_{cld} related to the condensed water amount and by the condensed water mass absorption coefficient k_{abs}. The emissivity ε_{cld} is related to the condensed water amount by:

$$\varepsilon_{cld} = 1 - \exp(-k_{abs} u_{LWP}) \tag{13}$$

where k_{abs} is the condensed water mass absorption coefficient obtained following Smith and Shi (1992) for the water clouds and Ebert and Curry (1992) for the ice clouds. u_{LWP} is the condensed water path. k_{abs} depends upon the water phase (ice or water) and upon temperature. A spectral dependency can also be included.

2.3 Cloud parametrization schemes

2.3.1 The prognostic cloud scheme

The ECMWF prognostic cloud scheme developed by Tiedtke (1993) has been put in the operational model in April 1995. This scheme includes prognostic equations for cloud fraction and liquid/ice water content and has been shown to provide a much more realistic description of the cloud cover than the previous diagnostic scheme described by Slingo (1987). The inclusion of the cloud fraction as a prognostic variable is an original feature of this scheme since most of the prognostic cloud schemes treat cloud fraction by means of a diagnostic relation (e.g. Sundqvist, 1988, Smith,1990).

The prognostic scheme consists of two prognostic equations, one for liquid/ice water l and one for cloud fraction a:

$$\frac{\partial l}{\partial t} = A(l) + S^l_{conv} + S^l_{bl} + C^l - E - P - D_{entr} \tag{14}$$

$$\frac{\partial a}{\partial t} = A(a) + S^a_{conv} + S^a_{bl} + C^a - D_{evap} \tag{15}$$

where $A(l)$ and $A(a)$ represent the advection of liquid/ice water and cloud fraction, S^l_{conv} and S^a_{conv} represent the source terms of liquid/ice water and cloud fraction from moist convection processes, S^l_{bl} and S^a_{bl} represent the source terms of liquid/ice water and cloud fraction due to boundary layer turbulence, C^l and C^a are the formation of liquid/ice water and cloud fraction by stratiform condensation processes, E is the evaporation rate, P is the precipitation rate, D_{entr} is the destruction of liquid/ice water due to cloud top entrainment and D_{evap} is the reduction of cloud fraction by evaporation.

The prognostic cloud scheme allows the ice and liquid water to co-exist (mixed phase) based on a simple quadratic temperature dependence between 0°C and -23°C as from Matveev, 1984 (see also Jakob, 1995).

This scheme accounts explicitly for the physical sources and sinks leading to the production and dissipation of clouds. It is therefore strongly coupled to the other physical parametrizations described in the ECMWF model (radiation, turbulence, deep and shallow convection). Clouds formed by convective processes are parametrized by considering them to be condensates produced by cumulus updrafts and detrained in the environmental air. Clouds are also assumed to be formed by non-convective processes (e.g. large-scale lifting of moist air, radiative cooling, etc). Evaporation of clouds is described by two processes in connection with large-scale and cumulus-induced descent and diabatic heating and by turbulent mixing of cloud air with unsaturated environmental air. Precipitation processes are represented differently for pure ice clouds and for mixed phase and pure water clouds. The rain and snow formed are removed from the atmospheric column immediately but can evaporate and interact with the cloud water in the layers they pass through. The precipitation process in ice clouds is treated as a sedimentation of the ice particles with a terminal fall speed of :

$$w_{ice} = 3.29(\rho l/a)^{0.16} \tag{16}$$

based on Heymsfield and Donner (1990), where ρ is the air density.

The precipitation from pure ice can then be written as:

$$P = \frac{1}{\rho}\frac{\partial}{\partial z}(\rho w_{ice} l) \tag{17}$$

Ice settling into cloudy areas is treated as a source for cloud ice in the layer below, whereas ice settling into clear-sky is converted into snowfall. For mixed phase and pure water clouds a parametrization describing the conversion of cloud droplets into raindrops is taken from Sundqvist (1978). It represents both the collision process and the Bergeron-Findeisen mechanism. Evaporation of rain/snow is described by a scheme following Kessler (1969) and only takes place when the grid mean relative humidity is below a threshold value.

2.3.2 The diagnostic cloud scheme

Before the implementation of the prognostic scheme (described above), the diagnostic cloud scheme (Slingo, 1987) was used in the ECMWF model. This scheme is simpler than the prognostic one, but describes physical processes more empirically.

The cloud scheme allows for four cloud types: convective cloud and three types of layer clouds (high, middle and low level).

The convective clouds are parametrized using the scale-averaged precipitation rate ($\bar{P}$) from the model convective scheme as:

$$C_{conv} = 0.4\ min(0.8,\ 0.125\ ln\bar{P} - 1.5) \tag{18}$$

Base and top heights are also derived from the convection scheme.

The layer clouds are determined from a function of the layer relative humidity (RH_e) after adjustment for the presence of convective clouds (C_{conv}), $RH_e = RH - C_{conv}$, as:

$$f(RH_e) = \left\{ max\left[\frac{RH_e - b}{1-b}, 0\right] \right\}^2 \tag{19}$$

where b is equal to 0.8 for high and middle level clouds and to 0.7 for low level clouds. The middle level clouds and low level clouds associated with the extra-tropical fronts are then modified by a linear transition up to weak ascent using vertical velocity. There are no such clouds in subsidence areas.

Liquid water l_{lwc} and ice water l_{iwc} are proportional to the specific humidity at saturation q_{sat}. They are defined as

$$l_{lwc} = \alpha l_{lc} \tag{20}$$
$$l_{iwc} = (1-\alpha) l_{lc} \tag{21}$$

where α is the fraction of condensate held as liquid water. l_{lc} is the function of the saturation q_{sat} and cloud cover of individual layer C_i defined as:

$$l_{lc} = 0.05\ C_i\ q_{sat} \tag{22}$$

2.4 Cloud overlap assumptions

Cloud overlap assumptions must be made in atmospheric models in order to organize the cloud distribution used for radiation and precipitation/evaporation computations. Indeed, given the grid size of global NWP models (10^4 km^2) cloudiness cannot be considered as an all or nothing process. A cloud overlap assumption of some sort appears to be necessary to account for the fact that clouds are likely not to fill the whole grid box, particularly when the radiative transfer is not computed at every time-step of the model. The global atmospheric models mostly use the random, the maximum-random and the maximum overlap assumptions in the radiation schemes. The definition of cloud overlap assumptions is given from the point of view of cloudiness $CC_{i,j}$ encountered between any two levels i and j in the atmosphere. Let C_k be the cloud fraction of the layer k located between levels k and $k+1$.

The maximum overlap assumption gives:

$$CC_{i,j} = \max(C_i, C_{i+1}, ..., C_{j-1}) \tag{23}$$

The random overlap assumption gives:

$$CC_{i,j} = 1 - \prod_{k=1}^{j-1} (1 - C_k) \tag{24}$$

The maximum-random overlap assumption gives:

$$CC_{i,j} = 1 - \prod_{k=1}^{j-1} \left[\frac{1 - \max(C_k, C_{k-1})}{1 - C_{k-1}}\right] \tag{25}$$

Tian and Curry (1989) have tested the previous cloud overlap assumptions by applying them to the U.S. Air Force three dimensional nephanalysis in January 1979 over the North Atlantic Ocean. This data set is believed to be the best available information on the vertical distribution of clouds since it integrates both satellite and conventional observations over a large area with relatively good data coverage. They compared the observed total cloud amount to the computed total cloudiness obtained with the three different assumptions. Their conclusion is somewhat in favour of the maximum-random overlap assumption first proposed by Geleyn and Hollingsworth (1979): adjacent layers containing cloud are combined by using maximum overlap to form a contiguous cloud and discrete layers separated by clear-sky are combined randomly. The maximum-random overlap assumption is operationally used in the ECMWF model.

3 Validation studies on clouds and radiative fluxes at ECMWF

3.1 Comparisons with satellite data

This section illustrates how model changes related to clouds and radiation are currently evaluated in the ECMWF forecasting system in order to emphasize the need for complementary datasets such as those proposed by ERM.

In December 1997, important changes to the physics were introduced in the operational ECMWF model. The water vapour absorption continuum formulation was changed according to Zhong and Haigh (1995) from tests with line-by-line models. The longwave properties of ice clouds were modified using the formulation of Ebert and Curry (1992) instead of Smith and Shi (1992). The effective radius of ice particles was changed from a constant value of 40 μm to a dependency with temperature previously described (see Equation (8)). A treatment of cloud inhomogeneities following Tiedtke (1996) was introduced in the shortwave radiation scheme, where cloud water path is multiplied by 0.7. The numerical treatment of ice fallout in the cloud scheme was improved and the closure assumption of the moist convection scheme was changed.

Seasonal forecasts were run at low resolution (T63) from which three month averages of various fields were compared with associated satellite climatologies. Some illustrative results are presented for the winter period of 1987/1988 (December/January/February).

The spatial pattern of cloudiness can be compared with ISCCP estimates (Fig. 1). The revised physics increases cloud cover in many regions in the tropics. In the storm track regions of the Northern hemisphere the area covered by cloud amounts greater than 80 % is increased, in better agreement with observations. The extent of regions with cloudiness above 80 % in the Equatorial Pacific is too large with the revised physics compared to ISCCP estimates. In the sub-tropical regions over the Pacific and Atlantic total cloud amount is slightly increased although still strongly underestimated by the model.

When compared with ERBE data, the increased cloud fraction with the revised physics lead to reduced errors in top of atmosphere (TOA) radiative fluxes. Overestimates of OLR (Outgoing

Longwave Radiation) seen in the control simulation over Indonesia and northern South America (Fig. 2) are greatly reduced with the revised physics leading to a better comparison with ERBE OLR estimates. However, over some regions (for example along the Pacific ITCZ) OLR is underestimated with the revised physics, providing some evidence that tropical high cloud amounts may be too large in these regions as also indicated by comparison with ISCCP. However, it is important to stress that radiative optical properties and cloud water/ice content may also play a role. Measurements from ERM should be able to provide additional information to better understand the source of model errors. Biases in the Southern Hemisphere of the control simulation (Fig. 2) are also reduced by the revised physics as a consequence of the revisions to the longwave radiation scheme.

Errors in the estimation of TOA absorbed shortwave radiation in the tropics and sub-tropics (Fig. 3 - negative values indicating an overestimation of albedo) are slightly reduced by the revised physics, specifically along the Pacific ITCZ and the sub-tropics of the Pacific and Atlantic oceans. A treatment of the inhomogeneity of clouds tends to reduce excessive albedos seen in the control simulation but this is counter balanced to a great extent by increased high level cloudiness. In southern mid-latitudes, the revised physics produces too large an TOA absorbed shortwave flux compared to ERBE. Although high cloud cover is increased in these regions by the revised physics, the inclusion of an effective radius which increases with temperature reduces the albedo of these mid-latitude clouds.

The results of these experiments underline the importance for future cloud satellite missions to generate consistent measurements of radiative fluxes, cloud fractional coverage and cloud water/ice contents to allow more comprehensive and consistent evaluations of cloud-radiation interactions in NWP models.

Although the type of comparisons illustrated above provides useful general information on the model's performance in the representation of clouds it is obvious that they are insufficient to uncover the reasons for model errors. One approach to improve our understanding of model deficiencies is to link them to dynamical regimes. A more detailed evaluation of the performance of the cloud and radiation schemes has been undertaken using ISCCP data and simple weather regime classifications (Klein and Jakob, 1999; Mahfouf *et al.*, 1999). The studies have shown that the model is able to reproduce the general cloud structure in the cyclones very well. However, a number of shortcomings has been noticed. The low-top clouds ahead and behind cyclone systems appear to be too thick. The high top clouds appear to be optically too thin. Overall, such validation studies show the potential of combining satellite data with information about the large-scale flow, an approach intrinsic in 4D-Var assimilation when applied to cloud fields.

Another new approach to the validation of cloud parametrizations is made possible by the use of new advanced active instruments, as they are planned for the Earth Radiation Mission. As a feasibility study for a lidar in space, the Lidar In-space Technology Experiment (LITE) was carried out aboard the space shuttle Discovery. Miller *et al.* (1999) examined the performance of the ECMWF prognostic cloud scheme against data from LITE during September 1994. Details on atmospheric profiles of cloud cover are available from this active sensor. Short-range (24 to 30 hours) forecasts were run for validation purposes over 15 different LITE orbit overpasses. Qualitatively, the vertical extent and placement of deep convection in the ITCZ, migratory mid-

latitude disturbances, and large-scale subsidence zones appear to be in good agreement with the observations for this case. The analysis of the 15 orbits indicates possible underestimation of the frequency of high-altitude cirrus and overestimation of lower tropospheric clouds by the ECMWF model.

3.2 Comparisons with field experiments datasets

As shown in the previous section one difficulty in the validation of the cloud parametrizations in global circulation models comes from the fact that current satellites only provide TOA fluxes, total cloud cover and optical thickness which are insufficient to identify precisely the origin of deficiencies in the cloud and radiation schemes.

However, for specific field experiment datasets, the vertical structure of observed clouds is available and comparisons with clouds described by the ECWMF forecast model have started.

A preliminary comparison between model profiles of clouds and precipitation and active sensor has been performed by Mace *et al.* (1998) using data from a vertically pointing millimeter wave radar (35 GHz) at a research site in North Central Oklahoma during three months (December 1996, January and February 1997). The ECMWF model has shown very good skill at predicting the vertical frequency distribution of clouds and precipitation that occured over this site during this period. However, it has a tendency to predict the onset of cloudiness too early, predict too great a layer depth and predict the dissipation of the layer too late.

The comparison has shown that overall the ECMWF model is sufficiently skillful to allow for more in depth analysis of individual cases where the macroscale and microphysical properties of the predicted clouds can be evaluated.

Although of obvious importance, the correct simulation of cloud occurrence is only a necessary, but not sufficient condition for capturing the main hydrological and radiative effects of clouds in GCMs. A further requirement is to correctly simulate the amount of condensate present in the cloud. Mace *et al.* (1997) have recently derived ice contents for isolated cirrus clouds from combined radar reflectivity and infrared interferometer data. An attempt has been made to use this information for a first evaluation of the ECMWF model performance in simulating the ice content in those clouds (Mahfouf *et al.*, 1999). The first results indicate that the model overestimates the frequency of very low ice contents and underestimates the number of events with intermediate values. It is a major step forward in model evaluation, that for the first time long time series of observations of cloud ice exist and can be compared to GCM results at least in a statistical way.

Another crucially important parameter in the simulation of clouds and their radiative effects is the cloud fraction and its vertical distribution. Figure 4 shows a comparison of cloud cover derived from a 94 GHz radar during the Cloud Lidar And Radar Experiment (CLARE) over Chilbolton (U.K.) from 24 October to 8 November 1998 with those from ECMWF short-range forecasts. It is evident that the model is able to correctly capture the major cloud events in that period although errors in the details are clearly visible. This figure shows the potential of the

use of space-borne radar to derive vertical cloud fraction distributions for model comparison.

The above comparisons of the model to data (for more details about those studies, see Mahfouf *et al.* 1999) are only a small sample of the possibilities that both the new remotely sensed data and the short-range forecast approach to evaluation of model clouds could provide . This approach will gain importance with the use of data provided by space-borne radar systems which will form part of ERM.

3.3 Influence of cloud and radiative processes on NWP products

As it was mentioned in Section 2.4, cloud overlap assumptions must be made in atmospheric models in order to organize the cloud distribution used for radiation and precipitation/evaporation computations. The most common cloud overlap assumptions in radiation schemes presently used in global atmospheric models are the random, the maximum-random and the maximum overlap assumptions, neither of which is completely justifiable on a global scale from limited observations of the actual atmosphere. Only little is known about the actual vertical distribution of clouds and the results from Morcrette and Jakob (2000) show that radiation fields are sensitive to the cloud overlap assumption. Some studies have also been done with cloud overlap derived from radar (Hogan and Illingworth, 2000; Hogan *et al.*, 2000). One of the original features of the ERM mission would be to provide some description of the vertical structure of cloud layers that could help to define better cloud overlap assumptions in NWP and climate models.

The sensitivity of the climate of the ECMWF global model to the value of the fall speed of ice has been investigated (Mahfouf *et al.*, 1999). The operational version formulates ice settling from Equation (16). The fall speed w_{ice} is a function of the ice content proposed by Heymsfield and Donner (1990). The results of the experimentation have shown that through the modification of the assumed fall speed of the ice particles, the climate of the ECMWF model, in particular that of the tropics, can be changed dramatically. Small changes to the fall speed parametrization can substantially modify the model climate. Unfortunately the accuracy of the available global observations is not sufficient to draw firm conclusions about the right value of IWP in the sensitivity experiments.

4 The ECMWF 4D-Var data assimilation system

The general problem of assimilation of observations in a NWP context consists in defining the initial conditions of a forecast model using all the available information on the atmospheric state in an optimal way. Since November 1997 the operational data assimilation system at ECMWF is a four-dimensional variational (4D-Var) system (Rabier *et al.*, 2000; Mahfouf and Rabier, 2000).

4.1 General formalism

4D-Var seeks an optimal balance between observations and the dynamics of the atmosphere by finding a model trajectory $\mathbf{x}(t)$ which is as close as possible, in a least-square sense, to the observations available during a given time period $[t_0, t_n]$. The model trajectory $\mathbf{x}(t)$ is completely defined by the initial state $\mathbf{x}_0$ at time t_0.

The misfit to given observations $\mathbf{y}^o$ and to an *a-priori* model state $\mathbf{x}^b$ called background and usually provided by a short-range forecast is measured by an objective cost-function defined as:

$$\mathcal{J}(\mathbf{x}_0) = \frac{1}{2}(\mathbf{x}_0 - \mathbf{x}_0^b)^T \mathbf{B}^{-1}(\mathbf{x}_0 - \mathbf{x}_0^b) + \frac{1}{2}\sum_{i=0}^{n}(H_i[\mathbf{x}(t_i)] - \mathbf{y}_i^o)^T \mathbf{R}_i^{-1}(H_i[\mathbf{x}(t_i)] - \mathbf{y}_i^o) \tag{26}$$

where at any time t_i, $\mathbf{y}_i^o$ is the vector of observations, H_i is the operator providing the equivalent of the observed data from the model variable $\mathbf{x}(t_i)$, $\mathbf{R}_i$ the observation error covariance matrix (including measurement and representativeness errors), and $\mathbf{B}$ the background error covariance matrix of the state $\mathbf{x}^b$. The *observation operator* H_i describes the spatial interpolations to the observation locations, the calculation of the observation variables (for example, a radiative transfer model is used to compute radiances) and also the action of the forecast model to propagate the initial state $\mathbf{x}_0$ to the time of observation. The background information valid at time t_0 summarizes all information used before that time. Superscripts -1 and T denote respectively matrix inverse and transpose. The subscript i denotes the time index.

The model state $\mathbf{x}(t_i)$ is defined as :

$$\mathbf{x}(t_i) = M(t_i, t_0)[\mathbf{x}_0] \tag{27}$$

where M is the non-linear forecast model integrated from time t_0 to time t_i. The control vector $\mathbf{x}_0$ includes the prognostic variables to be initialised in the forecast model : vorticity, divergence, temperature, specific humidity and surface pressure. The prognostic cloud variables previously defined are not part of the control vector. The minimization of the objective function $\mathcal{J}$ is performed in spectral space, since it allows an easier specification of the balance constraints between wind and mass imposed in the background error covariance matrix (Derber and Bouttier, 1999). The minimization uses a descent algorithm which requires several computations of the gradient of $\mathcal{J}$ with respect to the initial state $\mathbf{x}_0$. Given the dimension of the state vector the adjoint technique is used to provide an efficient estimate of $\nabla\mathcal{J}$ (Le Dimet and Talagrand, 1986) :

$$\nabla\mathcal{J}(\mathbf{x}_0) = \mathbf{B}^{-1}(\mathbf{x}_0 - \mathbf{x}_0^b) + \sum_{i=0}^{n}\mathbf{H}_i^{\mathbf{T}}\mathbf{R}_i^{-1}(H_i[\mathbf{x}(t_i)] - \mathbf{y}_i^o) \tag{28}$$

The numerical coding of the transpose of tangent-linear versions of both the forecast model and of the observation operators $\mathbf{H}_i$ is required for such an efficient computation. Moreover the trajectory of the non-linear model around which the linearization is performed needs to be stored.

4.2 The incremental approach

The current operational model describes the state of the atmosphere in spectral space up to wavenumber 511 corresponding to a physical resolution of about 40 km. The vertical dimension is discretized over 60 layers. As a consequence the dimension of the control variable (about 10^7) is such that the full 4D-Var problem cannot be solved on present-day computers. Moreover only part of the forecast model has been linearized (the dynamics and a set of simplified physical parametrizations). Courtier et al. (1994) have proposed an incremental approach in order to reduce significantly the computational cost of 4D-Var. The incremental 4D-Var consists of computing the background trajectory and the departures (observations minus model) using the full non-linear model at high resolution including a full set of physical parametrizations, and minimizing the cost-function in a low resolution space for the increments at initial time using a tangent-linear model $\mathbf{M}$ and its adjoint with a limited set of physical parametrizations.

Writing:

$$\mathbf{x}_0 = \mathbf{x}_0^b + \delta\mathbf{x}_0 \tag{29}$$

and

$$H_i[\mathbf{x}(t_i)] = H_i[\mathbf{x}^b(t_i)] + \mathbf{H}_i\delta\mathbf{x}(t_i) \tag{30}$$

with $\mathbf{H}_i$ the linearization of the observation operator H_i in the vicinity of the background $\mathbf{x}^b$ and :

$$\delta\mathbf{x}(t_i) = \mathbf{M}(t_i, t_0)[\delta\mathbf{x}_0] \tag{31}$$

the new cost-function becomes:

$$\mathcal{J}(\delta\mathbf{x}) = \frac{1}{2}(\delta\mathbf{x}_0)^T\mathbf{B}^{-1}(\delta\mathbf{x}_0) + \frac{1}{2}\sum_{i=0}^{n}(\mathbf{H}_i\delta\mathbf{x}(t_i) - \mathbf{d}_i)^T\mathbf{R}_i^{-1}(\mathbf{H_i}\delta\mathbf{x}(t_i) - \mathbf{d}_i) \tag{32}$$

where $\mathbf{d}_i = \mathbf{y}_i^o - H_i[\mathbf{x}^b(t_i)]$ the innovation vector.

The optimum $\delta\mathbf{x}^a$ is added to the background $\mathbf{x}^b$ in order to provide the analysis $\mathbf{x}^a$:

$$\mathbf{x}^a = \mathbf{x}^b + \delta\mathbf{x}^a \tag{33}$$

It is possible to take into account the non-linearities introduced by the physical processes by updating iteratively the trajectory in the vicinity of which the model is linearized. In the current ECMWF operational 4D-Var, the increments are computed at T159 resolution (about 120 km) and two external updates of the trajectory are performed. The first inner-loop minimization is performed through 50 iterations with an adiabatic tangent-linear model. The second minimization consists of 25 iterations with a set of linear physical processes (Mahfouf and Rabier, 2000). The time window of the observations is currently 12 hours. The developed adjoint of the semi-lagrangian integration scheme allows to compute higher resolution increments at a reasonable computing cost. By the end of 2001, increments should be computed at 80 km (T_L255) resolution with a non-linear trajectory computed at 40 km (T_L511).

5 Development of the linearized radiation and cloud schemes

The variational approach has been described in the previous section. In order to enable the assimilation of cloud properties derived from the passive and active satellite instruments, important adaptations and improvements to the current 4D-Var system are required.

Current ECMWF operational 4D-Var uses a very simplified linearized radiation code, as the radiative transfer is only modelled for the longwave spectrum using a constant emissivity formulation (Mahfouf, 1999). Effective emissivity arrays are stored from the full non-linear radiation scheme. No dependency of radiation on cloudiness is taken into account in this approach. However, a proper consideration of cloud-radiation interactions requires the development of a linearized cloud scheme and a more sophisticated radiation scheme, which enables to take into account cloudiness. They should be included in the tangent-linear model $\mathbf{M}$ (Equation 31) for the propagation in time of analysis increments and in its adjoint version $\mathbf{M}^T$ for the estimation of the gradient of the objective function. However, such a linearization is not straightforward, since the on/off nature of clouds can make the tangent-linear approximation inadequate. The development of linearized observation operators ($\mathbf{H}_i$ in Equation 28) including the cloud description are needed in order to compare the satellite products with their model counterparts.

5.1 The linearized radiation schemes

The ECMWF shortwave radiation scheme is less expensive than the longwave radiation one. Therefore the scheme has been linearized without a priori modifications.

The complexity of the radiation scheme for the longwave part of the spectrum makes accurate computations expensive. In the assimilation framework, simplifications are required to reduce its computational cost.

The longwave radiative fluxes depend upon the temperature, water vapour, cloud cover and liquid and ice water contents. The design of the scheme allows to separate the contribution of temperature and water vapour from that of cloud parameters by using the concept of effective emissivity. More precisely, the upward and downward longwave fluxes at certain height z_i can be expressed as:

$$F(z_i) = \sum_k a_k(z_i) F_k(z_i) \tag{34}$$

where the coefficients a_k are function of the cloudiness and overlap assumptions. A differentiation of the above equation leads to:

$$dF(z_i) = \sum_k [a_k(z_i) dF_k(z_i) + F_k(z_i) da_k(z_i)] \tag{35}$$

In the proposed approach, the flux perturbation is approximated by:

$$\Delta F(z_i) \simeq \sum_k [a_k(z_i)\Delta F_k(z_i) + F_k(z_i)\Delta a_k(z_i)] \tag{36}$$

NL model — Jacobian matrices — NeuroFlux — TL model

The coefficients a_k are computed using the non-linear (NL) model (part of the operational radiation code computing cloud optical properties). Perturbations of radiative fluxes $\Delta F_k(z_i)$ with respect to temperature and water vapour are obtained using pre-computed Jacobians averaged globally (Mahfouf *et al.* 1999) . Perturbations of radiative fluxes with respect to cloud parameters $\Delta a_k(z_i)$ are computed using a tangent-linear (TL) scheme. The trajectory of radiative fluxes required in the tangent-linear and adjoint computations are efficiently estimated from a neural network version (called NeuroFlux) of the ECMWF longwave radiative transfer model (Chevallier *et al.* 2000).

5.2 The linearized cloud scheme

The operational prognostic cloud scheme is too complex to be used as such in data assimilation. It contains many thresholds which can degrade the validity of the tangent-linear approximation and its prognostic variables (cloud fraction, cloud liquid and ice water contents) cannot be initialized without major changes to the current data assimilation system. This poses difficulties for including grid-point control variables in the current 4D-Var system, and for specifying the statistics of background errors. Some simplifications of the prognostic cloud scheme are required to get a diagnostic relation for prognostic variables. Moreover, the development of a linearized prognostic cloud scheme will also require a revision of the linearized mass-flux convection scheme in order to improve the coupling with convection.

Currently, a simplified linearized prognostic cloud scheme is under development. For the time being, the ECMWF diagnostic cloud scheme (described in Section 2.3.2), used before the implementation of the prognostic scheme, has been linearized to be used with the linearized radiation scheme.

6 Validation of the linearized model including cloud-radiation processes

The classical verification of the correctness of the tangent-linear model is done through the Taylor formula:

$$\lim_{\lambda \to 0} \frac{M(\mathbf{x} + \lambda\delta\mathbf{x}) - M(\mathbf{x})}{\mathbf{M}(\lambda\delta\mathbf{x})} = 1 \tag{37}$$

where M is a discretized primitive equation model of the atmosphere, $\mathbf{M}$ is the tangent-linear model of M and $\mathbf{x}$ represents a model state at a certain time. For the verification of the adjoint,

one tests the identity between inner products for given $\mathbf{x}$ and $\mathbf{y}$ vectors, as

$$\forall \mathbf{x}, \forall \mathbf{y} \qquad < \mathbf{M}.\mathbf{x}, \mathbf{y} >=< \mathbf{x}, \mathbf{M}^T.\mathbf{y} > \tag{38}$$

In the above equation, the linear operator $\mathbf{M}^T$ is the adjoint of linear operator $\mathbf{M}$.

Then the accuracy of the linearization of both radiation and diagnostic cloud schemes has been studied with respect to pairs of non-linear results. The tangent-linear integrations propagating in time analysis increments have been performed with the trajectory computed using either the diagnostic cloud scheme (as it was used in 4D-Var) or the prognostic cloud scheme (now operational in 4D-Var).

Singular vector computations have also been done to verify that the new schemes do not produce spurious unstable modes (Janisková *et al.* 2000).

6.1 Validation of the tangent-linear approximation

6.1.1 Experimental framework

To evaluate the impact of including radiation and cloud schemes within existing linearized parametrizations, sets of experiments have been performed for different dates (15 March 1999 at 12 UTC, 15 June 1999 at 12 UTC, 20 September 1999 at 12 UTC and 15 December 1998 at 12 UTC) with integrations up to 24 hours using model resolution T63L31 (200 km horizontal resolution and 31 vertical levels) of the ECMWF global spectral model. The radiation and cloud schemes have been used at each time step and at every grid point. In the operational ECMWF model, the full radiation computations are presently done on a reduced horizontal grid and not for every time step (as explained in section 2.1). However, the assimilation of cloud properties will require calling the linearized radiation more often and at the full spatial resolution for an improved description of cloud-radiation interactions.

In the validation experiments, the difference between two non-linear integrations (one starting from a background field $\mathbf{x}_{fg}$ and the other one starting from an analysis $\mathbf{x}_{an}$) is computed using the full physics. This difference is then used as the standard reference for the tangent-linear integrations which propagate in time the analysis increments $\delta\mathbf{x} = \mathbf{x}_{an} - \mathbf{x}_{fg}$ with the trajectory taken from the background field (Janisková *et al.* 1999, Mahfouf 1999).

For a quantitative evaluation of the impact of the cloud and radiation schemes, their relative importance is evaluated using mean absolute errors between tangent-linear and non-linear integrations as

$$\varepsilon = \overline{\left| [M(\mathbf{x}_{an}) - M(\mathbf{x}_{fg})] - \mathbf{M}(\mathbf{x}_{an} - \mathbf{x}_{fg}) \right|} \tag{39}$$

where M is the forecast model starting from different initial conditions:
$\mathbf{x}_{an}$ - from analysis,
$\mathbf{x}_{fg}$ - from the first guess,
$\mathbf{M}$ is the tangent-linear model starting from the initial conditions $(\mathbf{x}_{an} - \mathbf{x}_{fg})$,
$\overline{(...)}$ represents the mean over a particular domain.

As a reference for the comparisons, an absolute mean error for the tangent-linear model without any radiation or with the old radiation ε_{ref} is taken. ε_i represents the absolute mean error for the tangent-linear model with new shortwave, longwave radiation and cloud schemes included with respect to pairs of non-linear integrations with the full physics. Then an improvement coming from including more physics in the tangent-linear model should be expressed by:

$$\varepsilon_i < \varepsilon_{ref} \tag{40}$$

The impact of including the new radiation and cloudiness schemes has been evaluated by studying the time evolution of analysis increments at different model levels and using the zonal mean diagnostics of the mean absolute errors. Global zonal mean errors as well as zonal mean errors for 20N - 90N (North20), 20S - 90S (South20) and 20N - 20S (Tropics) have been evaluated separately.

It is assumed that the radiation directly influences the temperature field and as a consequence of these temperature changes one could observe the impact of the radiation on other quantities. This is why, results are mostly presented for temperature perturbations, though during the validation, the results from other fields have been compared as well.

6.1.2 Impact of including the new schemes within the existing linearized parametrizations

The relative importance of the different tangent-linear radiation schemes has been evaluated. For that purpose, zonal mean absolute errors between non-linear and tangent-linear integrations have been computed. The results of our experiments have shown that the inclusion of a more sophisticated radiation package improves the fit to the non-linear model. However, the impact of the linearized diagnostic cloud scheme is small (Janisková *et al.* 2000).

Figure 5 shows comparisons of the tangent-linear (TL) integrations where the trajectory is computed either with the diagnostic cloud scheme (as it was used in 4D-Var) or with the prognostic cloud scheme (as it is now used in 4D-Var). The TL models using the whole physics with either the old radiation scheme or with the new radiation and cloud schemes are compared to the TL model without any radiation (reference TL model). Negative values (resp. positive values) correspond to an improvement (resp. deterioration) of the TL model with respect to the reference one. When using the diagnostic cloud scheme in the trajectory computations, one can see that the old longwave radiation scheme (Fig. 5a) only gives a slight global improvement of 0.31 %. Negative impacts appear in the upper troposphere. This problem comes from the use of the constant emissivity approach, which is not appropriate in the stratosphere. The new longwave and shortwave radiation schemes (Fig. 5b) give a global improvement of 4.71 %. There are only few places showing a some small negative impact.

When the prognostic cloud scheme is used in trajectory computations, the run with the old radiation scheme (Fig. 5c) is only slightly influenced, since the effective emissivity arrays are stored from the full non-linear radiation scheme. Therefore the arrays used in the TL model are obtained from the non-linear integration with the prognostic cloud scheme. It means that there is a consistency between the non-linear and tangent-linear integrations. However, when the TL

model containing the new radiation and diagnostic cloud scheme uses the trajectory computed with the prognostic cloud scheme (Fig. 5d), results are worse than in the run with the trajectory obtained using the diagnostic cloud scheme (Fig. 5b). In this case, different cloud schemes are used in the trajectory computation and in the linearized model, therefore having an influence on the accuracy of the TL approximation. One of the reasons for developing a simplified version of the prognostic cloud scheme is to avoid such discrepancy.

The vertical profiles for the mean values of $\varepsilon_i - \varepsilon_{ref}$ (see equations 39, 40) are presented in Fig. 6 for a 24-hour integration and for the different domains (North20, South20 and Tropics). The results for temperature, specific humidity and u-wind component are on the left, middle and right panels, respectively. The comparisons are displayed for the old (simplified) longwave radiation scheme (dashed line) as well as for the new radiation (longwave and shortwave) with simplified cloud scheme (solid line) and for clear sky (dot-dashed line).

By comparing the impact of the schemes on temperature (Fig. 6a, d, g), one can see that including the new radiation to the linearized physics improves the fit of the tangent-linear model to the nonlinear one through the whole vertical profile in North20 and Tropics. It is also the case for South20, except levels between 900 and 700 hPa. Adding the cloudiness scheme to the radiation has a very small impact and is mainly negative except in the tropics. The old radiation scheme improves the results only in the lower troposphere and degrades them for higher levels.

The results for specific humidity (Fig. 6b, e, h) show that there is an improvement close to the surface and in the lower troposphere when using the new radiation scheme. The impact is only slightly negative elsewhere. The largest improvement is observed in the lower and middle troposphere of the tropics. The old radiation scheme has only a slight influence on specific humidity. It often improves or worsens the results at the same levels as the new radiation scheme, but the magnitude of the impact of the old radiation schemes is always smaller.

The results for the u-wind component are displayed in Fig. 6c, f, i. When using the new radiation scheme, it is interesting to notice an improvement in the wind considering it is not an input to either the longwave or shortwave radiation schemes. The improvement is observed nearly through the whole vertical profiles for all domains. The impact of the old radiation scheme on u-wind is negligible and it is mainly negative in the upper part of the atmosphere. A positive impact of using cloudiness together with the radiation is seen especially in the Tropics.

The relative comparison between the different tangent-linear models have shown a general improvement at the lowest model levels when the new radiation and cloud schemes are used. The results are also better for the tropics suggesting that a proper balance between shortwave, longwave radiation and moist processes is crucial.

Table 1 summarizes the results of the relative comparisons for the 24-hour integration of the different situations and for North20, South20, Tropics domains as well as globally. The tables contain the results from experiments run with the old radiation scheme, with the new radiation schemes for clear sky or using the diagnostic cloud scheme.

The largest improvement is achieved when using the new radiation scheme. The results are

slightly better, except in the Tropics, for the clear sky radiation than for the radiation with clouds. In the Tropics, cloudiness always has a positive impact when used in the linearized model. The results are situation dependent. The worst results (however still leading to an improvement after 24-hour integration, except within South20) were obtained for the June situation (Table 1). Actually, this was a situation for which no configuration including radiation improves significantly the results.

Including more sophisticated radiation schemes gives a general improvement in the Tropics and a large error reduction as well as a reduction of some existing negative impacts for longer integrations. The impact of using cloudiness with the radiation is not as large as one would expect and not always positive. The negative impacts are possibly a consequence of introducing more non-linearities in the linearized physics with the cloud processes.

According to our experiments, the improvement coming from the new radiation scheme with respect to the old one represents up to 10 % of the perturbation value. It can reach locally several Kelvins for some specific situations (Janisková *et al.* 2000).

7 1D-Var assimilation experiments

To investigate the potential of the developed radiation and cloud schemes to modify the model profiles of temperature, humidity and cloudiness to produce a better match to the observations of the radiation fluxes, preliminary 1D-Var experiments with simulated observations have been carried out. The sensitivity of the radiation scheme to the temperature, humidity and cloud properties has been investigated using adjoint technique. Feasibility studies in a 1D-Var framework using data from the Atmospheric Radiation Measurement Program (ARM - Stokes and Schwartz, 1994) have also been done. Results of these experiments are discussed below.

7.1 Description of the system

Let $\mathbf{x}$ be the vector representing an atmospheric state described by temperature T, humidity q and surface pressure p_s (control variables of 1D-Var). The goal of 1D-Var is to define the atmospheric state $\mathbf{x}$ such that the distance between the model variables and the observations is minimum. The model is constrained to fit the observations by adjusting its initial conditions. Then the minimization problem consists in finding the optimum profile $\mathbf{x}$ which minimizes the objective function:

$$\mathcal{J}(\mathbf{x}) = \frac{1}{2}(\mathbf{x}-\mathbf{x}^b)^T\mathbf{B}^{-1}(\mathbf{x}-\mathbf{x}^b) + \frac{1}{2}\sum_{i=1}^{n}\left[\frac{F_i(\mathbf{x})-F_{oi}}{\sigma_{oi}}\right]^2 \qquad (41)$$

where $\mathbf{B}$ is the covariance matrix of the background error taken from the operational ECMWF 4D-Var (described in more details in Section 7.4.1 Background error statistics). $\mathbf{x}^b$ is the background vector (short term forecast profile). F_{oi} represents a set of observations i ($i = 1, \cdots, n$) with observation errors σ_{oi}. Different types of observations have been used, such as the surface and/or top of atmosphere radiation fluxes, total column water vapour and liquid water path. Pseudo-observations of vertical profiles for temperature and humidity have been used in the case of experiments with simulated observations. $F_i(\mathbf{x})$ is the observation operator providing the equivalent of the data from the model variable $\mathbf{x}$. In 1D-Var experiments, $F_i(\mathbf{x})$ includes the shortwave and longwave radiation schemes together with the cloud scheme. The minimization requires an estimation of the gradient of the objective function:

$$\nabla \mathcal{J}(\mathbf{x}) = \mathbf{B}^{-1}(\mathbf{x} - \mathbf{x}^b) + \sum_{i=1}^{n} \mathbf{F}_i^T \left[\frac{F_i(\mathbf{x}) - F_{oi}}{\sigma_{oi}^2} \right] \tag{42}$$

The transpose of the observation operator $\mathbf{F}^T$ can be obtained explicitly through the Jacobian matrix computed in finite differences by a perturbation method. Such approach is affordable due to the low dimension of the control vector in 1D-Var. Using the adjoint of the tangent-linear physical processes to compute $\mathbf{F}^T$ reduces significantly the computational cost. An estimation of the gradient of $\mathcal{J}$ is done using a limited memory quasi-Newton optimization routine (M1QN3), which requires an estimation of the gradient of the objective function at each iteration (Gilbert and Lemaréchal 1989).

1D-Var computations contain forward modelling of cloudy radiation fluxes (F operator) and corresponding adjoint modelling ($\mathbf{F}^T$ operator). In the case of forward modelling (Fig. 7a), the computation starts from the control variables T, q, p_s, which are input variables for the cloud scheme. The outputs of the cloud scheme are the cloud cover, cloud liquid water and ice water contents. Those variables together with the control variables are inputs to the radiation scheme. The cloud-radiation interactions are taken into account there. The incorporation of the effects of clouds on radiation fluxes is achieved through the cloud optical properties and the effective cloud cover computed using the maximum-random overlap assumption. Then from the radiation scheme, one can get cloudy (or clear sky) radiation fluxes. Backward computation of the cloudy radiation fluxes (Fig. 7b) starts from the departure of cloudy radiation fluxes, which are entering the adjoint of the radiation scheme. Integration of the adjoint scheme gives increments of the cloud variables. Those are then used as inputs for the adjoint of the cloud scheme (for the time being, there is only adjoint of the diagnostic cloud scheme). After its integration, one gets the gradient of the objective function with respect to the control variables.

7.2 Sensitivity studies using simulated observations

1D-Var experiments have been undertaken using simulated observations. In those experiments, the first-guess data are taken from 3D-model integrations. The simulated observations are obtained from a 1D-model integration (over one time step) of the cloud and radiation schemes by modifying the vertical profiles of temperature and humidity. The observation operator can be obtained explicitly through a Jacobian matrix in the case of the finite-differences approach or it can be obtained using the adjoint technique. In our experiments, the observation operator includes the shortwave and longwave radiation schemes together with the diagnostic cloud

scheme. There is a very strong relationship between temperature and liquid/ice water contents in the diagnostic cloud scheme. This might not be similar once the prognostic cloud scheme is used. Several experiments have been done using simulated observations of the longwave downward radiation flux at the surface, longwave upward radiation flux at the top of atmosphere, shortwave downward radiation flux at the surface or the combination of all those fluxes. Profiles of temperature and specific humidity have been used in some experiments as well.

One of the questions, which we tried to answer in our experiments, was whether it is possible to modify significantly the cloud cover when using the 1D-Var approach to improve the fit of the model to radiative fluxes. Experiments have been run for different model profiles simulating a nearly clear sky or cloudy "observed" atmosphere, while the first-guess was describing the opposite situation. Three types of observations were used: longwave downward radiation flux at the surface (LWDs), longwave upward radiation flux at the top of atmosphere (LWUPtoa) and shortwave downward radiation flux at the surface (SWDs). The observations were assumed to be nearly perfect, since the observation error σ_o was set up to 2 W.m^{-2}. For instance, Baseline Surface Radiation Network's (BSRN) standard is something around 2 W.m^{-2} for LWD, but more like 10 W.m^{-2} for SWD (Ohmura *et al.*, 1998).

The capacity of 1D-Var to remove clouds is shown in Fig. 8. The first-guess (b) and analyzed (c) cloud cover are compared to the pseudo-observed cloud cover (simulated observation) for 100 consecutive points. The observed situation is a clear sky (a), while the first guess shows significant cloud cover. As seen in Fig. 8c, 1D-Var is quite efficient at removing clouds. Figure 9 displays the results for a cloudy "observed" atmosphere and a first guess with a small amount of clouds. It shows that 1D-Var is able to increase the cloudiness or even to create new clouds. However, our experiments have shown that to create new clouds, the atmospheric state must be already close to cloud formation.

The potential of the radiation and cloud schemes to modify the model temperature, humidity and cloud profiles in order to get closer to the observations is presented in more details in Fig. 10-13. Figure 10 shows the results for one of the vertical profiles from the study of the 1D-Var ability to create clouds. In that experiment, the simulated observations indicate larger amount of clouds than given by the first-guess. The values of observed, first-guess and analyzed radiation fluxes are written in Fig. 10. Analysis increments of the specific humidity (solid line), temperature (dashed line) and cloud profiles (observed, first-guess and analyzed) are presented on the left panel (a) of the figure. This figure shows that the analyzed cloud cover is much larger than the first-guess. Except for the highest model levels, it nearly reaches the amount of observed clouds. This result is presented in more details on the right panel (Fig. 10b), which also shows information about cloud liquid water and ice water contents. At the same time, analyzed radiation fluxes are close to the observed ones. Our experiments have shown (not presented here) that the clouds can be created even when they are completely missing in the first-guess. However, in this case the atmospheric state must be close to the state of cloud formation. It is important to mention that the radiation has a sensitivity of the same sign for cloudy and clear sky conditions (see below in the section 7.3 Sensitivity of radiation scheme to input variables). If there are no clouds in the model even though indicated by observations, the radiation scheme has some skill to increase humidity in order to make the atmosphere less transparent. When the atmospheric state is close to the threshold value for cloud formation, such positive humidity

increments can be sufficient to trigger the creation of clouds. Once a small amount of cloudiness appears at some level, the background error correlation may help to spread it over the vertical.

Results from the experiment studying whether 1D-Var is able to remove the clouds are presented in Fig. 11. The same information as in the previous figure is included. In this case, the first-guess has a significant amount of clouds and the simulated observation is clear-sky one. One can see that analyzed cloud cover is significantly reduced and the analyzed radiation fluxes are adjusted to the observed ones. However, analysis increments of specific humidity around 500 hPa are very large. Some explanation about such a behaviour is given at the end of this section.

To illustrate a situation when 1D-Var fails to get closer to the observations, an experiment has been done using only a simulated observation of longwave downward radiation flux at the surface (LWDs). Figure 12 shows a situation where the model first guess (fg) gives a profile with cloud cover close to one at several levels with an observation (obs) larger than the first guess ($obs = 1.05fg$). In such case, 1D-Var is not able to improve the fit to the observations, since this would require to create clouds in the lowest model levels and 1D-Var is not able to trigger them. This is proven by an additional experiment where small amount of clouds below existing ones are added to the first guess (Fig. 13). In that case, the 1D-Var is able to get close to the observation by modifying the profiles of temperature and humidity which leads to a significant increase of the cloud cover at low levels.

Our experiments have shown that 1D-Var is, to some extent, able to modify the temperature and humidity profiles (analysis increments of temperature and humidity are presented in Fig. 10a and 11a) in order to reduce or increase the cloud cover. However, there are some potential problems. One of them is a difficulty to trigger new clouds in certain situations, as described above. Another one is that it is possible to adjust the model state to the observed fluxes with very different profiles than the reference ones. An example of such situation is presented in Fig. 14. This figure shows comparisons of the first-guess (dashed line) and analyzed (solid line) vertical profiles of specific humidity (a) and temperature (b) against observations from the previous study when reducing cloud cover (Fig. 11). Though the cloud cover is reduced using 1D-Var, one cannot be satisfied with the retrieved temperature and humidity profiles. Especially with the specific humidity when the very large analysis increments around 500 hPa actually increase the difference between analysis and observations compared to the difference between first-guess and observations. One would rather expect to obtain opposite results after the performed analysis. This demonstrates the ambiguity of the surface or top of atmosphere fluxes on the retrievals. Experiments have shown that using some observations on the vertical helps to retrieve more accurate profiles. The differences between observations and improved analysis when using temperature and humidity observations on the vertical are displayed on Fig.14 (solid line with symbols). One must admit that too large humidity increments may also appear due to the very small observation error for radiation fluxes ($\sigma_o = 2$ W.m^{-2}) used in our experiments. 1D-Var tries then to satisfy such perfect observation by creating too large increments of the control variables. This stresses the importance of defining observation error relevant for the future observation systems.

7.3 Sensitivity of the radiation scheme to input variables

The adjoint models can be used not only for the data assimilation, but also for sensitivity studies. They allow to compute the gradient of one output parameter of a numerical model with respect to all input parameters (Le Dimet and Talagrand, 1986) and therefore to be applied to the study of sensitivity problems. When such technique is applied to a particular physical parametrization scheme, it can provide information on the meteorological variables to which the parametrization scheme is the most sensitive. From a data assimilation point of view, it can give some indications related to the importance and efficiency of particular types of observations. For instance, the vertical extension of the sensitive areas corresponding to a given surface radiation observation may support increasing the number of upper-level observations of a certain kind in order to improve this surface radiation flux. Improved radiation can in turn improve the quality of the forecasts (two-metre temperature, humidity, ...).

7.3.1 Methodology

Let us briefly explain the formulation of a sensitivity problem for the radiation scheme. Using the parametrization schemes for the shortwave and longwave radiations, let $\mathbf{y}$ denote the vector of the outputs (radiation fluxes) from the radiation schemes. It can be expressed as

$$\mathbf{y} = F(\mathbf{x}) \tag{43}$$

where $\mathbf{x}$ is the vector representing an atmospheric state described by T, q, p_s (control variables as in Eq. 41) together with cloud characteristics (cloud fraction, liquid water and ice water contents). The operator $F(\mathbf{x})$ includes only the shortwave and longwave radiation schemes in this case.

A small perturbation $\delta\mathbf{y}$ can be estimated to the first order approximation by the tangent linear equation of the radiation scheme as:

$$\delta\mathbf{y} = \mathbf{F}(\mathbf{x})\delta\mathbf{x} \tag{44}$$

where $\mathbf{F}$ is the Jacobian operator of F.

Given the definition of the adjoint of a linear operator for the scalar product:

$$< \mathbf{x} \mid \mathbf{F}(\mathbf{y}) > = < \mathbf{F}^T(\mathbf{x}) \mid \mathbf{y} > \tag{45}$$

the linear operator $\mathbf{F}^T$ provides the gradient of an objective function $\mathcal{J}$ with respect to $\mathbf{x}$ (input variables) given the gradient of $\mathcal{J}$ with respect to $\mathbf{y}$ (output variables):

$$\frac{\partial \mathcal{J}}{\partial \mathbf{x}} = \mathbf{F}^T(\mathbf{x})\frac{\partial \mathcal{J}}{\partial \mathbf{y}} \quad \text{or} \quad \nabla_{\mathbf{x}}\mathcal{J} = \mathbf{F}^T(\mathbf{x})\nabla_{\mathbf{y}}\mathcal{J} \tag{46}$$

In our experiments, the gradient with respect to $\mathbf{y}$ of unity size (i.e. perturbation of some of the radiation fluxes which are output variables of the radiation scheme) is provided to the adjoint of

radiation schemes in order to get the sensitivity of this scheme with respect to its input variables, i.e. temperature, specific humidity and cloud characteristics. This leads to

$$\nabla_{\mathbf{x}}\mathcal{J} = \frac{\partial F}{\partial \mathbf{x}} \tag{47}$$

where $\partial F/\partial \mathbf{x}$ is the corresponding Jacobian matrix.

7.3.2 Numerical results

The method described above has been used in order to examine the sensitivity of the radiation schemes described in section 5. The results are presented in Fig. 15-20.

The perturbations of the different radiation fluxes with the unity size (± 1 W.m^{-2}) have been used one by one as input for the adjoint of the radiation schemes. The sensitivity of the downward longwave (b part of the figures) and shortwave (c) radiation fluxes at the surface, as well as the upward longwave (d) and shortwave (e) radiation fluxes at the top of atmosphere has been investigated with respect to the input variables. The parametrization schemes produce fluxes which are counted positive downwards. Then the sign plus or minus is used for the perturbation to study the same type of situation in all experiments. It was chosen to investigate the situation when the increase/decrease (± 1) of radiation should be a consequence of more cloudiness (or less transparent atmosphere).

As mentioned in section 2.4, cloud overlap assumptions must be made in atmospheric models in order to organize the vertical cloud distribution used for radiation computations. The linearized model is used for investigation of sensitivity. Such a model is sensitive to any thresholds as those represented by the max-function either in the maximum overlap assumption (Eq. 23) or the maximum-random overlap assumption (Eq. 25). Therefore for simplicity, the experiments have been done using the random overlap assumption (Eq. 24). Such results are presented in Fig. 15-18 for the different cloud cover and solar zenith angle. Figure 19 shows the sensitivity of the radiation fluxes for clear sky conditions. The impact of using different cloud overlap assumptions is displayed in Fig. 20. In all those figures, (a) shows the cloud fraction (yellow filled area) together with the cloud liquid content (green solid line) and cloud ice water content (red solid line). The sensitivity of the different radiation fluxes is displayed in (b)-(e) with respect to the following input variables: temperature $\partial F_{Ri}/\partial T$ (black solid line), specific humidity $\partial F_{Ri}/\partial q$ (black dashed line), cloud cover $\partial F_{Ri}/\partial a$ (blue dotted line), cloud liquid water content $\partial F_{Ri}/\partial q_{lw}$ (green solid line) and cloud ice water content $\partial F_{Ri}/\partial q_{iw}$ (red solid line). All those input variables are of different orders of magnitude. Therefore to get a relative evaluation of the sensitivity, the particular $\partial F_{Ri}/\partial \mathbf{x}_i$ had to be normalized. This has been done by multiplying $\partial F_{Ri}/\partial T$ and $\partial F_{Ri}/\partial q$ by their background errors σ_{bT} and σ_{bq}, respectively. The background errors for the cloud variables are not known. Therefore a rough estimate has been used for them instead:

$$\begin{aligned} \sigma_{ba} &= 0.1 && \text{for cloud cover} \\ \sigma_{bq_{lw}} &= \sigma_{bq_{iw}} = 0.05\sigma_{bq} && \text{for cloud water} \end{aligned} \tag{48}$$

Though the cloud cover is different in Fig. 15 and 16, the main difference in the sensitivity of the shortwave radiation is linked to the different solar zenith angle $\mu = cos\theta$ ($\mu = 0.93$ in Fig. 15 and 0.25 in Fig. 16). Otherwise the results for those experiments can be summarized together. When looking at the sensitivity of the downward radiation flux at the surface with respect to the input variables, one can see that the most important role is played by temperature in the lower levels (up to model level 45-50, i.e. pressure levels around 700-850 hPa) and by cloud fraction. The sensitivity to the cloud fraction depends on the actual cloud cover. When there are no clouds in the lowest levels (Fig. 15), the cloud fraction sensitivity has a similar vertical extent (with a maximum in the lowest clouds) as the temperature contribution. However, when the base of the clouds is very low and the cloud cover is maximum at around 850 hPa (Fig. 16), the sensitive area extends from the surface up to the level with the maximum cloud fraction. The sensitivity to the specific humidity is quite small and does not differ significantly from case to case. The downward shortwave radiation (c) is mostly sensitive to the cloud parameters. The sensitivity of specific humidity and that of the cloud parameters increase with higher sun.

When investigating the upward longwave radiation flux at the top of atmosphere (d), one can see that the sensitivity to input variables is maximum in the highest layers of the clouds from the top of atmosphere and it diminishes below. There is mostly a sensitivity to the temperature and the cloud parameters. However, when the clouds are lower, below level 35 (around 350 hPa), the contribution of humidity above the clouds is also significant (see Fig. 16 - 18). When studying the behaviour of the upward shortwave radiation flux at the top of atmosphere, it is important to mention that this flux represents the shortwave radiation flux reflected either from the clouds or from the surface. It means that it also contains information on the downward shortwave radiation and the sensitivity is then more complex. There is a similar level of sensitivity to the cloud variables as for the downward shortwave (sw) radiation. In the case of the downward sw radiation, the scheme tends to create more clouds in order to decrease this radiation flux by 1 W.m^{-2}. It does similarly for the upward sw radiation. In order to reflect more radiation, it creates more and denser clouds. At the same time, it shows that a 1 W.m^{-2} increase in the upward shortwave radiation flux at the top of atmosphere is also achieved through a decrease in specific humidity. This may look paradoxical. However, this comes from the sw radiation going downward before being reflected. To get more upward sw radiation at the TOA, the scheme tends to reduce the atmospheric absorption by water vapour so that more downward radiation is reflected. The upward component of the sw radiation is responsible for the tendency to create more clouds for the reflection. There is almost no sensitivity of the shortwave radiation to temperature.

Figure 17 displays the results for a highly cloudy atmosphere (cloudiness equal to one through several levels) around midday (solar zenith angle equal to 0.93). In this case, the sensitivity is mostly seen either below the maximum cloud cover for the downward longwave (lw) radiation or above the maximum cloud cover for the upward sw and lw radiation at the TOA. The downward shortwave radiation shows very small sensitivity in such situation. It is obvious that this small sensitivity is due to the saturation effects occuring at several levels.

The results in Fig. 18 can be compared with those in Fig. 16. The results presented in this figure underline that the upward lw radiation at the TOA shows a maximum sensitivity to the specific humidity above the clouds and to the temperature together with the cloud variables at

the top of cloud, wherever this top is located (Fig. 16-18).

The sensitivity in clear sky conditions is displayed in Fig. 19. The downward lw radiation at the surface has a similar sensitivity to temperature at the lowest model levels as for the situations with clouds before reaching the first cloudy level. There is a significantly higher sensitivity to specific humidity. Since there are no clouds, less transparent atmosphere can only be achieved through increasing humidity. In the case of the upward lw radiation at the TOA, the sensitivity to temperature and specific humidity is smaller than in presence of clouds and it is more regularly distributed through the vertical. The shortwave radiation (b, d) shows only sensitivity to humidity. Without clouds, sensitivity of the downward longwave and shortwave radiation fluxes to the specific humidity in the lower troposphere is higher than in their presence, though only a small amount of clouds. In a data assimilation, one can imagine a situation when the model does not produce any cloud even though some cloudiness is present in reality. If the assimilation system does not succeed at triggering clouds by modifying the control variables in the minimization process and no other observations are used, this could lead to an inadequate modification of the specific humidity in order to get closer to the radiation observation. On the other hand as $\partial F/\partial q\ |_{clear}$ has the same sign as $\partial F/\partial q\ |_{cloudy}$, the positive sensitivity to specific humidity in clear sky conditions can help to trigger new clouds for the situations close to cloud formation.

There is also a sensitivity of the radiation fluxes to the cloud overlap assumption. The results are shown only for the upward longwave radiation at the top of atmosphere (Fig. 20) using maximum-random (b), maximum (c) and random (d) overlap assumptions. The sensitivity to temperature and humidity is not significantly modified when using the different overlap assumptions contrary to the sensitivity to cloud variables. Except that the sensitivity is maximum for the highest clouds in any overlap assumption, the results are otherwise quite different. Using maximum-random overlap assumption (MRN) shows that the radiation scheme tends to increase cloudiness at those levels where the cloud fraction is high and decrease them at intermediate levels. The scheme with maximum overlap (MAX) is insensitive at intermediate levels and it displays a higher sensitivity to lower clouds than MRN. The only positive sensitivity (i.e. leading to increasing cloud variables) through the top level clouds is given by the radiation scheme with the random overlap assumption (RAN). The question is then, which assumption is the most appropriate one. In the operational forecast model, MRN is used. From the linearization point of view, one would prefer to use RAN which gives a smoother sensitivity response due to the absence of thresholds in this formulation. This sensitivity study confirms the results obtained by Morcrette and Jakob (2000) showing that the radiation fields are sensitive to the cloud overlap assumptions and that there is still limited information about the actual vertical distribution of clouds for the time being.

In summary, the sensitivity study with the adjoint version of the radiation schemes not surprisingly confirms known results: The radiation scheme increases the downward longwave radiation flux at the surface through increasing cloudiness and temperature below the clouds and mainly close to the surface (in the case of temperature). The reduction of the downward shortwave radiation at the surface is also achieved through increased cloudiness and increased humidity. To decrease the upward longwave radiation flux at the TOA, the scheme increases the cloudiness, which comes with an increase of the specific humidity and a decrease in temperature. When

some clouds already exist, the sensitivity is located at the highest layers of clouds reached by the upward radiation flux. The scheme tends mainly to increase cloudiness (cloud cover, water and ice content) to increase upward shortwave radiation at the TOA. The study also shows at which levels and which variables can be modified when the observations of the surface and/or TOA radiation fluxes are used in data assimilation.

7.4 Assimilation of ARM data

The performance of 1D-Var using real observations has also been examined. Some observations from the ARM program (Stokes and Schwartz, 1994) at the SGP (South Great Plains) site, where measurements of both cloud properties and radiative fluxes are available, have been used in our feasibility studies.

7.4.1 Experimental framework

(a) Background profiles

A set of background temperature and specific humidity profiles and surface pressure have been produced by short-range 6-hour forecasts from the ECMWF model with a T_L319 spectral truncation and 50 vertical levels for the period of April-May 1999 and from the model with the same horizontal resolution, but with 60 vertical levels for the period between 29 April and 7 May 2000.

The surface pressure p_s and the profiles of T and q (control variables) together with the vertical velocity, skin temperature, albedo and soil moisture are used in the observation operator to calculate first the cloud properties (cloud cover, liquid water and ice water content) and then the corresponding radiation fluxes (Fig. 7). More precisely, the vertical velocity is an input of the diagnostic cloud parametrization scheme. The soil moisture and albedo are used for the computation of soil emissivity. Only the control variables are modified during the minimization. All other input variables remain constant.

In the 1D-Var experiments, the convective precipitation, which is an input variable to the cloud parametrization scheme, has not been taken into account. Any supersaturation is then released by the stratiform clouds. It is a simplification of the original diagnostic scheme (Slingo, 1987).

The problem of this link between the convection and the cloudiness remains to be solved. During the period from 29 April to 7 May 2000, the first guess gives some convective precipitation just for 4 hours, between 7 and 10 UTC on 30 April 2000. It means that most of the clouds produced by the diagnostic cloud scheme are of a stratiform nature. There are several situations with convective precipitation during the period of April-May 1999. However, the stratiform cloudiness is generally dominant during that period. One can see it in Fig. 27 (for April 1999) and Fig. 30 (for May 1999), which display the time-series of the cloud cover from the first guess obtained using the diagnostic cloud scheme with (a) and without (b) convective precipitation.

(b) Background error statistics

The role of the background error covariance matrix **B** is to pass to the variational analysis the appropriate information about the 3D statistical structure of the forecast errors. It means that **B** gives the information on how to spread the observation departures in the vertical in the case of 1D-Var. In the experiments, the covariance matrix of the background error **B** is taken from the operational ECMWF 4D-Var system (Rabier *et al.* 1998, Derber and Bouttier 1999). The covariances are computed statistically using the National Meteorological Center method (Parish and Derber 1992) from differences between 48-h and 24-h forecasts. No cross correlations between the background errors of specific humidity and temperature are considered, as in the ECMWF 4D-Var analysis system. The standard deviations of temperature (Fig. 21) over the vertical are about 1 K up to around 200 hPa, then they grow in the stratosphere up to 4.5 K. The standard deviation for specific humidity has been empirically specified by Rabier *et al.* (1998). The vertical distribution has a maximum around 850 hPa, an exponential decrease above and lower values in the boundary layer.

(c) Observations

The experiments have been carried out using observations from the Atmospheric Radiation Measurement Program (ARM) at the South Great Plains (SGP) site over the April-May 1999 and 29 April - 7 May 2000 periods. The ARM-SGP site (Lamont, Oklahoma) is located at 36.605°N and 97.485°W. Some measurements from the observational systems located at the Central Facility have been used. The surface downward shortwave (SWD) and longwave (LWD) radiation are measured by pyrgeometers and pyranometers (SIRS - Solar Infrared Radiation Stations). The total column water vapour (TCWV) and cloud liquid water path (LWP) are derived from the Microwave Radiometer (MWR). A comparison was also made with the vertically integrated water vapour derived from the humidity information in the radiosoundings at Lamont, close to the Central Facility. The TCWV derived from the radiosonde is slightly smaller than the MWR-derived value (Morcrette, 2001).

All observations are averaged over 1-hour intervals as described by Morcrette (2001). For radiative fluxes, the averaging is carried out taking all values after rejecting the few unrealistic values. The same procedure has been applied to the measurements from the Microwave Radiometer. The measurements of the total column water vapour and liquid water path are sometimes contaminated by precipitation and the presence of condensation on the optics. The wet index is thus marked on the figures presenting the results from 1D-Var assimilation experiments in order to indicate when those measurements have not been assimilated since they are unreliable.

In order to evaluate the cloud cover modified by the assimilation of the above observations, the first guess and analyzed liquid water content (LWC) and ice water content (IWC) fields have been used to simulate Ze-reflectivity using the relationships from Frisch *et al.* (1995) for LWC-Ze and Atlas *et al.* (1995) for IWC-Ze. Details of the procedure follows Beesley *et al.* (2000) and are described in Morcrette (2001). The corresponding Ze-reflectivity is derived from the Multi-Mode Cloud Radar (MMCR) by Clothiaux *et al.* (2000). Such evaluation has been done for the period April-May 1999, since the measurements from MMCR were only available for that period.

(d) Observation errors

The observation errors for the radiation measurements used observations in this study are defined as 5 W.m^{-2} for the longwave radiation and 10 W.m^{-2} for the shortwave radiation (BSRN standard - Ohmura *et al.*, 1998). However, our experiments have shown (see Section 7.4.2) that larger errors by a factor 2 should be used in order to achieve a compromise for better usage of the radiation and moisture observations at the same time.

The MWR only measures LWP. The model produces both LWP and ice water path (IWP) from temperature. In presence of ice clouds, the LWP measurement cannot be used to check the model LWP+IWP. Therefore the observation error for LWP measurements has been set-up as large as 50 % of the observed value.

For the observation error of TCWV, the error specification defined for the assimilation of SSM/I[9] has been used (Gérard and Saunders, 1999):

$$\sigma_{TCWV_{obs}} = 7.27\ .\ 10^{-2}\ TCWV_{obs} + 1.63 \tag{49}$$

7.4.2 Case study for the period of 29 April - 7 May 2000

This short period of measurements has been used to find an optimal set-up for the 1D-Var assimilation with real observations. Different experiments have been run in order to decide which observations among the available ones are reasonable to assimilate. The problem of the observation errors and of how to control the size of the increments (difference between the analyzed and the background states for the control variables) had to be assessed as well.

The results of experiments are displayed for each hour starting from 29 April in Fig. 22-24. Figure 22 shows a comparison of the first guess and analysis against the observations (obs_rs - radiosonde, obs_mr - microwave) of the total column water vapour. As it was mentioned above, the wet index marked in the figures means that MWR observation was not used (either it was unreliable or unavailable). On the left corner of the figures (a)-(d), there are values of the absolute mean differences between analysis and observation, as well as between the first guess and observation for the whole period.

It was decided to start with an assimilation of the downward longwave and shortwave radiation at the surface from the radiometers together with the total column water vapour and liquid water path from the Microwave Radiometer. A sensitivity study has shown that, as expected, the upward longwave radiation at the surface has very small sensitivity to the control variables (not shown) and the upward sw radiation at the surface would not bring much additional information with respect to the downward sw, since the albedo and soil moisture are kept constant in 1D-Var computations. The observation errors have been used as defined in section 7.4.1 d.

Results of experiments using the first set-up are presented in Fig. 22a (exp_d2) and they are not very encouraging. Though 1D-Var succeeded to get close to the radiation observations (not

[9]Special Sensor Microwave Imager

shown), the humidity analysis was deteriorated, which is obvious from the analyzed TCWV. The mean absolute difference between analysis and observation for the whole period (2.914 $kg.m^{-2}$) is significantly worse than between the first guess and observation (2.144 $kg.m^{-2}$). The definition of the observation errors seems to favour more the radiation observations (error approximately 1 % of radiation) than the humidity ones (TCWV error is approximately 10 % and LWP is 50 % of their values). Then a relatively small correction to the radiation flux to make it closer to its observation can more easily contribute to decreasing the gradient of the objective function than corrections to the humidity and the minimization procedure usually takes such a direction. Therefore it was decided to increase the observation errors by a factor 2 for the radiation observations (i.e. 10 $W.m^{-2}$ for LWD and 20 $W.m^{-2}$ for SWD) in order to achieve a better compromise in using simultaneously the radiation and moisture observations. An improvement coming from the increased observation errors is seen in Fig. 22b (exp_d6), though the analyzed TCWV is still slightly worse than the first-guess one. For some periods the analysis increases TCWV too much. In those cases, humidity increments are large and not realistic. They may be a consequence of the discontinuous nature of the physical parametrization (Fillion and Errico 1997). We need to constrain them during the minimization to avoid their large values in the resulting analysis. The minimization procedure is assumed successful, when the size of increments for temperature, specific humidity and surface pressure is smaller than five-times of their background standard deviations. The 1D-Var with such control really tends to improve the humidity analysis (exp_d11 in Fig. 22c) and at the same time to preserve a generally improved fit of the radiation fluxes to the observations at the same time (Fig. 23a, c). However, the comparison of the first guess and analysis against the observations of the LWD and SWD at the surface (Fig. 23) shows some periods where 1D-Var makes the fit to the LWD observation worse in order to get close to the SWD observation . This is seen on 30 April and 6 May 1999 for the midday - afternoon period when SWD observation is available. In both cases, LWD observation indicates that there should be less clouds in order to bring the first guess closer to the observation, while to get closer to the SWD observation requires to create more clouds. On top of that, the differences between the first-guess and analyzed SWD are larger than in the case of LWD. There is no humidity observation during the problematic periods. In such situations, the minimization goes in the direction of an improvement of the shortwave downward radiation flux at the expense of the longwave downward radiation. To avoid such contradictory situations, which the 1D-Var is not able to deal with, it was decided not to use SWD observations in our experiments. A more sophisticated method would be to find a suitable quality control of the observations to remove those which look inconsistent. However, this would require to study longer series of data to define properly such check. For the time being, it was decided simply not to use SWD observations together with LWD ones.

The results of an experiment without SWD observations are shown in Fig. 22d (exp_d15) and Fig. 23b, d. One can see that TCWV analysis was further improved compared to exp_d11 (Fig. 22c). For instance, an improvement in the afternoon of 4 May 2000 can be explained using the results of the sensitivity study from the section 7.3. There are no clouds either in the first guess or analysis at that period (Fig. 24). The first-guess radiation fluxes are not too far from the observations. To fit these observations would require to have a slightly more opaque atmosphere. However, according to TCWV there should be less specific humidity than what is given by the first guess. Both SWD and LWD have a quite high sensitivity to humidity at clear sky conditions. At local noon, the sensitivity of SWD to humidity would be larger (about 3 times) than that the one presented in Fig. 19 for the solar zenith angle equal to 0.25. Such

sensitivity to humidity may create a situation where any fit to the observation may be done through the humidity modification. One can see (Fig. 23), that when SWD is used, there is a small improvement in the differences between analysis and observations for both SWD and LWD at the price of an incorrect humidity modification. Without SWD observations, 1D-Var improves very slightly the fit to observations of both LWD and TCWV.

Comparison of the first-guess and analyzed cloud cover for the experiments with and without SWD observations (Fig. 24) is quite similar for most of the period. The largest difference is seen in the afternoon period of 30 April 2000, which was one of the situations leading to the decision not to use SWD observations. When SWD observations are used, the cloud fraction is increased up to 800 hPa to match this observation. Without SWD observation, the cloudiness is slightly decreased compared to the first guess in order to get closer to LWD. Some observations on the vertical would be useful in this case to constrain the 1D-Var towards the right atmospheric state.

From the results of the experiments presented above, the set-up for 1D-Var experiments using the ARM data has been defined. It was decided to use the following observations: the downward longwave radiation at the surface with an observation error of 10 $W.m^{-2}$, the total column water vapour with the error defined by Eq. 49 and the liquid water path with an error as large as 50 %. The control of the size of the increments for temperature, specific humidity and surface pressure should also be used.

7.4.3 Case study for the period of April-May 1999

A one-dimensional variational assimilation of the observations from the ARM-SGP has been performed for a two-month period (April-May 1999) using the set-up previously defined. For this period, the measurements from MMCR are also available to evaluate the cloud cover modified by the assimilation. Unfortunately, there is a period between 19 April 1999 12 UTC and 3 May 1999 10UTC, when the radiation measurements are not available. The 1D-Var assimilation has been performed for the whole two-month period, though one must take the results of analyzed TCWV and LWP with extra caution during the period for which radiation observations are missing.

The results for April 1999 are displayed in Fig. 25-27 and those for May 1999 in Fig. 28-30. Improvement, resp. deterioration of the analysis with respect to the first guess after 1D-Var assimilation of the ARM observations are summarized for April and May 1999 in Fig. 25 and 28, respectively. The results are presented as the differences between the absolute value of the first guess minus observation and the absolute value of the analysis minus observation for the total column water vapour (a), the downward longwave radiation at the surface (b), the liquid water path (c) and the downward shortwave radiation at the surface (d). The positive values then indicate an improvement of the analysis compared to the first guess with respect to the observations. Figures 26 and 29 show the radar reflectivity measured at the ARM-SGP site (a) and the pseudo-radar reflectivity computed from the first-guess (b) and analyzed (c) data. As explained by Morcrette (2001), the model reflectivity depends on the method used for its computation. The model clouds are produced using the diagnostic cloud scheme, which derives the liquid water and ice water contents only from temperature through the saturation and cloud fraction (Eq. 20 and 21). One can see, that the first guess already shows generally too low model

reflectivity, though the comparison with the microwave observations of LWP (as seen in more details in Fig. 32) does not show that the model would produce too low amount of the liquid water. It is mostly rather opposite. The liquid water content produced by the diagnostic cloud scheme is usually larger (sometimes comparable) than the one obtained through the prognostic cloud scheme used in the ECMWF forecast model (not shown here). However, the amount of ice water content produced by the diagnostic cloud scheme used in the observation operator is smaller compared to the prognostic scheme of the forecast model (Fig. 31a for April 1999, b for May 1999). There seems to be a problem in partitioning between the liquid and ice water contents in the diagnostic cloud scheme. Therefore our 1D-model reflectivity can be used only for a relative comparison to the observations. The observed reflectivity can serve for the identification of the cloudy periods and vertical distribution of the clouds. It may help to check whether 1D-Var succeeded to modify the cloudiness in the right direction (location and increased/decreased reflectivity) through the modification of temperature and humidity. To get a direct information about the clouds produced by the model, time-series of the cloud cover in percentage from the first guess and from the analysis are presented in Fig. 27 and 30.

Though some deterioration of the analysis appears at some hours, generally 1D-Var is able to retrieve temperature and humidity profiles that provide LWD, TCWV and LWP closer to the observations (Fig. 25 and 28). For the shortwave radiation, the number of cases with an improvement only slightly dominates over the deterioration of SWD flux. There are cases, when the 1D-Var was not able to modify properly the model TCWV or LWP to get closer to the observations. A lot of them are situations with no clouds in the first guess (even though indicated by the measured radar reflectivity) and 1D-Var is not able to trigger them. One can find them, for instance, at the beginning of 2 April, on 6 May, 21 May 1999 (Fig. 26 with the reflectivity, Fig. 27 for the cloud cover in April and the same in Fig. 29, 30 , but for May). There are some situations when using 1D-Var led to a reduction of clouds not supported by the reflectivity observations. Such positive corrections are observed on 14 May 1999 (when low levels clouds were removed), 17 May 1999 around 10UTC or 25 May 1999 around 10-11UTC. There are a lot of cases, as those on 7-8 April 1999 (upper level cloud), 5 May 1999, 20 and 22 May 1999 (upper level clouds), 25 May 1999 (lower level clouds - up to 680 hPa), when the clouds became properly denser (as observed) and their vertical extent have been increased. It is even possible to find cases where new clouds have been created. Examples of such situations are small spots of new clouds on 4 April 1999 and 5 April 1999 or clouds from 600 and 780 hPa just between 4 and 5 May 1999. Improvement in cloud cover comes together with improved radiation, total column water vapour and liquid path produced from analyzed temperature and humidity.

The above mentioned situations are just examples of improvement/deterioration in cloud cover when using 1D-Var of radiation (LWD) and humidity (TCWV, LWP) observations. Certainly, a more detailed comparison of the results (e.g. plotting a zoom for certain periods) can show more situations of all described types. For this reason, additional results from the period between 20 and 28 May 1999 are presented in Fig. 32-34. In those figures, as before, the dates on x-axis are indicated as the days since 1 May 1999 00UTC starting from 0. For instance, the hourly data of 20 May 1999 are then plotted in the interval starting at 19 and finishing at 20. Figure 32 shows a comparison of the first guess and analysis against the observations for the total column water vapour (a), the downward longwave radiation at the surface (b), the liquid water path (c) and

the downward shortwave radiation at the surface (d). Figure 33 displays the radar reflectivity measured at the ARM-SGP site (a) as well as the pseudo-radar reflectivity computed from the first-guess (b) and analysis (c) for the same period. The time-series of the cloud cover from the first guess (a) used for 1D-Var experiment and from the analysis (b) are shown in Fig. 34. Looking at all those comparisons, one can get a detail picture when and how 1D-Var is successful to get closer to the observations through the modified profiles of temperature and humidity. Let us start with the first two-day period (20-21 May 1999). One can see, that there are some clouds, which were removed at the lower levels after 12UTC of 20 May 1999 and in the early hours of 21 May 1999 (Fig. 34). At the same time, upper level clouds as those from 500 to 600 hPa and from 280 to 430 hPa have been either created or became denser. The cloudiness is also intensified at 12UTC on 20 May 1999 and around 05-07UTC on 21 May 1999. All those cloud modifications went in the right direction as compared with the measured radar reflectivity (Fig. 33), though the model reflectivity is still smaller than the measured one. Possible reasons for such behaviour have been suggested earlier. The proper cloud modifications are also translated into improved analyzed LWP and TCWV compared to the MWR observations, when they are available (Fig. 32a, c). The analyzed LWD and SWD (Fig.32b, d), when the humidity is successfully modified, is closer to the observations than the first guess. The modifications of LWD are positive, though sometimes the improvements are too small. This is most obvious early after 12UTC on 21 May 1999, as 1D-Var has not succeeded to create the additional low level clouds observed by MMCR at that period. The MWR indicates that there should be less TCWV and more LWP than given by the first guess. The analyzed LWP is not changed and TCWV is even increased. It means that the humidity has been increased in order to get closer to the radiation observations, which show that there should be more clouds. Apparently in this short 3-4-hour period from the first two days, 1D-Var has not succeeded to modify correctly the temperature and specific humidity. It may be the case, that due to some thresholds in the physical parametrization schemes, the minimization procedure failed to find proper minima.

During the next two days (22-23 May 1999), there are some middle and higher level clouds not present in the first guess, nor in the analysis. There was no convection activity indicated by the first guess, so the missing clouds are not a consequence of neglecting the convective precipitation in the diagnostic cloud scheme. One can see that the model clouds between 230 and 370 hPa are intensified and some additional clouds between 370 and 430 hPa and below 690 hPa are created on 22 May 1999. New clouds are also triggered by 1D-Var around 06-07UTC and 12-13UTC on 23 May 1999. Those are positive corrections when compared to the radar reflectivity (MMCR). Any other missing clouds have not been created. The cloud cover correction is connected with improved analysis leading to a better fit of LWD radiation, TCWV and LWP to the observations. The analyzed SWD is also improved for 22 May 1999, while it is not modified at all for 23 May 1999 (however the distance of both, the first guess and analysis, to the observation is relatively small).

The period of three days between 24 and 26 May 1999 is again characterized by a lack of middle and high level clouds. To be objective, the clouds above 520 hPa between 07 and 11UTC of 25 May 1999 would appear there (see Fig. 30), if the convective precipitation are taken into account. However, the possibility to modify them through 1D-Var would be limited as explained in section 7.4.1 a (Background profiles). In this period, 1D-Var has not triggered missing middle level clouds on 25 May 1999 and high clouds on 26 May 1999, though there are

positive impacts brought by 1D-Var. Those are increasing cloudiness between 250 and 440 hPa on 24 May 1999, below 650 hPa after 12UTC on 25 May 1999 and removing the low and the middle level clouds at 05, 06 and 11UTC on 25 May 1999. There are some middle level clouds created between 05 and 07UTC on 26 May 1999. However, only those at 06UTC are observed by MMCR. When comparing with the radiation (LWD, SWD) and humidity (TCWV, LWP) observations, one can see that there is a general improvement of the analyzed quantities in Fig. 32 with respect to the first guess. Though no humidity observations are used after 12UTC of 25 May 1999, analyzed temperature and specific humidity produce the radiation fluxes with a better match to the observations. One can guess from TCWV of the radiosonde measurements and from the measured reflectivity, that the increased analyzed TCWV and LWP should then be a consequence of the right modification of the first guess.

Let us examine the last period of two days (27-28 May 1999). It is obvious, that there is too many low clouds and completely missing clouds above 600 hPa. While 1D-Var is able to slightly decrease the amount of low clouds, it does not succeed to trigger those high clouds indicated by the reflectivity observations. In this case, the analyzed TCWV is partly improved by removing the low level clouds as TCWV is reduced with respect to the first guess. Then the fit of the analysis to LWD observations is just slightly modified (sometimes improved, sometimes worsened). The same comment applies to the SWD (see also Fig. 28d). This two-day period shows an example of a situation when the 1D-Var fails to correct the first guess to get closer to the observations (though there is an improvement in TCWV).

One can hope that additional radiation observations at the top of the atmosphere or even some observations on the liquid and ice water content on the vertical could help to improve the analysis. As shown by the examination of the Jacobians (section 7.3), the influence of atmospheric profiles on surface observation of radiation is important up to a certain level (maximum 450 hPa for the clear sky spring-time conditions at ARM-SGP). Most of the missing clouds are above 600 hPa. Certainly, the surface measurements cannot have too much impact there.

The 1D-Var assimilation of observations from the ARM-SGP over a two-month period (April-May 1999) has shown a capability to improve the analysis of temperature and specific humidity through the assimilation of surface observations. However, it has also revealed some weaknesses of the 1D-Var (difficulty to trigger clouds, minimization favouring one type of observations sometimes) and also a lack of complementary observations for some situations.

8 Conclusions and perspectives

Some illustrations of the ECMWF model performance and of model changes related to clouds and radiation have been given in order to emphasize the need for complementary datasets such as those proposed for ERM. The results of the described experiments underline the importance for future satellite missions to generate consistent measurements of radiative fluxes, cloud fractional coverage and cloud water/ice contents to allow more comprehensive evaluations of cloud-radiation interactions in NWP models, and hence to improve their parametrization.

The cloud and radiation parametrizations used in the ECMWF model have been described. The linearized radiation and cloud schemes have been developed for variational data assimilation of cloud observations. The shortwave radiation is based on a linearization of the operational ECMWF code. To reduce the computational cost, a combination of artificial neural network and mean Jacobian matrices is used for the linearized longwave radiation scheme. For the time being, the ECMWF diagnostic cloud scheme has been linearized to be used with the linearized radiation. The results from the validation of the linearized model including cloud-radiation processes have shown that the inclusion of a more sophisticated radiation treatment to the existing linearized parametrizations improves the fit to the nonlinear model. However, the impact of the linearized diagnostic cloud scheme is small. A simplified linearized prognostic cloud scheme is under development in order to improve cloud-radiation interactions and the coupling with the convection scheme.

Preliminary 1D-Var experiments with simulated observations have been carried out to investigate the potential of the developed radiation and cloud schemes to modify the model temperature, humidity and cloud profiles to produce a better match to the observations of radiation fluxes. Our experiments have shown, that though 1D-Var is able to modify the temperature and humidity profiles in order to reduce or increase cloud cover, there are also some potential problems. One of them is a difficulty to trigger new clouds in certain situations. Another one is a possibility to adjust the model state to the observed fluxes with very different profiles than the reference ones in several cases. Experiments have shown that using some observations on the vertical helps to retrieve more accurate profiles.

A sensitivity of the radiation schemes to the temperature, humidity and cloud properties has been investigated using the adjoint technique. The study has shown which variables can be modified when certain observations of the surface and/or TOA radiation fluxes are used in data assimilation. It has also indicated how much in the vertical such observations have an influence. The limited extension on the vertical of the areas sensitive to cloud properties related to the value of surface/TOA radiation can be an argument for complementary observations of cloud properties.

The performance of 1D-Var using real observations has also been examined. The observations from the Atmospheric Radiation Measurement (ARM) Program, where measurements of both cloud properties and surface radiative fluxes are available, have been used in our feasibility studies. The first experiments have been performed to define the set-up for 1D-Var experiments using ARM surface observations. Two-month assimilation of those observations has shown a capability of 1D-Var to improve the analysis of temperature and specific humidity. Some weaknesses have also been identified, as a problem of triggering clouds and the lack of complementary observations to the surface ones in some situations.

Though not shown, we have tried to use the 1D-Var with the ECMWF prognostic cloud scheme using the finite differences approach without having an explicit coding of tangent-linear and adjoint versions of the scheme. The study has shown the difficulties to use the current prognostic cloud scheme as it is. The problem is connected mainly with the prognostic variables (cloud fraction, cloud liquid and ice water contents) not taken as control variables. It leads to very limited modifications of cloud properties in the 1D-Var context, as each iteration of the

minimization process starts from the same initial values of cloud variables. However, including prognostic cloud variables to the control variables would require major changes to the current data assimilation system and the specification of statistics of background errors. It has been generally agreed (ECMWF/EuroTRMM Workshop on Assimilation of clouds and precipitation) that it would not be cost effective to add separate cloud control variables. Clouds have a much smaller scale (temporal and spatial) and are discontinuous compared to the conventional observations (such as temperature and humidity). However, they are not independent variables since they are related to temperature and specific humidity. As a consequence, it would be difficult to define the cloud background errors. It means that we need to work on a simplification of the prognostic cloud scheme in a direction to get a diagnostic relationship for cloud variables.

Feasibility studies in a 1D-Var framework will continue using data from field experiments (e.g. ARM-SGP, ARM-TWP, CLARE) in order to assess further how cloud observations can be used for analysis purposes. Such kind of work is also being done with TOVS[10] (Chevallier *et al.*, 2000). Another objective of the studies will be to identify the most important (sensitive) processes to be included in the improved linearized cloud scheme. Data from the cloud radar at Chilbolton (UK), South Great Plains (Oklahoma), North Slope of Alaska and Tropical West Pacific will be used to demonstrate the importance of cloud profile observations collocated with radiative measurements. Sensitivity studies will be used to assess the importance of additional cloud retrievals (such as cloud boundaries, IWP, effective radius).

Acknowledgements

Many thanks belong to J.-F. Mahfouf and J.-J. Morcrette for their cooperation on the subject of this report and for their fruitful advices and instructive suggestions. I am grateful to F. Chevallier for providing neural networks and Jacobian matrices for the linearized longwave radiation scheme, as well as for constructive discussions and comments. The validation studies on clouds and radiative fluxes at ECMWF have been prepared thanks to the contributions of J.F. Mahfouf, A. Beljaars, F. Chevallier, D. Gregory, C. Jakob, J.-J. Morcrette, J. Teixeira and P. Viterbo. Their help was greatly appreciated. The CLARE radar comparison has been performed by R. Hogan from the University of Reading. A. Beljaars and M. Miller provided useful comments to improve the initial manuscript.
This work was funded by grants from ESA/ESTEC Contract 13151/98/NL/GD coordinated by J. Pedro V. Poiares Baptista.

[10] TIROS (Television Infrared Observation Satellite) Operational Vertical Sounder

9 References

Atlas, D., Matrosov, S.Y., Heymsfield, A.J., Chou, M.D. and Wolff, D.B. , 1995: Radar and radiation properties of ice clouds. *J. Appl. Meteor.*, **34**, 2329-2345.

Beesley, J.A., Bretherton, C.S., Jakob, C., Andreas, E.L., Intrieri, J.M. and Uttal, T.A. ,2000: A comparison of cloud and boundary layer variables in the ECMWF forecast model with observations at the Surface Heat Budget of the Arctic ocean (SHEBA) ice camp. *J. Geophys. Res.*, **105D**, 12337-12350.

Bonnel, B., Fouquart, Y., Vanhoutte, J.-C., Fravalo, C. and Rosset, R. , 1983: Radiative properties of some African and mid-latitude stratocumulus. *Beitr. Phys. Atmos.*, **56**, 409-428.

Cess, R.D., Potter, G.L., Blanchet, J.-P., Boer, G.J., DelGenio, A.D., Déqué, M., Dymnikov, V., Galin., V., Gates, W.L., Ghan, S.J., Kiehl, J.T., Lacis, A.A., Le Treut, H., Li, Z.-X, Liang, Z.-X., McAvaney, B.J., Meleshko, V.P., Mitchell, J.F.B., Morcrette, J.-J., Randall, D.A., Rikus, L., Roekner, E., Royer, J.-F., Schlese, U., Scheinin, D.A., Slingo, A., Sokolov, A.P., Taylor, K.E., Washington, W.M., Wetherald, R.T., Yagai, I. and Zhang, M.-H. , 1990 : Intercomparison and interpretation of climate feedback processes in 19 general circulation models. *J. Geophys. Res.*, **95**, 16601-16615

Cess, R.D., Zhang, M.H., Ingram, W.J., Potter, G.L., Alekseev, V., Barker, H.W., Cohen-Solal, E., Colman, R.A., Dazlich, D.A., Del Genio, A.D., Dix, M.R., Dymnikov, V., Esch, M., Fowler, L.D., Fraser, J.R., Galin, V., Gates, W.L., Jack, J.J., Kiehl, J.T., Le Treut, H., Lo, K. K.-W., McAvaney, B.J., Meleshko, V.P., Morcrette, J.-J., Randall, D.A., Roeckner, E., Royer, J.-F., Schlesinger, M.E., Sporyshev, P.V., Timbal, B., Volodin, E.M., Taylor, K.E., Wang, W. and Wetherald, R.T. , 1996: Cloud feedback in atmospheric general circulation models: An update. *J. Geophys. Res.*, **101D**, 12791-12794.

Chevallier, F., Morcrette, J.-J., Chéruy, F. and Scott, N.A. , 2000: Use of a neural network-based longwave radiative transfer scheme in the ECMWF atmospheric model. *Q. J. R. Meteor. Soc.*,**126**, 761-776.

Chevallier, F., Bauer, P., Kelly, G., Mahfouf, J.-F., Jakob, C. and McNally, T. , 2000: Requirements for the assimilation of cloudy radiances. ECMWF/EuroTRMM Workshop on Assimilation of Clouds and Precipitation. Reading, UK, 6-9 November 2000

Clothiaux, E.E., Ackerman, T.P., Mace, G.G., Moran, K.P., Marchand, R.T., Miller, M.A. and Martner, B.E. ,2000: Objective determination of cloud heights and radar reflectivities using a combination of active remote sensors at the ARM CART sites. *J. Appl. Meteor.*, **39**, 645-665.

Derber, J. and Bouttier, F. ,1999: A reformulation of the background error covariance in the ECMWF global data assimilation system. *Tellus*, **51A**, 195-221.

Ebert, E.E. and Curry, J.A. , 1992: A parametrization of ice optical properties for climate models. *J. Geophys. Res.*, **97D**, 3831-3836.

Fillion, L. and Errico, R. , 1997: Variational assimilation of precipitation data using moist convection parametrization schemes: A 1D-Var study. *Mon. Wea. Rev.*, **125**, 2917-2942.

Fouquart, Y. , 1987: Radiative transfer in climate models. *Physically Based Modelling and Simulation of Climate and Climatic Changes*, M.E. Schlesinger, Ed., Kluwer Acad. Publ., 223-284.

Fouquart, Y. and Bonnel, B. , 1980: Computations of solar heating of the earth's atmosphere: a new parametrization. *Beitr. Phys. Atmos.*, **53**, 35-62.

Fowler, L.D., Randall, D.A. and Rutledge, S.A. , 1996: Liquid and ice cloud microphysics in the CSU general circulation model. Part I : Model description and simulated microphysical processes. *J. Climate*, **6**, 498-529.

Frisch, A.S., Fairall, C.W. and Snider, J.B. , 1995: Measurement of stratus cloud and drizzle parameters in ASTEX with a Ka-band Doppler radar and a microwave radiometer. *J. Atmos. Sci.*, **52**, 2788-2799.

Geleyn, J.-F. and Hollingsworth, A. , 1979: An economical analytical method for the computation of the interaction between scattering and line absorption in radiation. *Beitr. Phys. Atmos.*, **52**, 1-16.

Gérard, E. and Saunders, R.W. ,1999: Four-dimensional variational assimilation of Special Sensor Microwave/Imager total column water vapour in the ECMWF model. *Quart. J. Roy. Meteor. Soc.*, **125**, 3077-3101.

Gilbert, J.-C. and Lemaréchal, C. , 1989: Some numerical experiments with variable-storage quasi-Newton algorithms. *Math. Programming*, **45**, 407-435.

Heise, E. and Roekner, E. , 1990: The performance of physically based cloud schemes in general circulation models. *Beitr. Phys. Atmos.*, **93**, 1-14.

Heymsfield, A.J. and Donner, L.J. , 1990: A scheme for parameterising ice cloud water content in general circulation models. *J. Atmos. Sci.*,**47**, 1865-1877.

Hogan, R.J. and Illingworth, A.J. , 2000: Deriving cloud overlap statistics from radar. *Quart. J. Roy. Meteor. Soc.*, **126A**, 2903-2910.

Hogan, R.J., Jakob, C. and Illingworth, A.J. , 2000: Comparison of ECMWF cloud fraction with radar derived values. *J. Appl. Meteor.*, submitted.

Houghton, J.T., Meira Filho, L.G., Callander, B.A., Harris, N., Kattenberg, A. and Maskel, K. , 1995: Climate change 1995. The science of climate change. Cambridge University Press, 572pp.

Ingmann, P. , 1998: The Earth Radiation Mission, Proceedings of the Workshop on Synergy of Active Instruments in the Earth Radiation Mission, 12-14 November 1997, GKSS, Geesthacht,

Germany, 47-50.

Jakob, C. , 1995: The impact of the new cloud scheme on ECMWF's Integrated Forecasting System (IFS). Proceedings of ECMWF/GEWEX Wokshop on Modelling, Validation and Assimilation of clouds, November 1994, ECMWF, Reading, United Kingdom, 277-294.

Jakob, C. and Klein, S.A. , 2000: A parametrization of the effects of cloud and precipitation overlap for use in general circulation models. *Quart. J. Roy. Meteor. Soc.*, **126C**, 2525-2544.

Janisková, M., Thépaut, J.-N. and Geleyn, J.-F. , 1999: Simplified and regular physical parametrizations for incremental four-dimensional variational assimilation. *Mon. Wea. Rev.*, **127**, 26-45.

Janisková, M., Mahfouf, J.-F., Morcrette, J.-J. and Chevallier, F. , 2000: Development of linearized radiation and cloud schemes for the assimilation of cloud properties. *ECMWF Technical Memorandum*, **301**, 31 pp.

Kessler, E. , 1969: On the distribution and continuity of water substance in atmospheric circulation. *Meteorol. Monog.*, **10**, American Meteor. Soc., Boston, Mass.

Klein, S. A. and Jakob, C. ,1999: Validation and sensitivities of frontal clouds simulated by the ECMWF model. *Mon. Wea. Rev.*, **127**, 2514-2531.

Le Dimet, F.-X. and Talagrand, O. , 1986: Variational algorithms for analysis and assimilation of meteorological observations. *Tellus*, **38A**, 97-110.

Mace, G.G., Ackermann, T.P. and Clothiaux, E.E. , 1997: A study of composite cirrus morphology using data from a 94-Ghz radar and correlations with temperature and large-scale vertical motion. *J. Geophys. Res.*, **D12**, 13581-13593.

Mace, G.G., Jakob, C. and Moran, K.P. , 1998: Validation of hydrometeor occurence predicted by the ECMWF model using millimeter wave radar data. *Geophys. Res. Lett.*, **25**, 1645-1648.

Mahfouf, J.-F. , 1999: Influence of physical processes on the tangent-linear approximation. *Tellus*, **51A**, 147-166.

Mahfouf, J.-F., Beljaars, A., Chevallier, F., Gregory, D., Jakob, C., Janisková, M., Morcrette, J.-J., Teixeira, J. and Viterbo, P. , 1999: The importance of the Earth Radiation Mission for numerical weather prediction. *ECMWF Technical Memorandum*, **288**, 77 pp.

Mahfouf, J.-F. and Rabier, F. , 2000: The ECMWF operational implementation of four-dimensional variational assimilation. Part II: Experimental results with improved physics. *Quart. J. Roy. Meteor. Soc.*, **126**, 1171-1190.

Marécal, V. and Mahfouf, J.-F. ,2000: Variational retrieval of temperature and humidity profiles from TRMM precipitation data. *Mon. Wea. Rev.*, **128**, 3853-3866.

Matveev, Yu.L. , 1984: Cloud dynamics. D. Reidel Publishing Co., Dordrecht, 340 pp.

Miller, S.D., Stephens, G.L. and Beljaars, A.C.M. ,1999: A validation survey of the ECMWF prognostic cloud scheme using LITE, *Geophys. Res. Lett.*, **26**, 1417-1420.

Morcrette, J.-J., Smith, L. and Fouquart, Y. , 1986: Pressure and temperature dependence of absorption in longwave radiation parametrizations. *Beitr. Phys. Atmos.*, **59**, 455-469.

Morcrette, J.-J. , 1989: Description of the radiation scheme in the ECMWF operational weather forecast model. *Research Department Tech.Memo*, **165**, 26 pp.

Morcrette, J.-J. , 1991: Radiation and cloud radiative properties in the ECMWF operational forecast model. *J. Geophys. Res.*, **96D**, 9121-9132.

Morcrette, J.-J. , 1998: Impact of validated radiative transfer scheme, RRTM on the ECMWF model climate and 10-day forecasts. *ECMWF Technical Memorandum*, **252**, 47 pp.

Morcrette, J.-J. , 2000: On the effects of the temporal and spatial sampling of radiation fields on the ECMWF forecasts and analyses. *Mon. Wea. Rev.*, **128**, 876-887.

Morcrette, J.-J. and Jakob, C. ,2000: The response of the ECMWF model to changes in the cloud overlap assumption. *Mon. Wea. Rev.*, **128**, 876-887.

Morcrette, J.-J. ,2001: Assessment of the ECMWF model cloudiness and surface radiation fields at ARM-SGP site. *ECMWF Technical Memorandum*, **327**, 41pp.

Ohmura, A., Dutton, E.G., Forgan, B., Frohlich, C., Gilgen, H., Hegner, H., Heimo, A., Konig-Langlo, G., McArthur, B., Muller, G., Philipona, R., Pinker, R., Whitlock, C.H., Dehne, K., and Wild, M. , 1998: Baseline Surface Radiation Network (BSRN/WCRP): New precision radiometry for climate research. *Bull. Amer. Meteor. Soc.*, 79, 2115-2136.

Ou, S.C. and Liou, K.-N. , 1995: Ice microphysics and climate temperature feedback. *Atmosph. Research*, **35**, 127-138.

Parrish, D.F. and Derber, J,C. , 1992: The National Meteorological Center's Spectral Statistical Interpolation Analysis System. *Mon. Wea. Rev.*, **120**, 1747-1763.

Rabier, F., McNally, A., Andersson, E., Courtier, P., Unden, P., Eyre, J., Hollingsworth, A. and Bouttier, F. ,1998: The ECWMF implementation of three dimensional variational assimilation (3D-Var). Part II: Structure functions. *Quart. J. Roy. Meteor. Soc.*, **124**, 1809-1829.

Rabier, F., Järvinen, H., Klinker, E., Mahfouf, J.-F. and Simmons, A. , 2000: The ECMWF operational implementation of four-dimensional variational assimilation. Part I: Experimental results with simplified physics. *Quart. J. Roy. Meteor. Soc.*, **126**, 1143-1170.

Ricard, J.-L. and Royer, J.-F. , 1993: A statistical cloud scheme for use in an AGCM. *Ann. Geophysicae*, **11**, 1095-1115.

Senior, C. A. and Mitchell, J.F.B. , 1993: Carbon dioxide and climate : the impact of cloud parameterization. *J. Climate*, **6**, 393-418.

Slingo, J.M. , 1987: The development and verification of cloud prediction scheme in the ECMWF model. *Quart. J. Roy. Meteor. Soc.*, **113**, 899-927.

Smith, E.A. and Shi, L. , 1992: Surface forcing of the infrared cooling profile over the Tibetan plateau. Part I: Influence of relative longwave radiative heating at high altitude. *J. Atmos. Sci.*, **49**, 805-822.

Smith, R.N.B. , 1990: A scheme for predicting layer clouds and their water content in a general circulation model. *Quart. J. Roy. Meteor. Soc.*, **116**, 435-460.

Stokes, G.M. and Schwartz, S.E. ,1994: The Atmospheric Radiation Measurement (ARM) Program: Programmatic background and design of the cloud and radiation tested. *Bull. Amer. Soc.*, **75**, 1201-1221.

Sundqvist, H. , 1978: A parameterisation scheme for non-convective condensation including prediction of cloud water content. *Quart. J. Roy. Meteor. Soc.*, **104**, 677-690.

Sundqvist, H. , 1988: Parameterization of condensation and associated clouds in models for weather prediction and general circulation simulation. *Physically-Based Modelling and Simulation of Climate Change*, M.E. Schlesinger, Ed. Kluwer, 433-461.

Tian, L. and Curry, J. , 1989: Cloud overlap statistics. *J. Geophys. Res.*, **94D**, 9925-9936.

Tiedtke, M. , 1993: Representation of clouds in large-scale models. *Mon. Wea. Rev.*, **121**, 3040-3061.

Tiedtke, M. , 1996: An extension of cloud-radiation parameterization in the ECMWF model: The representation of sub-grid scale variations of optical depth. *Mon. Wea. Rev.*, **124**, 745-750.

Washington, W.M. and Williamson, D.L. , 1997: A description of the NCAR GCMs. "GCMs of the atmosphere." J. Chang, Ed., *Methods in computational physics*, Vol.**17**, Academic Press, 111-172.

Zhong, W. and Haigh, J.D. , 1995: Improved broadband emissivity parameterization for water vapor cooling rate calculations. *J. Atmos. Sci.*, **52**, 124-138.

10 Tables

15 March 1999

	radiation scheme		
Domain	old radiation	new radiation clear sky	new radiation cloud
global	-0.31%	-4.69%	-4.71%
Tropics	-1.93%	-2.72%	-3.09%
North20	+1.19%	-8.06%	-7.96%
South20	-0.16%	-3.09%	-2.82%

15 June 1999

	radiation scheme		
Domain	old radiation	new radiation clear sky	new radiation cloud
global	-0.13%	-1.10%	-0.41%
Tropics	-0.58%	-0.70%	-0.88%
North20	+0.02%	-1.25%	-0.95%
South20	+0.25%	+0.38%	+0.74%

20 September 1999

	radiation scheme		
Domain	old radiation	new radiation clear sky	new radiation cloud
global	+0.05%	-2.78%	-2.58%
Tropics	-0.55%	-3.09%	-3.16%
North20	+0.48%	-3.89%	-3.69%
South20	+0.35%	-0.80%	-0.20%

15 December 1998

	radiation scheme		
Domain	old radiation	new radiation clear sky	new radiation cloud
global	-0.65%	-3.28%	-3.22%
Tropics	-1.39%	-2.10%	-2.31%
North20	+0.47%	-1.54%	-1.39%
South20	-1.03%	-6.55%	-6.29%

Table 1: Percentage of an improvement(-)/worsening(+) of the TL model with some of the listed radiation schemes with respect to the TL model without any radiation scheme for temperature after 24-hour integration. (Initial dates of the integration: 15 March 1999 12UTC, 15 June 1999 at 12 UTC, 20 September 1999 12 UTC and 15 December 1998 12UTC.)

11 Figures

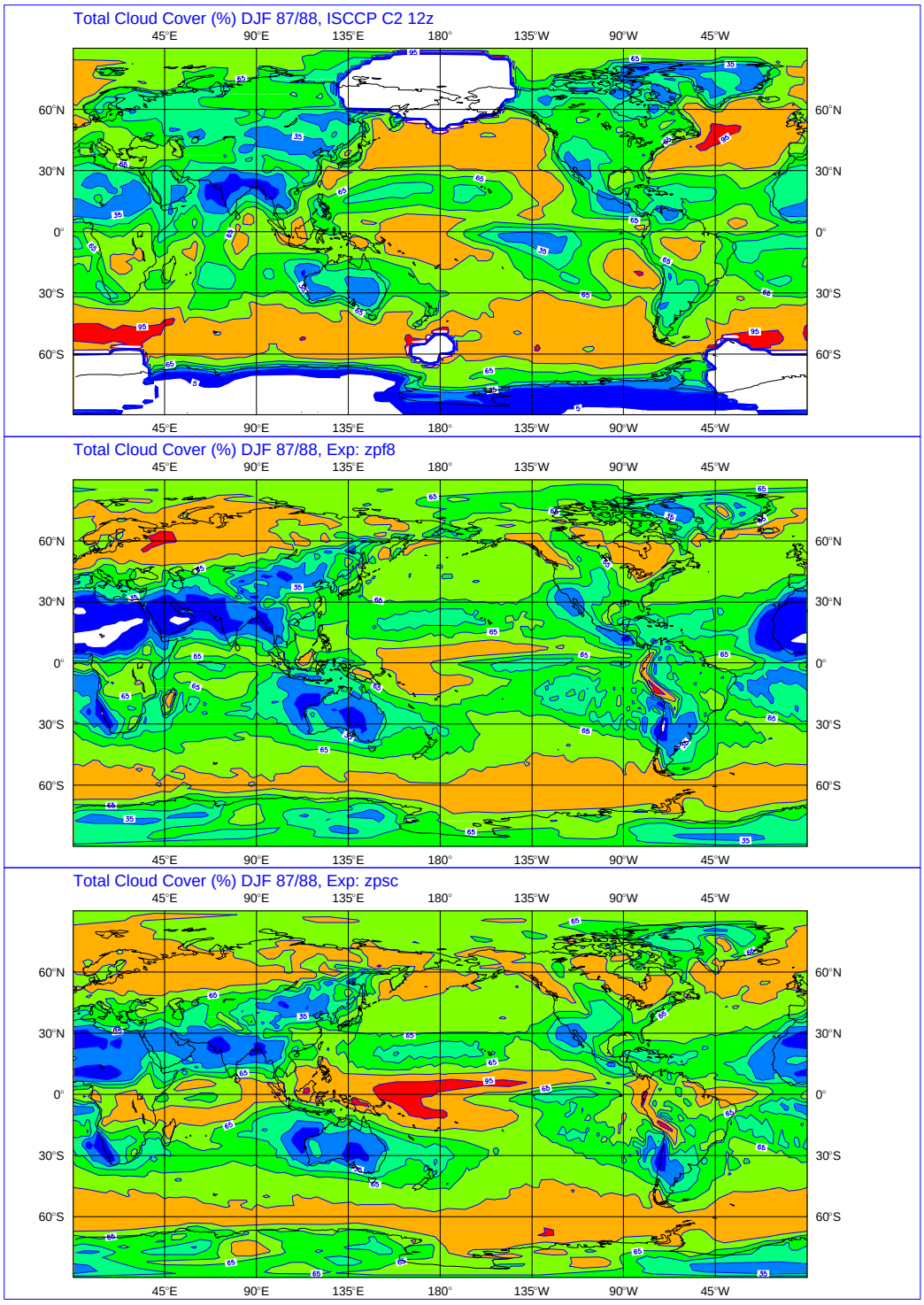

Figure 1: Total cloud cover (%) for December/January/February 1987-88 from T63L31 model simulations: ISCCP climatology (upper), control simulation (middle panel), revised package (lower panel). Model results are an average over an ensemble of three situations. Contours are 5, 20, 35, 50, 65, 80 and 95 %.

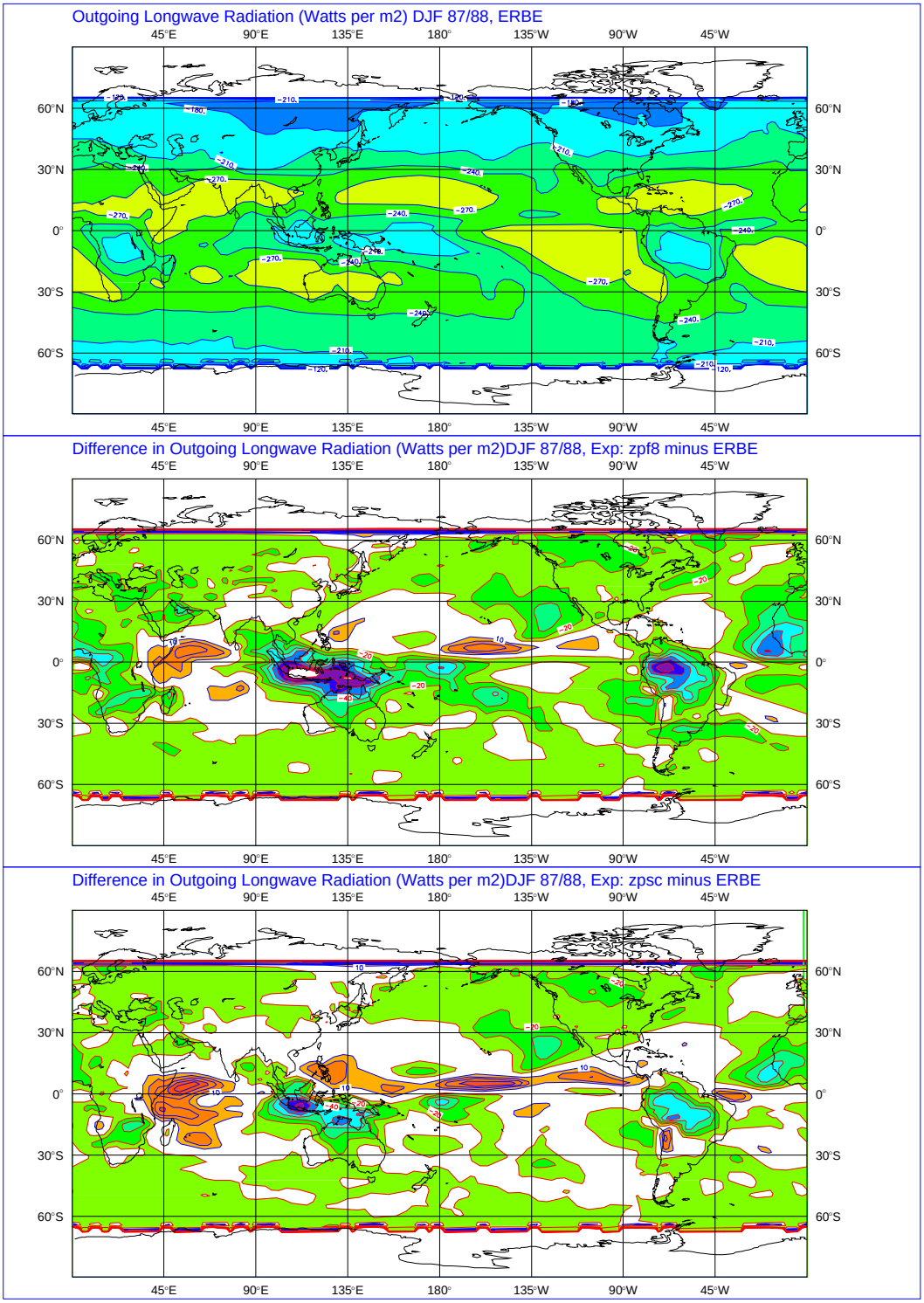

Figure 2: Outgoing Longwave Radiation (OLR - W.m^{-2}) for December/ January/February 1987-88 from ERBE (upper panel) and difference of OLR from T63L31 simulations from ERBE: control simulation (middle panel) and revised physical package (lower panel). Model results are an average over an ensemble of three simulations. On OLR plot, contour interval is 30 W.m^{-2}. On plot differences, contour interval is 10 W.m^{-2}.

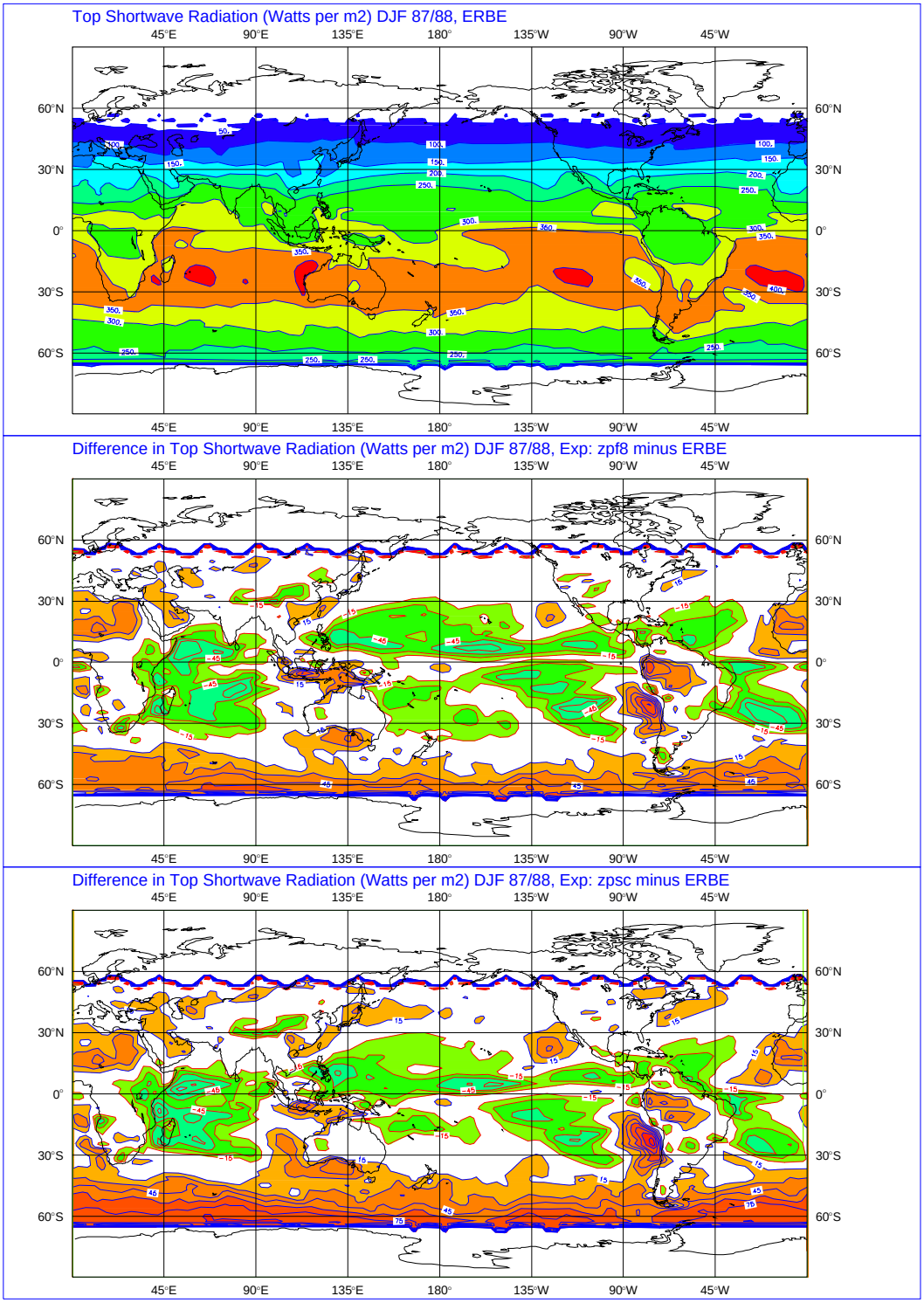

Figure 3: Top of atmosphere absorbed shortwave radiation (ASW - W.m^{-2}) for December/January/-February 1987-88 from ERBE (upper panel) and difference of ASW from T63L31 simulations from ERBE: control simulation (middle panel) and revised physical package (lower panel). Model results are an average over an ensemble of three simulations. On ASW plot, contour interval is 50 W.m^{-2}. On plot differences, contour interval is 15 W.m^{-2}.

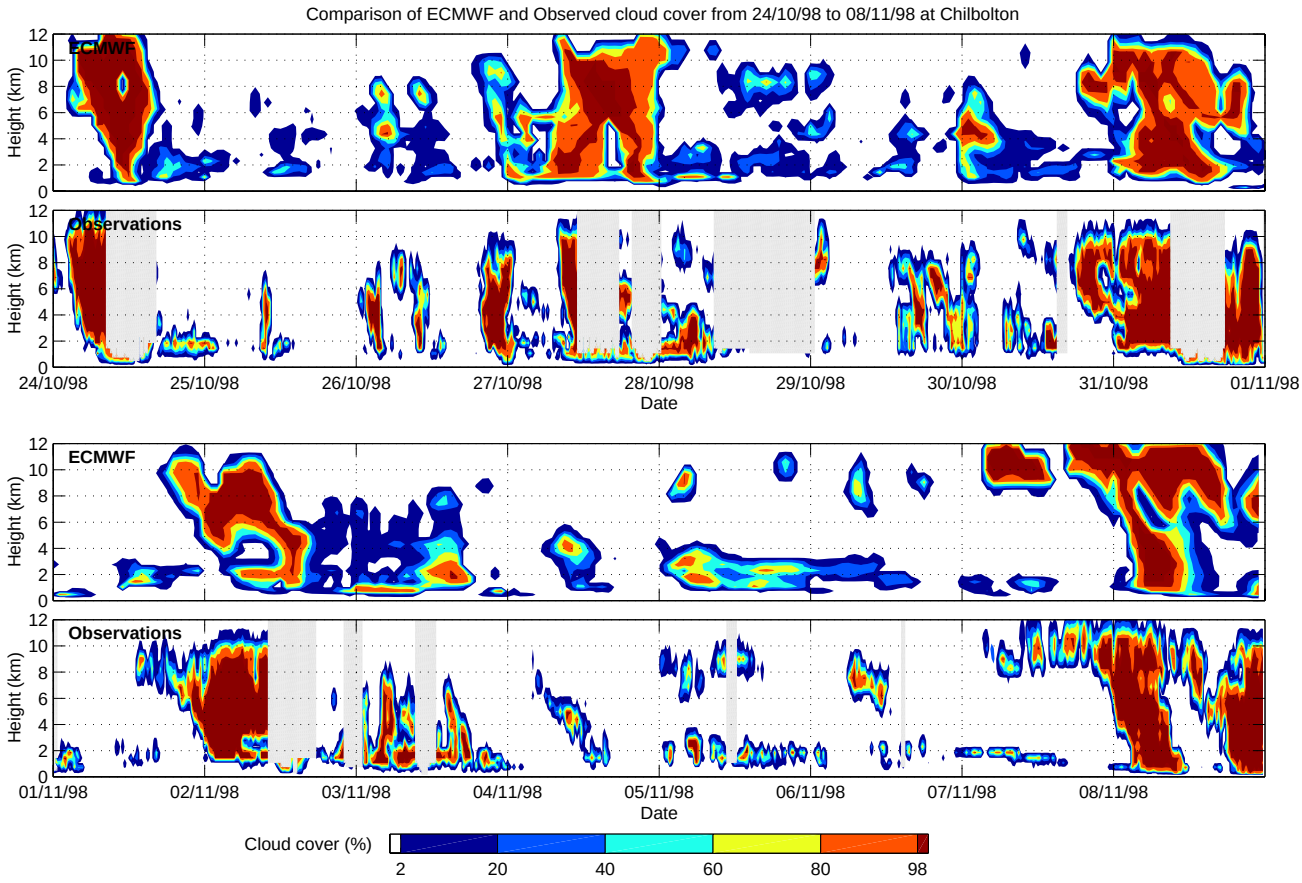

Figure 4: Comparison of ECMWF cloudiness profiles with radar estimates during CLARE experiment (25/10 - 08/11/98).

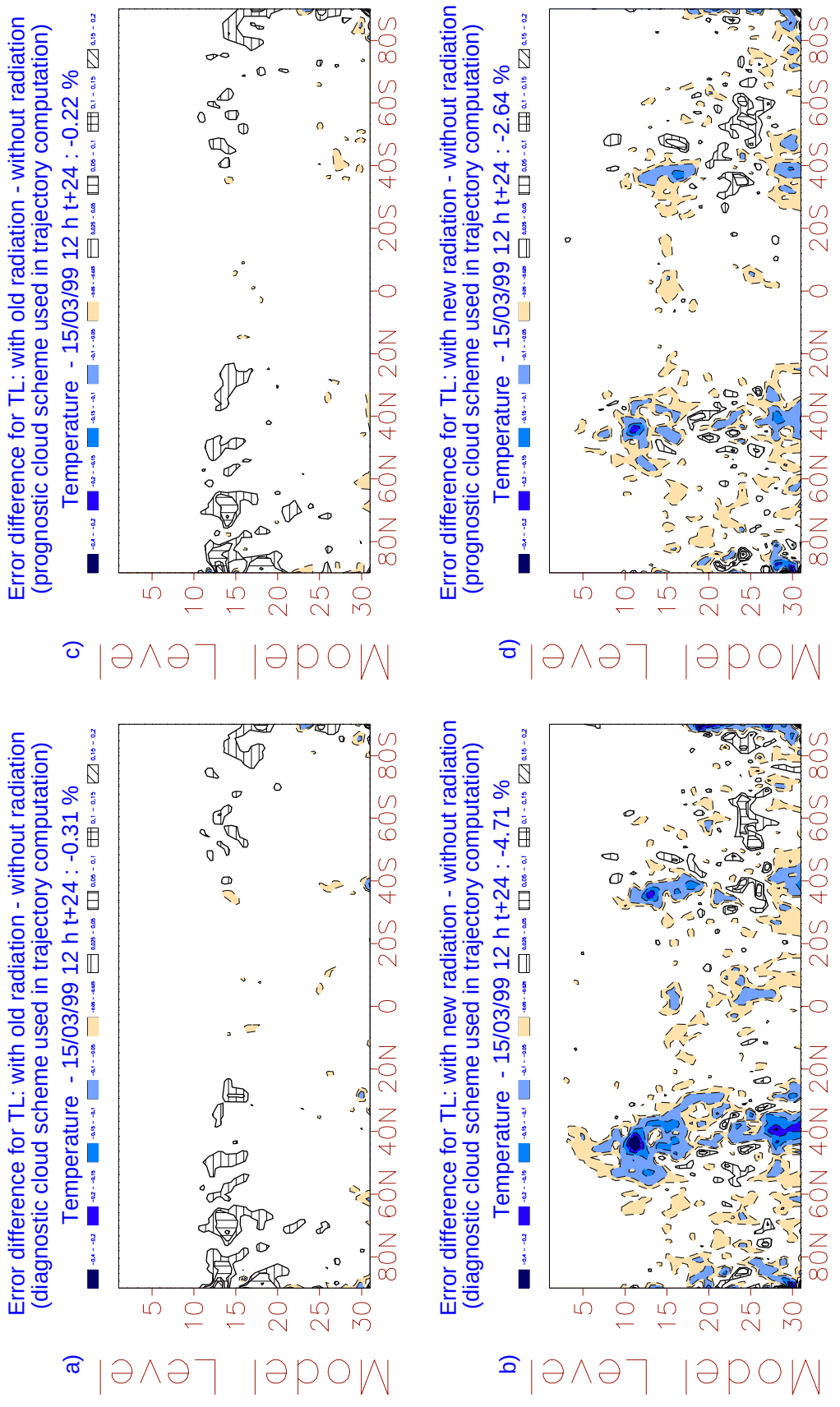

Figure 5: Influence of the different tangent-linear radiation schemes on the evolution of temperature increments with the trajectory computed using either diagnostic cloud scheme (a, b) or prognostic cloud scheme (c,d). Results are presented as the error differences (in terms of fit to the nonlinear model with full physics) between the tangent-linear (TL) model including operational linearized physics (old radiation) and the TL model without any radiation (a, c). (b) and (d) present the same, but for the TL model containing new radiation scheme with the simplified diagnostic cloud scheme. (24-hour forecast for the situation of 15 March 1999 12UTC, units: K)

Figure 5:

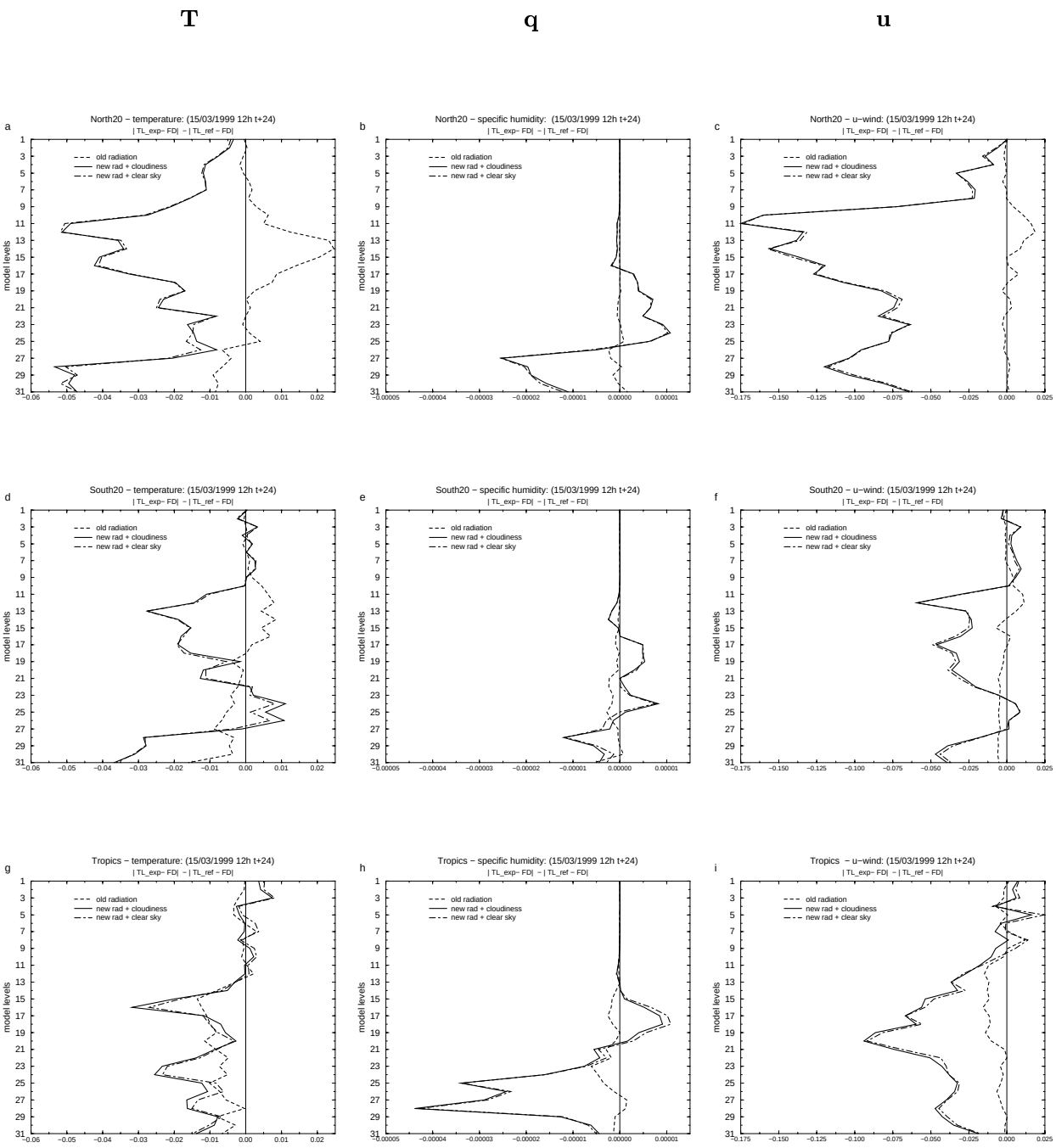

Figure 6: Vertical profiles of the mean values of error differences for temperature (units: K), specific humidity (units; kg kg^{-1}) and u-wind component (units: m s $^{-1}$) from 24-hour integration for North20 (a, b, c), South20 (d, e, f) and Tropics (g, h, i). The results are presented for currently used radiation scheme (dashed line) as well as for the new radiation scheme with cloudiness (solid line) and for clear sky (dot-dashed line). Initial date of the integration: 15 March 1999 12UTC.

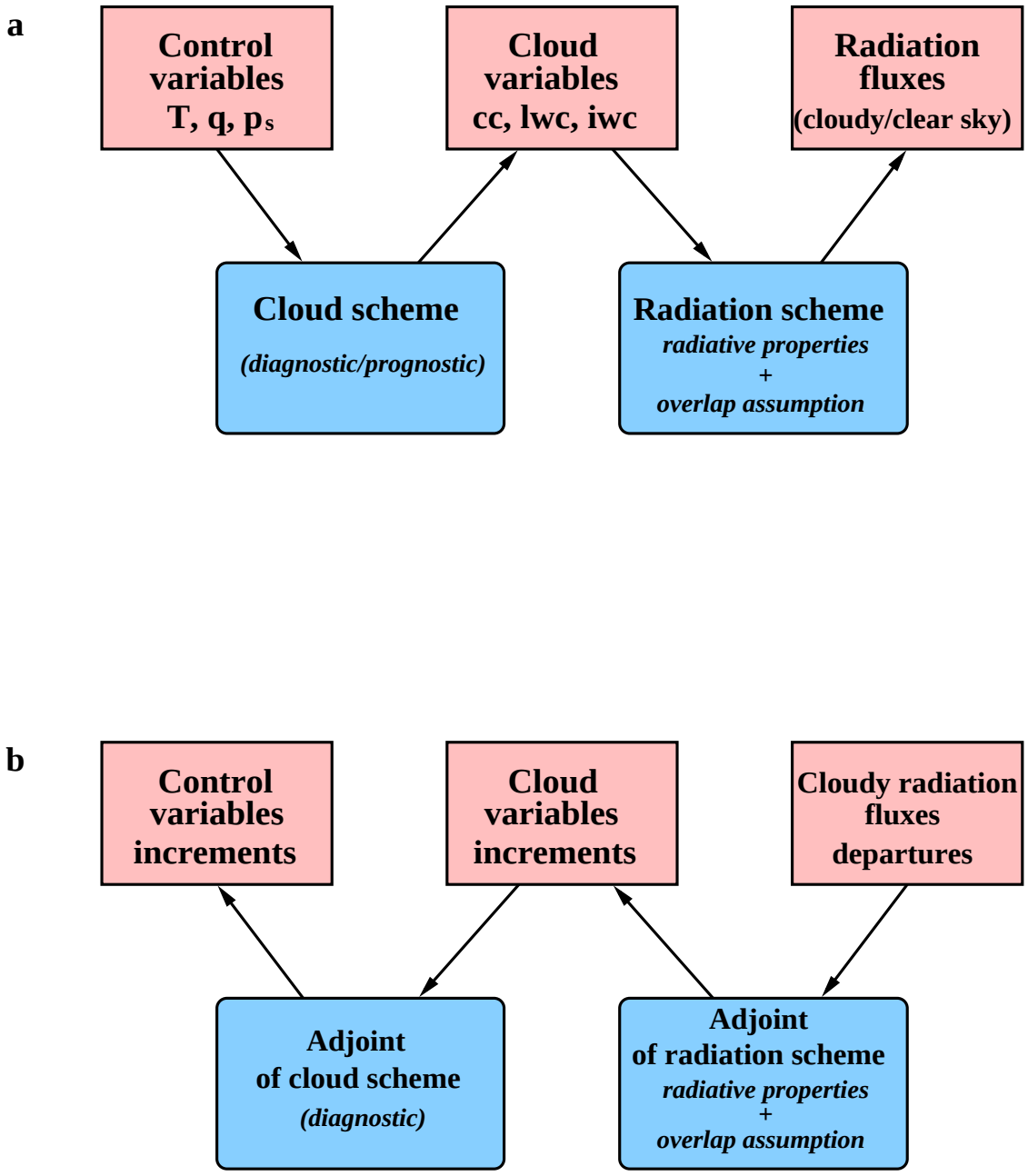

Figure 7: Schematic description of forward modelling of cloudy radiation fluxes (a) and their corresponding adjoint modelling (b).

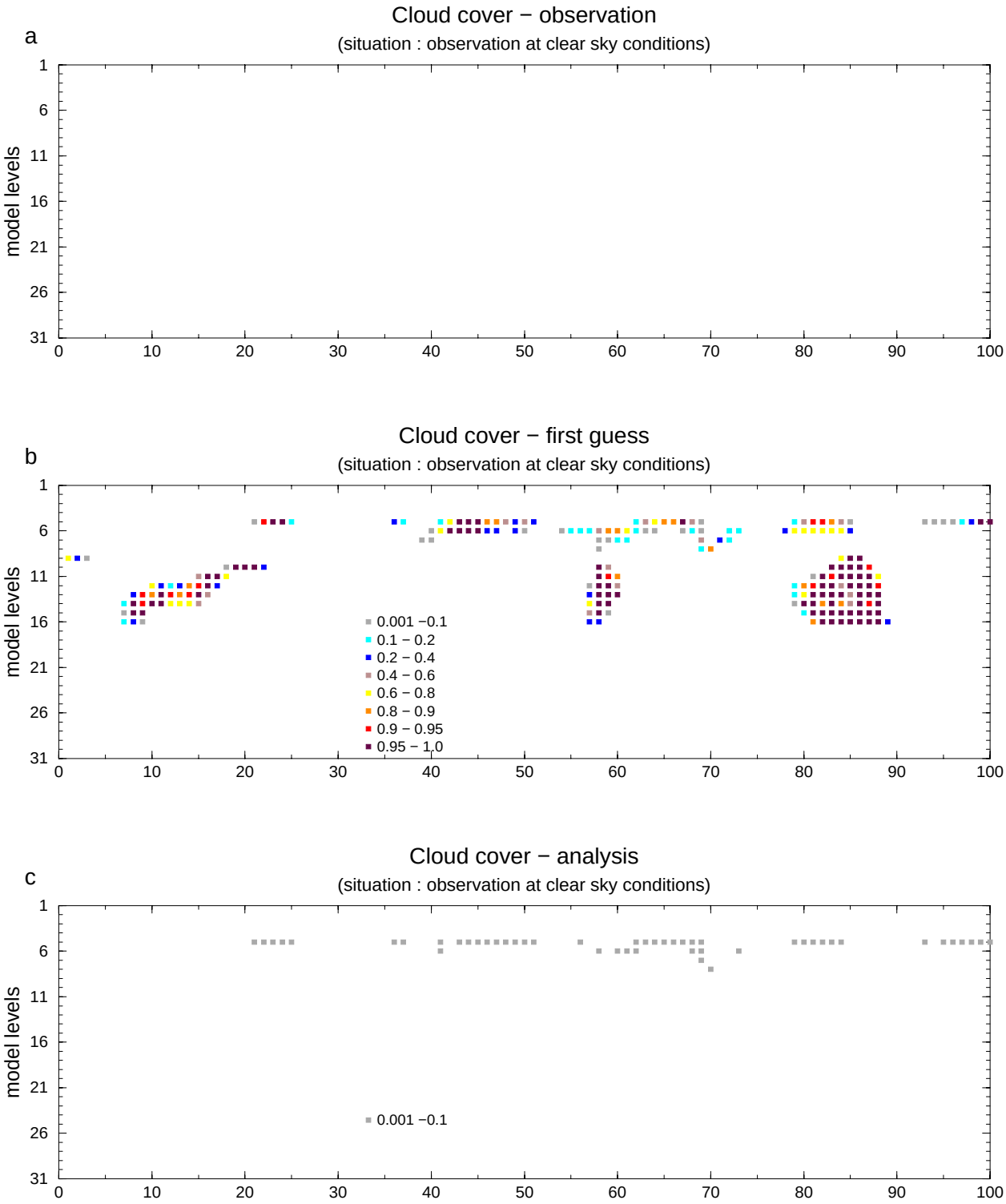

Figure 8: Comparison of the first-guess (b) and analyzed (c) cloud cover to the pseudo-observed cloud cover (a) when using simulated observations. The computations are done for 100 consecutive points and the simulated situation is clear sky one.

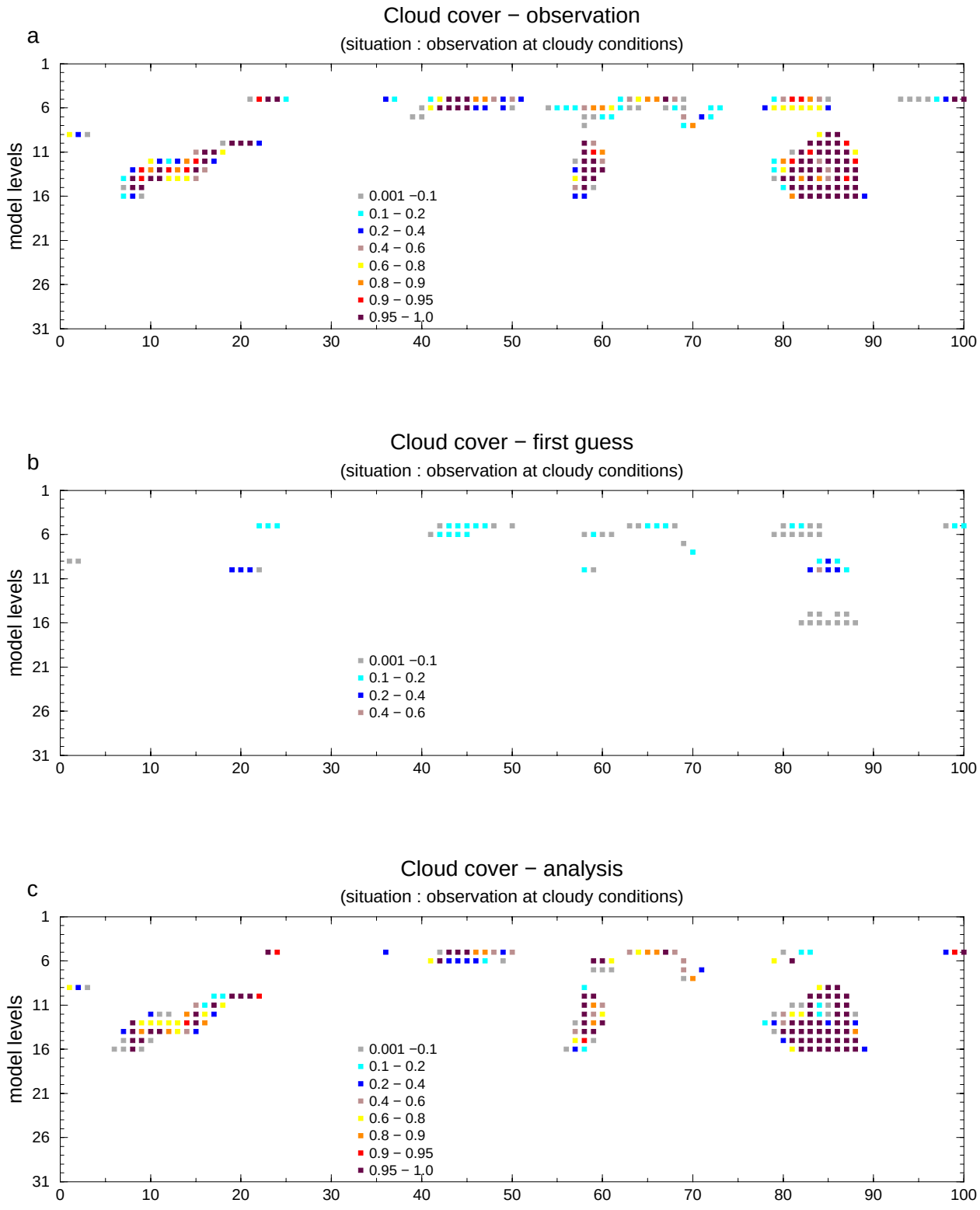

Figure 9: The same as in Fig: 8, but for cloudy situation.

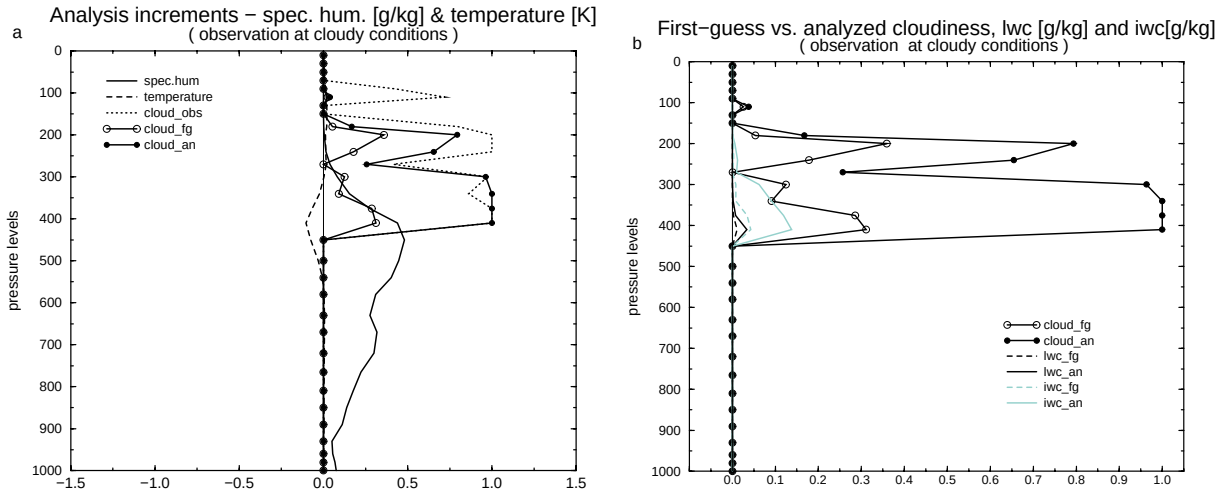

		LWDs	LWUPtoa	SWDs
obs	:	422.72 W.m^{-2}	-181.62 W.m^{-2}	227.68 W.m^{-2}
fg	:	409.49 W.m^{-2}	-242.15 W.m^{-2}	409.87 W.m^{-2}
anal	:	423.23 W.m^{-2}	-183.94 W.m^{-2}	227.52 W.m^{-2}

Figure 10: 1D-Var ability to increase/create clouds. (a) Analysis increments for specific humidity (solid line) and temperature (dashed line) together with the cloud profiles (observed - dotted line, first-guess - solid line with empty circles and analyzed - solid line with filled circles). (b) Cloud liquid water content (first-guess - black dashed line, analysis - black solid line) and cloud ice water content (grey lines). Values of observed, first-guess and analyzed radiation fluxes are also given.

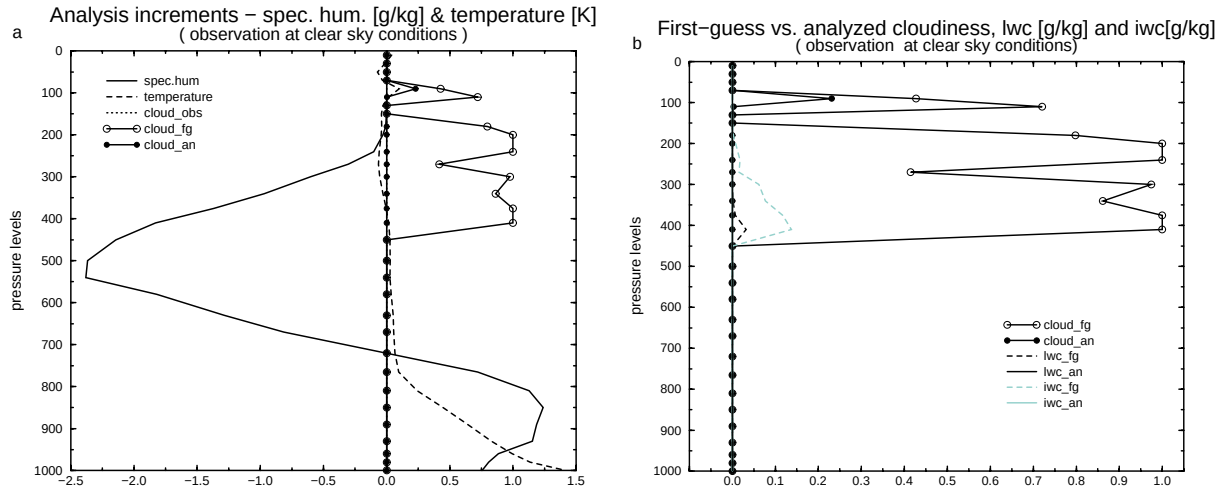

		LWDs	LWUPtoa	SWDs
obs	:	413.82 W.m^{-2}	-281.04 W.m^{-2}	493.17 W.m^{-2}
fg	:	422.48 W.m^{-2}	-182.52 W.m^{-2}	228.49 W.m^{-2}
anal	:	412.20 W.m^{-2}	-278.41 W.m^{-2}	493.23 W.m^{-2}

Figure 11: Same as Fig. 10, but for 1D-Var ability to remove clouds.

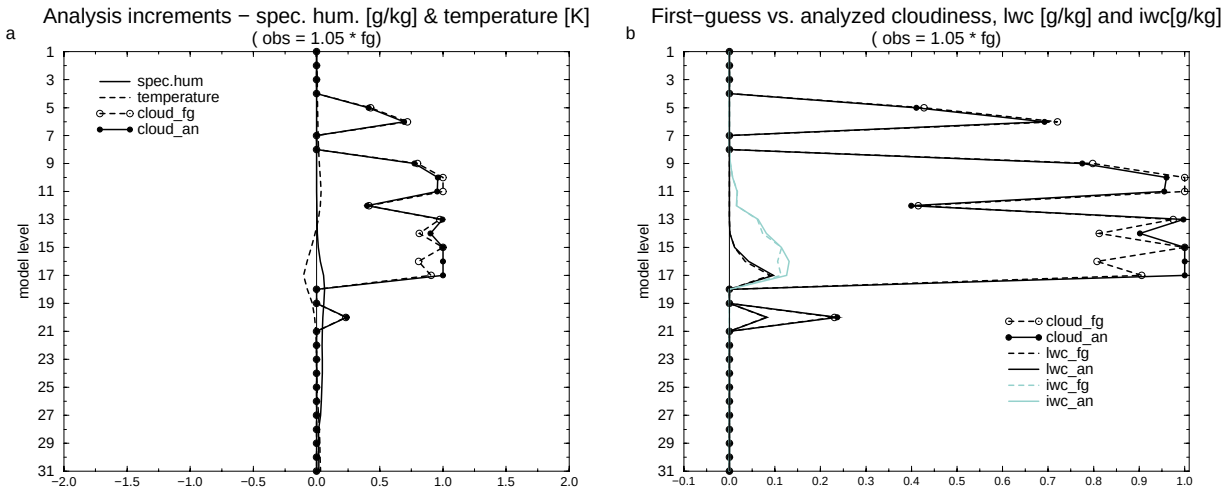

LWDs

obs : 444.67 W.m^{-2}

fg : 424.06 W.m^{-2}

anal : 425.61 W.m^{-2}

Figure 12: Same as Fig. 10, but for a potential problem of 1D-Var to trigger new clouds. The simulated observation of longwave downward radiation flux at the surface (LWDs) was only used in the experiment.

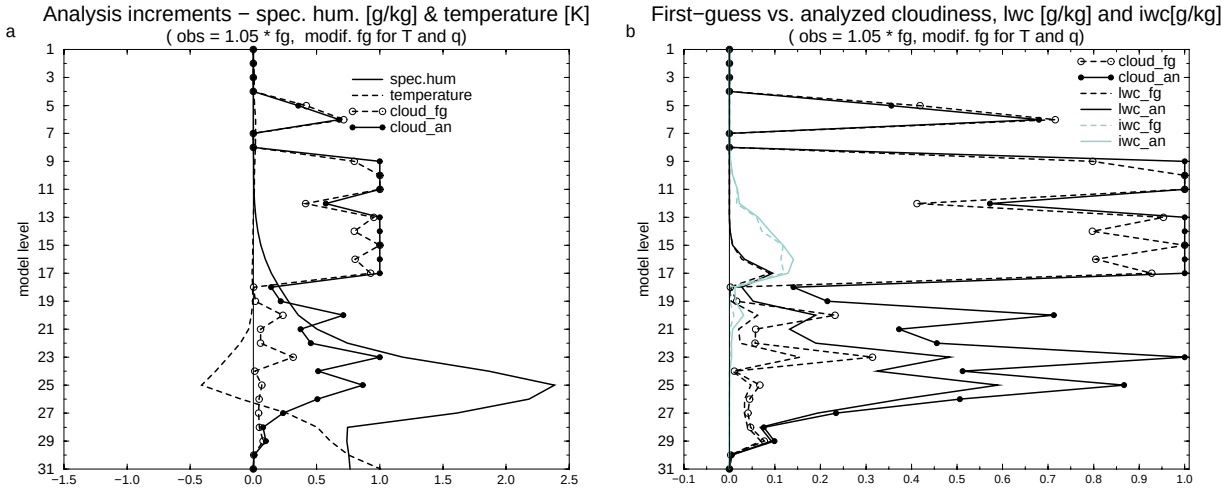

LWDs

obs : 444.67 W.m^{-2}

fg : 424.10 W.m^{-2}

anal : 442.91 W.m^{-2}

Figure 13: Same as Fig. 12, but when adding small amount of clouds below existing ones.

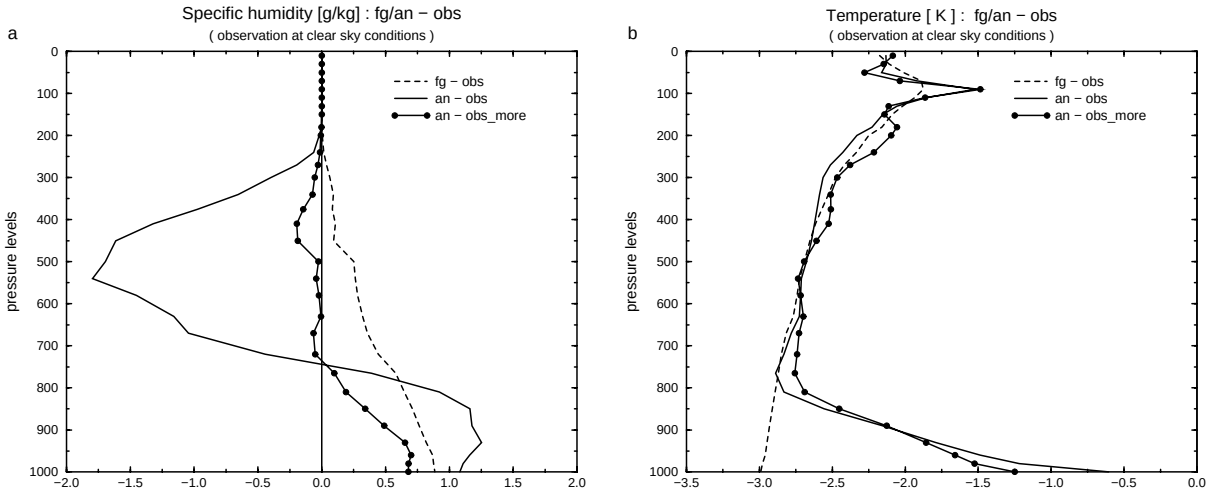

Figure 14: Comparisons of the first-guess (dashed line) and analyzed (solid line) vertical profiles of specific humidity (a) and temperature (b) against observations corresponding to the situation presented in Fig. 11. The differences between improved analysis and observations when using observations on vertical levels for temperature and humidity are presented as solid line with symbols.

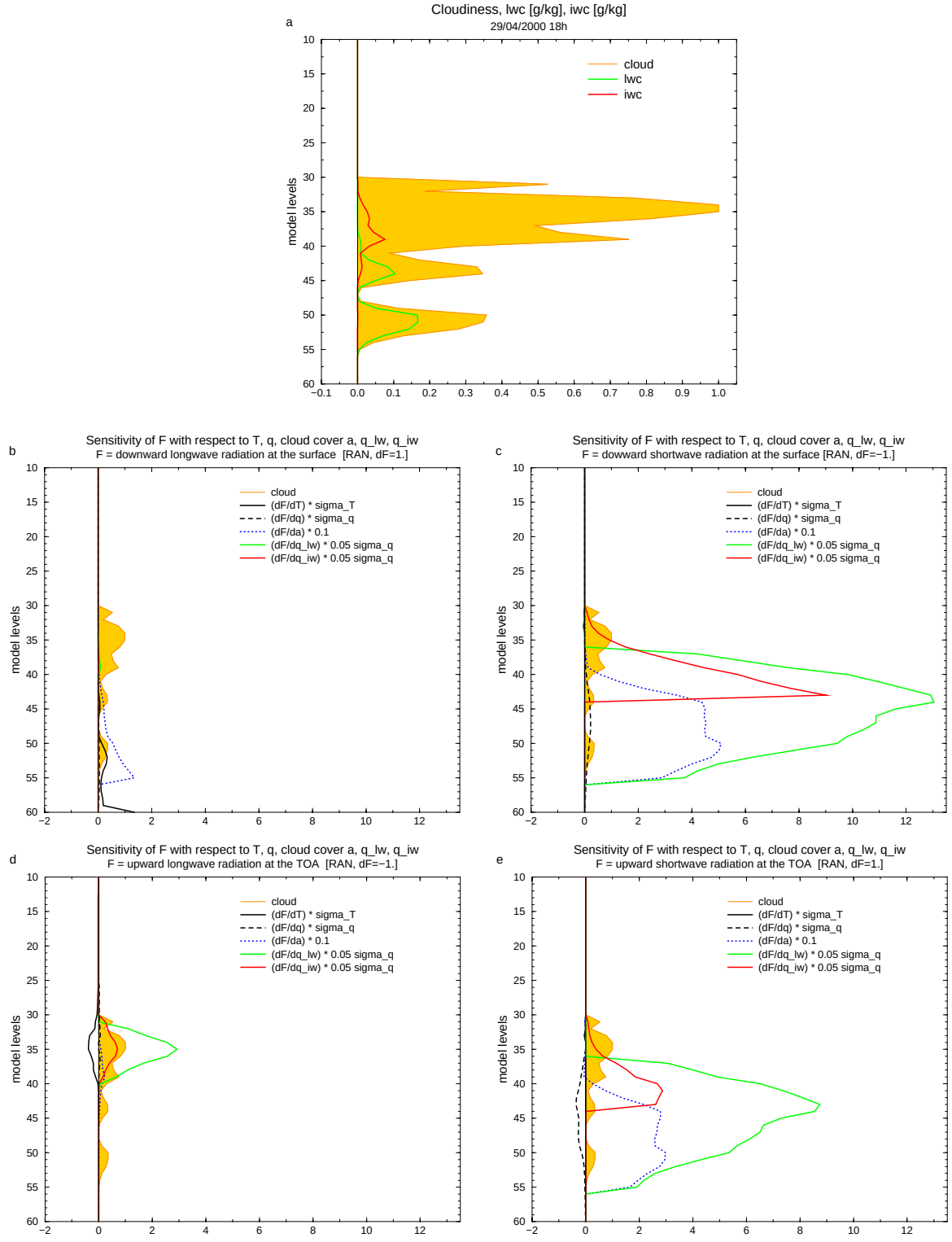

Figure 15: Sensitivity of the radiation fluxes with respect to temperature T, specific humidity q, cloud cover a, liquid water content q_{lw} and ice water content q_{iw}. The computation is done for the cloud type displayed in (a) and for solar zenith angle $cos\theta = 0.93$. The results are presented for the downward longwave (b) and shortwave (c) radiation fluxes at the surface, as well as for the upward longwave (d) and shortwave (e) radiation fluxes at the top of atmosphere.

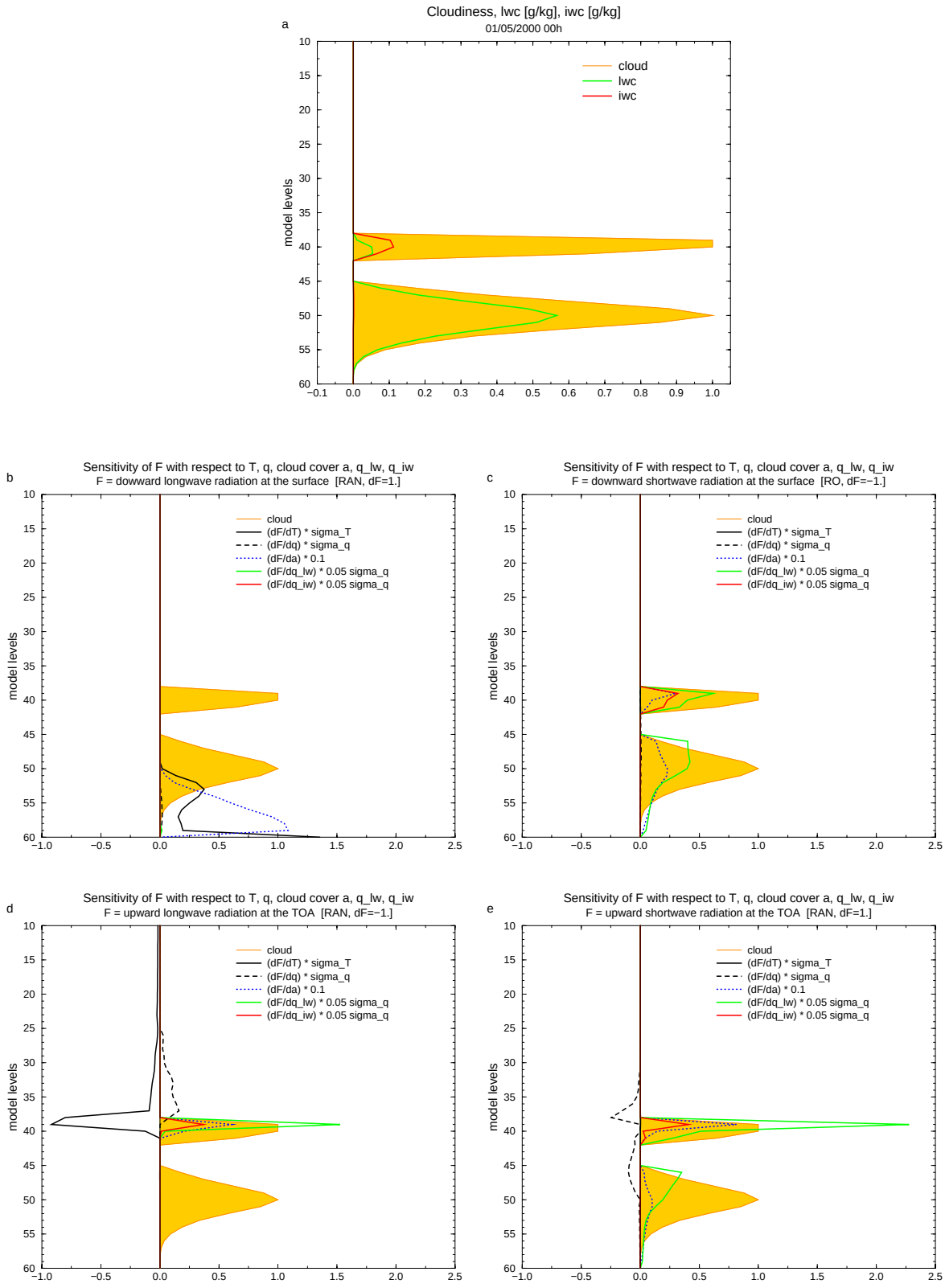

Figure 16: Same as Fig. 15, but for the different cloud cover and for solar zenith angle $cos\theta = 0.25$.

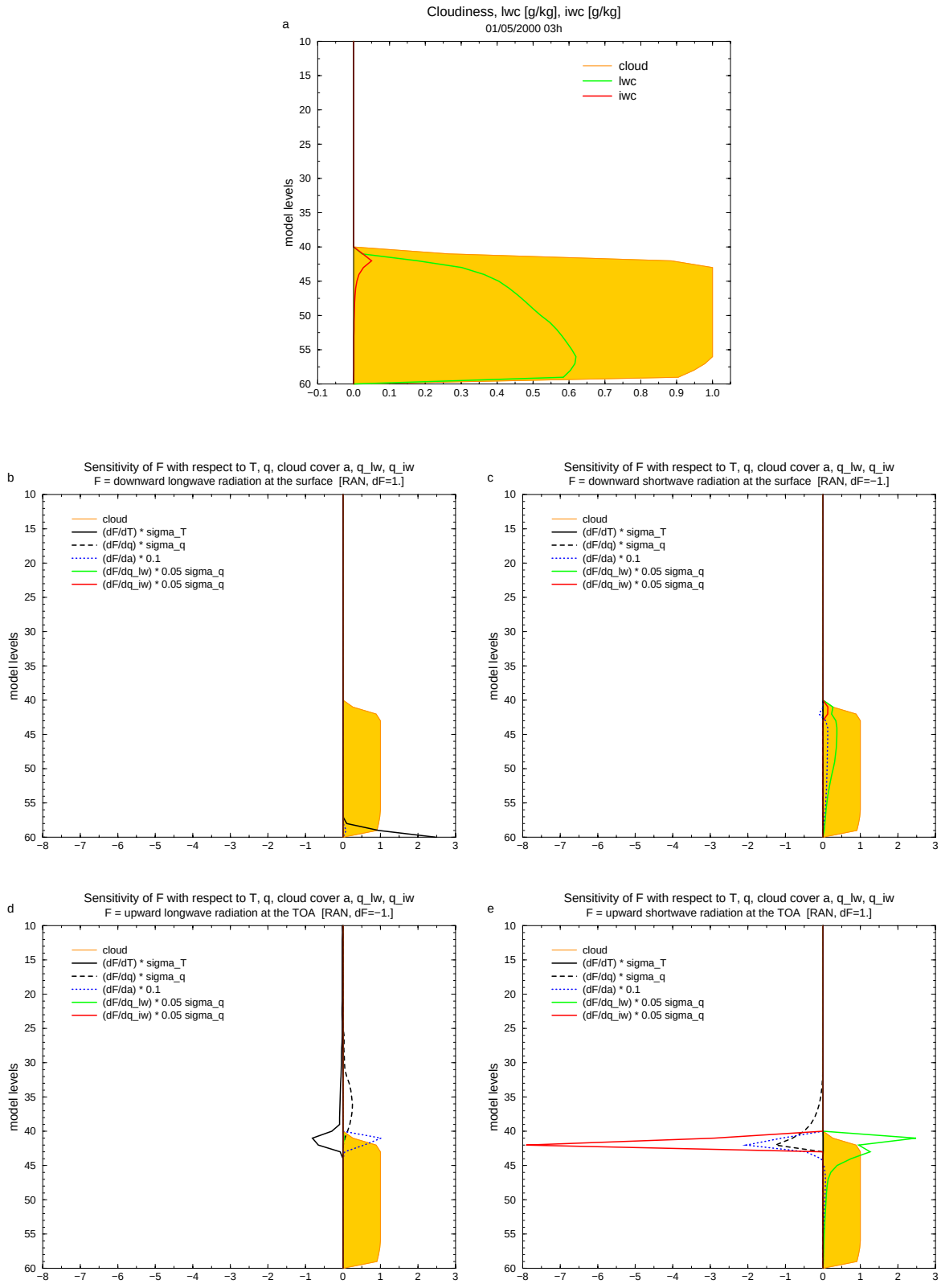

Figure 17: Same as Fig. 15, but for the different cloud cover.

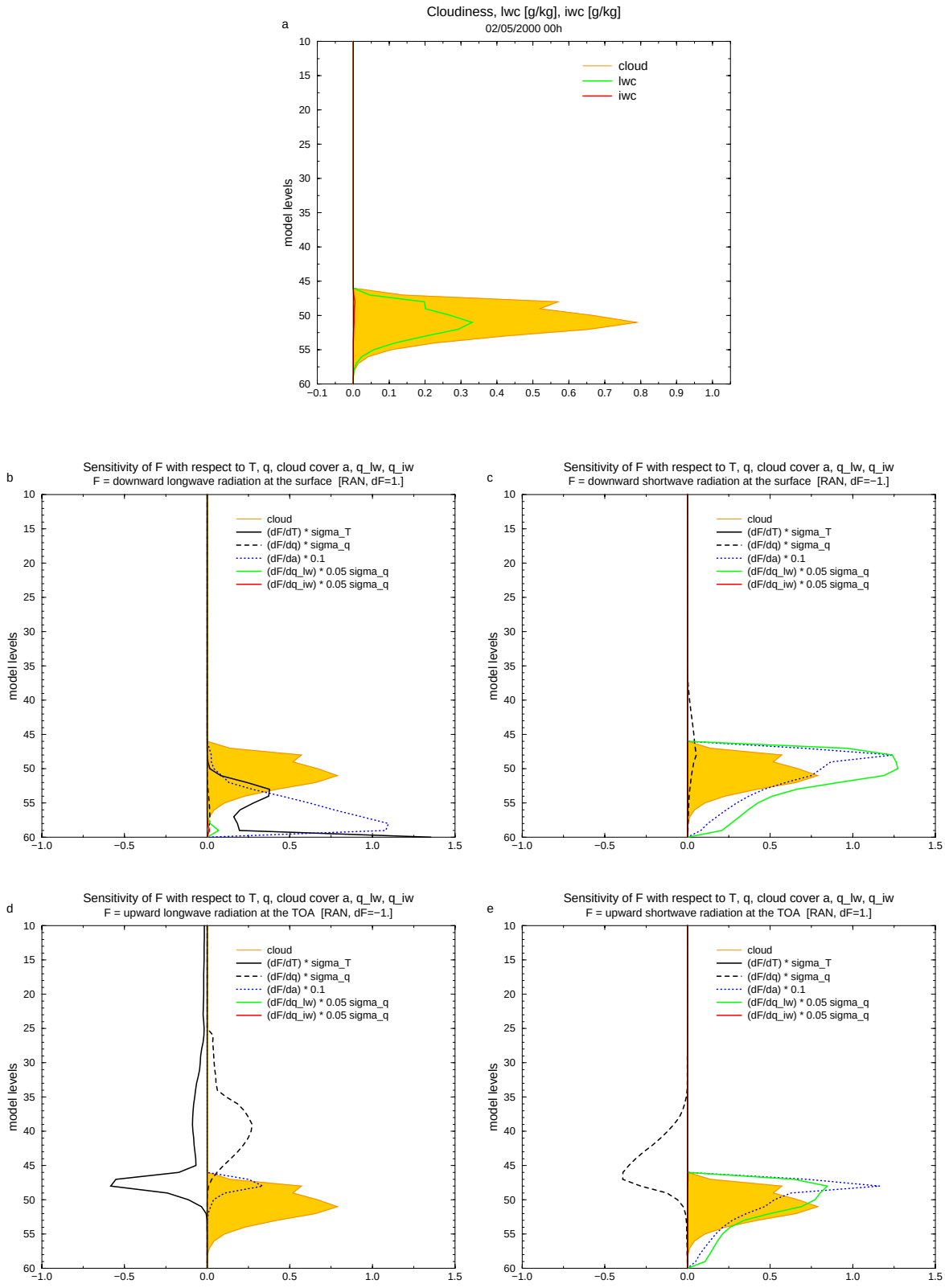

Figure 18: Same as Fig. 15, but for the different cloud cover and for solar zenith angle $cos\theta = 0.25$.

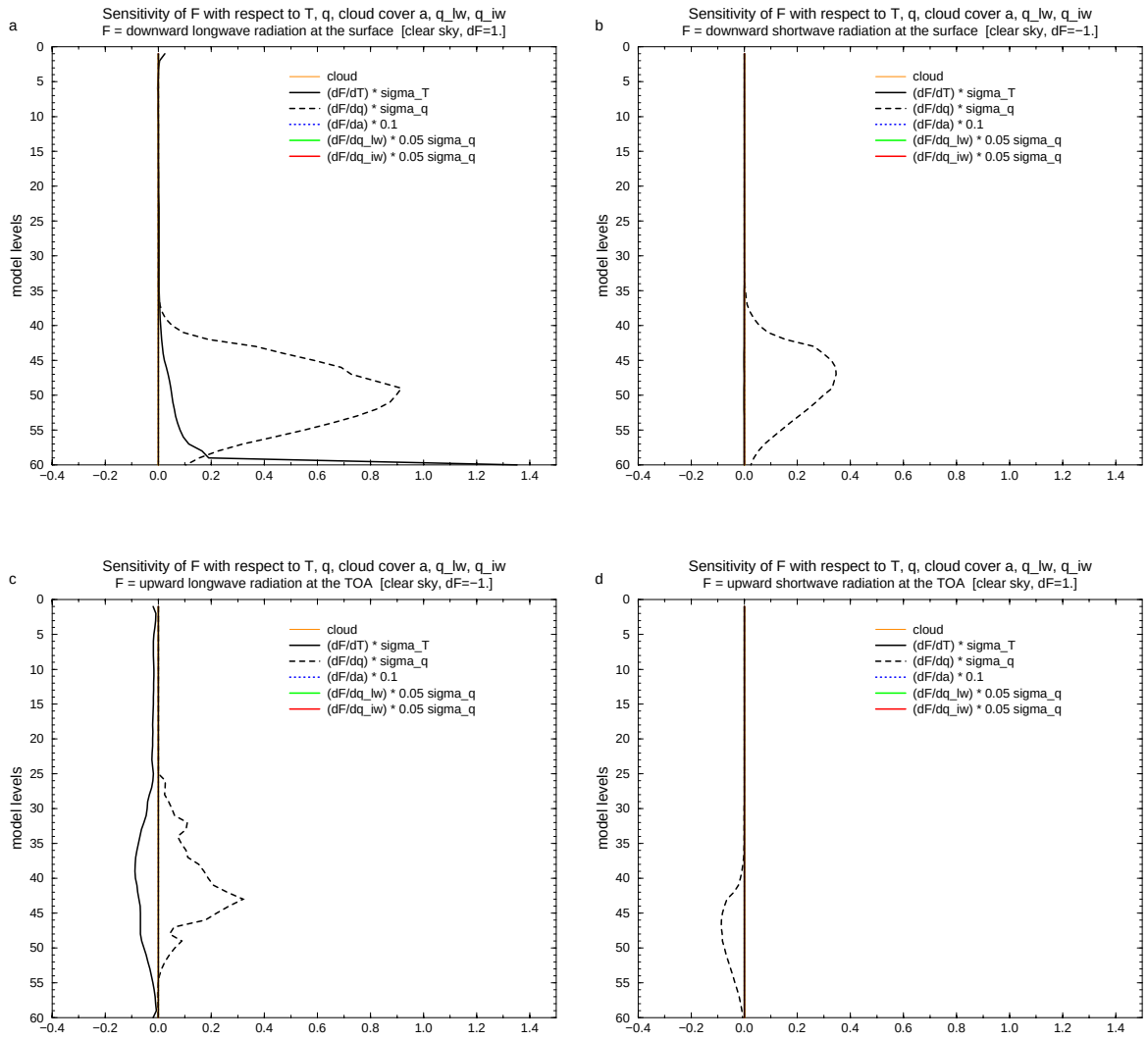

Figure 19: Same as Fig. 15, but for clear sky and for solar zenith angle $cos\theta = 0.25$.

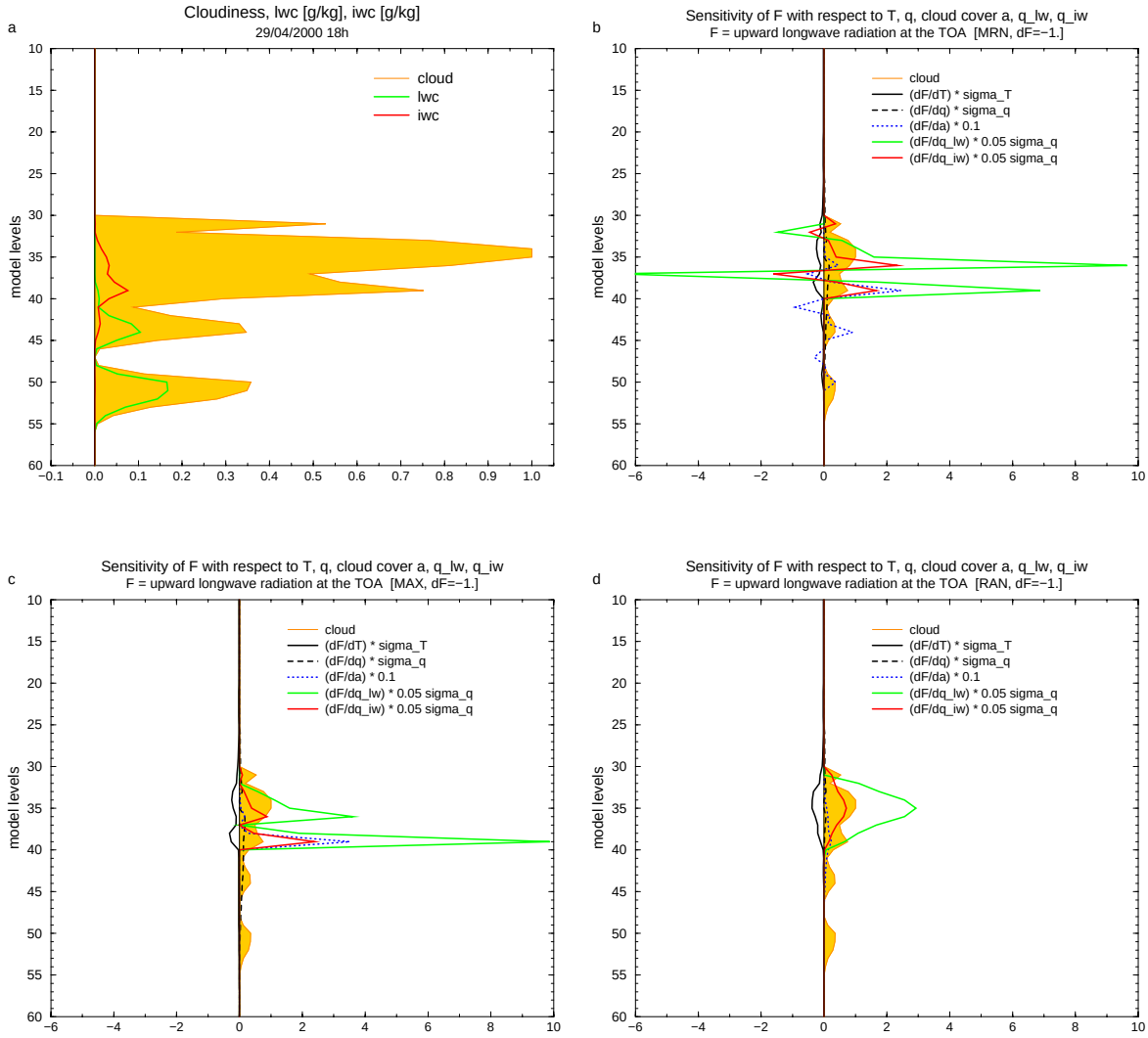

Figure 20: Same as Fig. 15, but the results are shown for the upward longwave radiation at the top of atmosphere using different cloud overlap assumptions: (b) maximum-random, (c) maximum and (d) random.

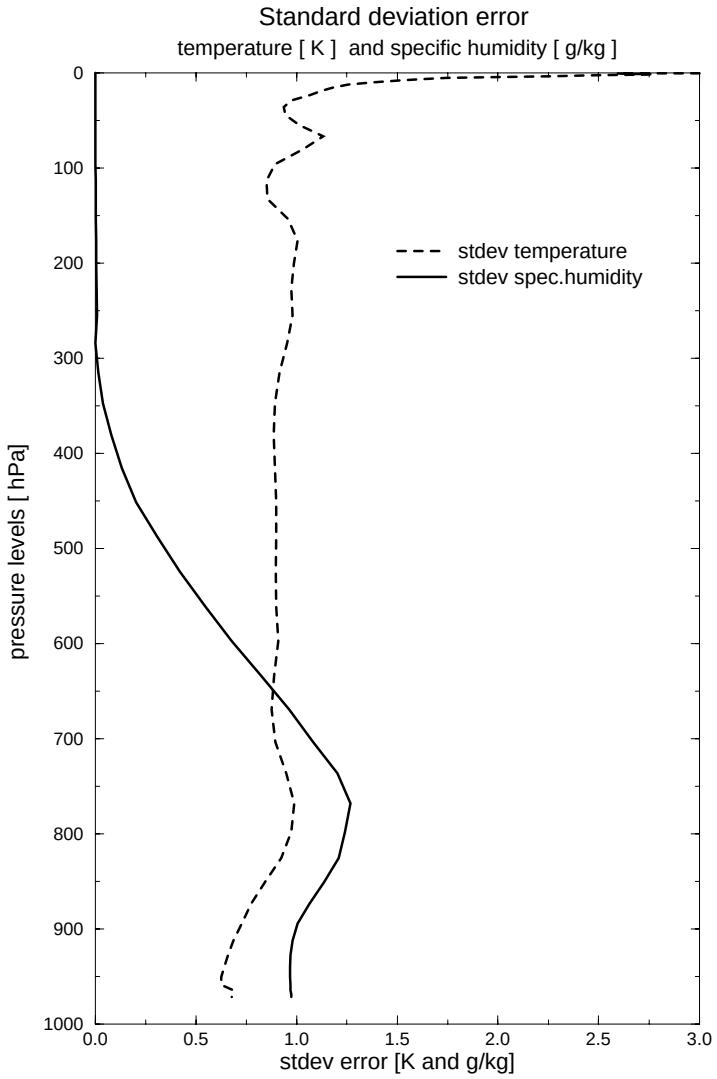

Figure 21: ECMWF background-error standard deviation for temperature (dashed line) and specific humidity (solid line).

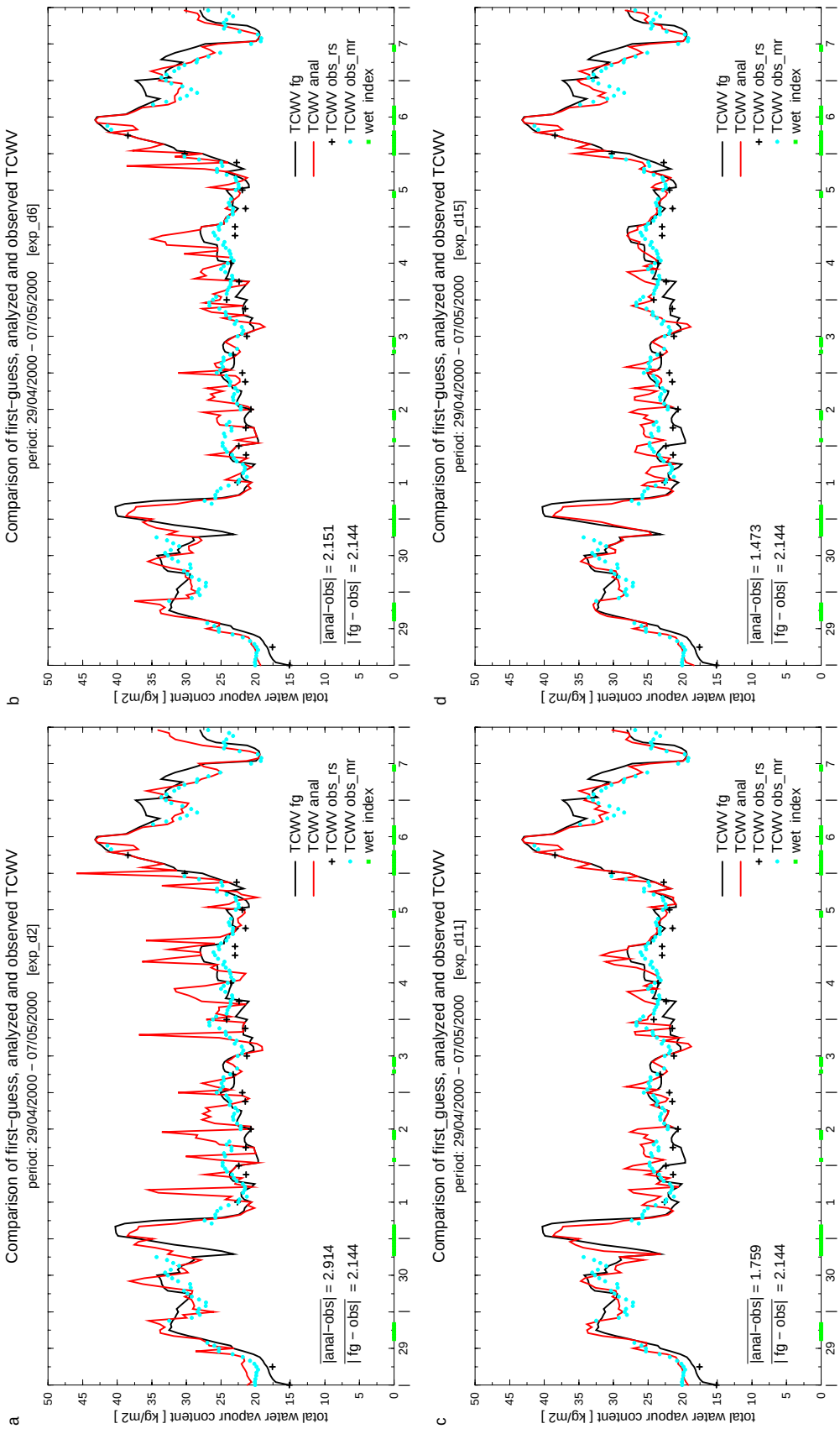

Figure 22: Comparison of the first guess and analysis against the observations (obs_rs - radiasonde, obs_mr - microwave) of the total column water vapour (units: $kg.m^{-2}$) over the ARM-SGP site in the period from 29 April to 7 May 2000. Hourly results are displayed for four different 1D-Var experiments explained in the text. Values of absolute mean differences between analysis and observations (obs_mr), as well as between the first guess and observations for the whole period are also given. x-axis indicates the days of experiment.

Figure 22:

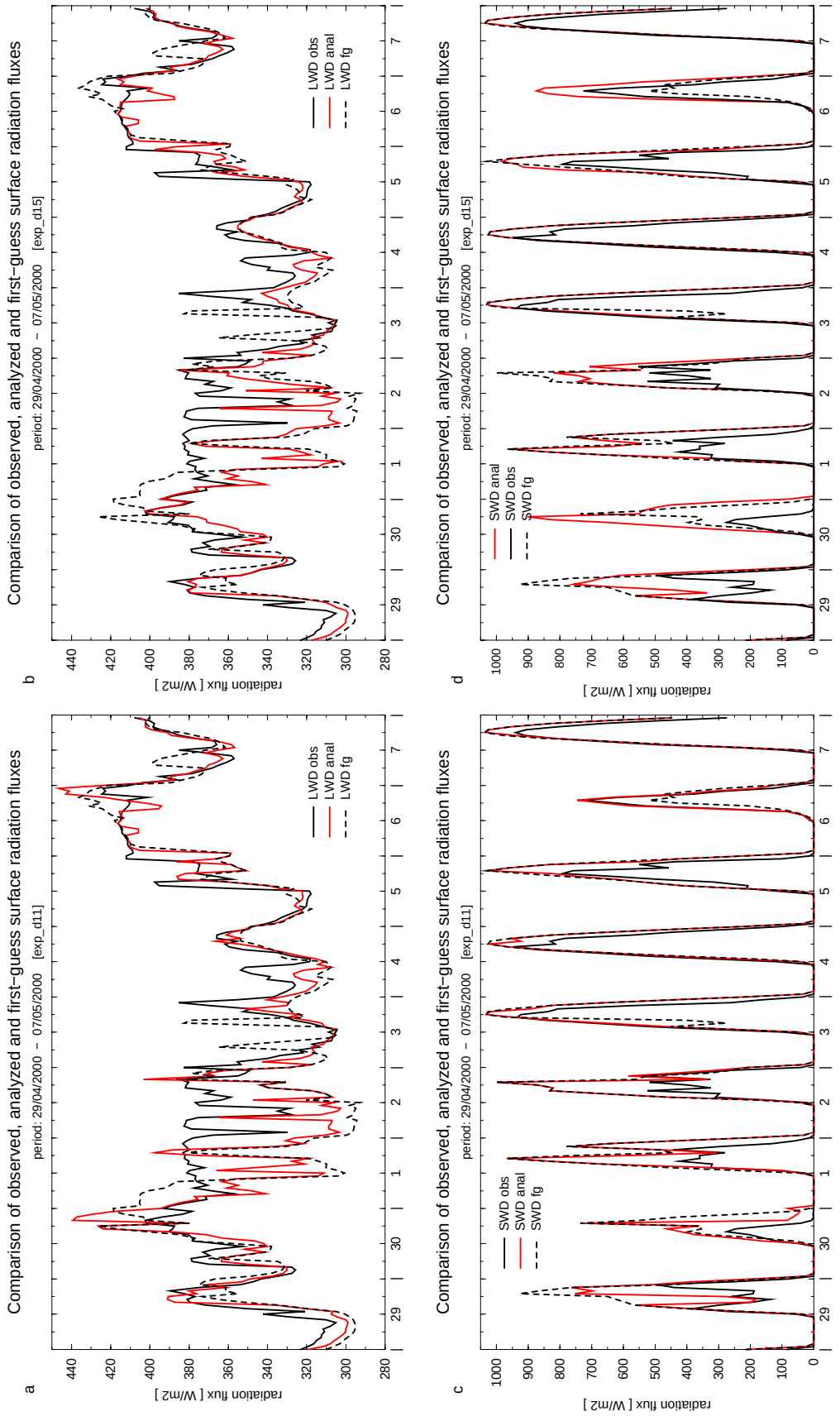

Figure 23: Comparison of the first guess and analysis against the observations of the downward longwave radiation at the surface (a, b) and downward shortwave radiation at the surface (c, d). (a) and (c) show the results from 1D-Var experiment when the downward shortwave radiation (SWD) observation at the surface is assimilated (exp_d11). (b) and (d) are the results from the experiment without assimilating this SWD observation (exp_d15).

Figure 23:

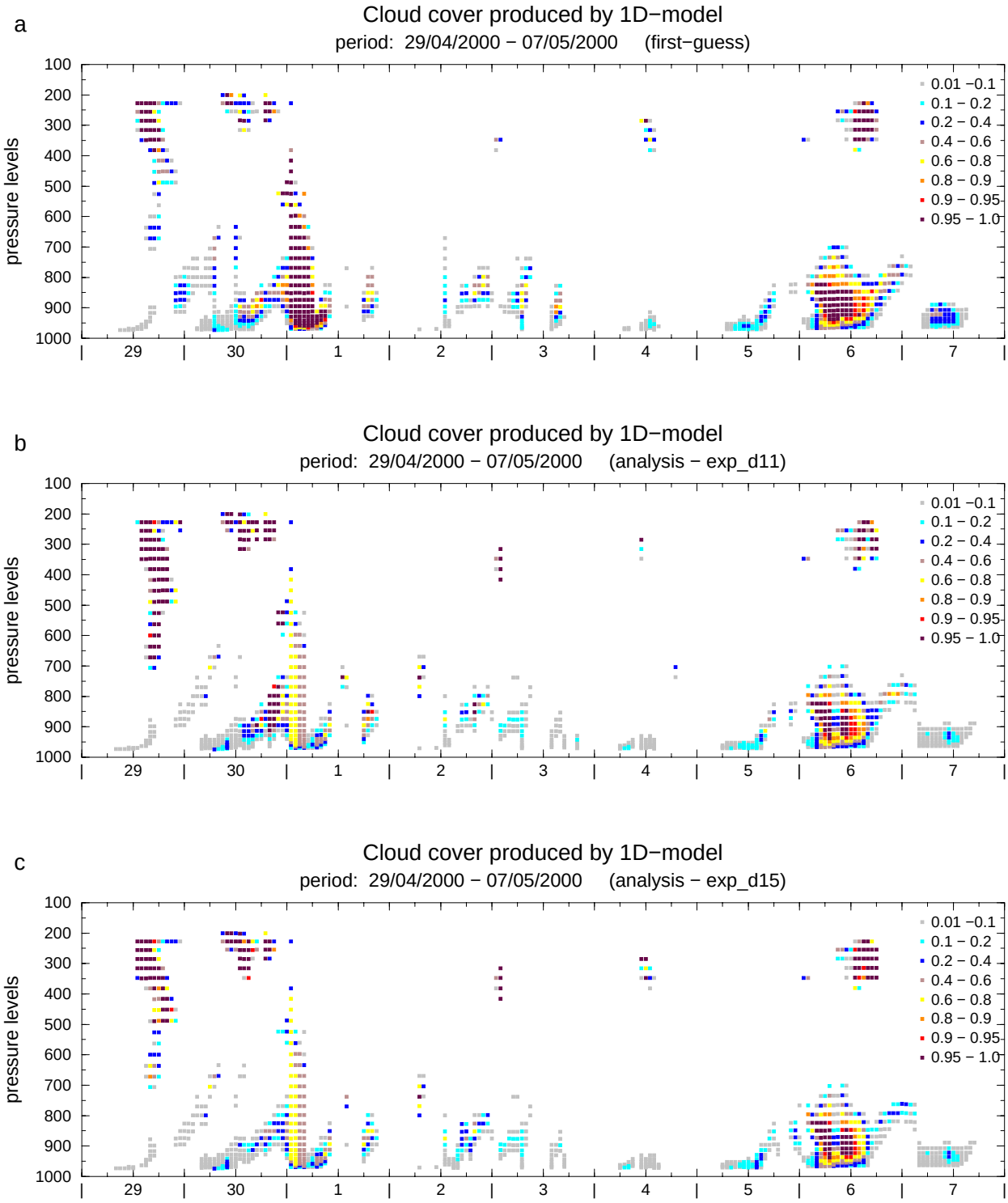

Figure 24: Comparison of the first-guess (a) and analyzed cloud cover (b, c) for the period from 29 April to 7 May 2000 at ARM-SGP side. (b) is analyzed cloud cover obtained when using the shortwave (SW) radiation observation in 1D-Var computations (exp_d11). (c) is the cloud cover from the run without SW radiation observation (exp_d15).

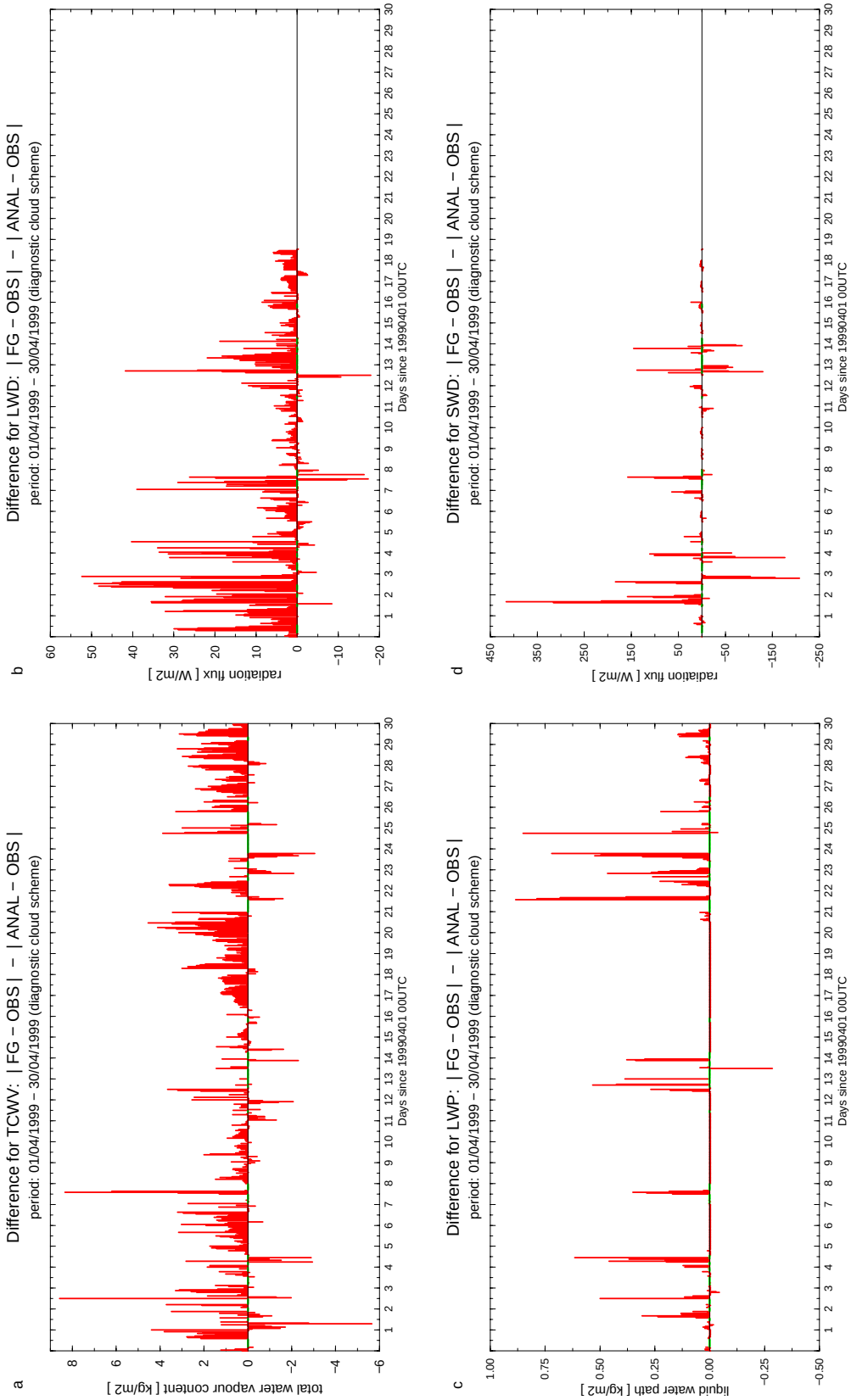

Figure 25: Improvement/deterioration of the analysis with respect to the first guess after 1D-Var assimilation using observations of the downward longwave radiation at the surface, the total column water vapour and the liquid water path over the ARM-SGP site in April 1999. The results are presented as differences between absolute value of the first guess minus observation and absolute value of the analysis minus observation for the total column water vapour (a), the downward longwave radiation at the surface (b), the liquid water path (c) and the downward shortwave radiation at the surface (d).

Figure 25:

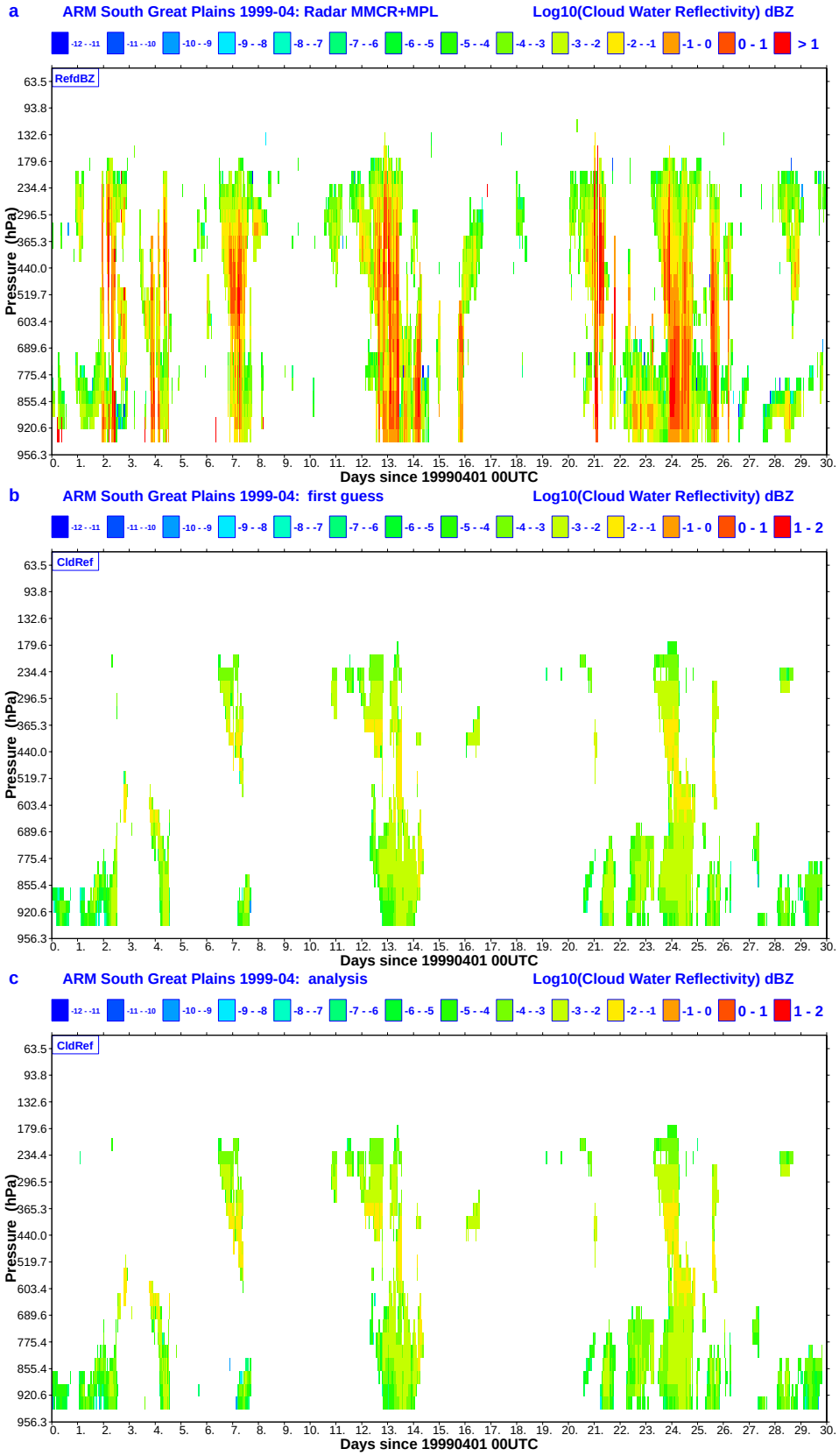

Figure 26: The radar reflectivity measured at the ARM-SGP site in April 1999 (a) and the pseudo-radar reflectivity computed from the first guess data (b) and from the analysis (c).

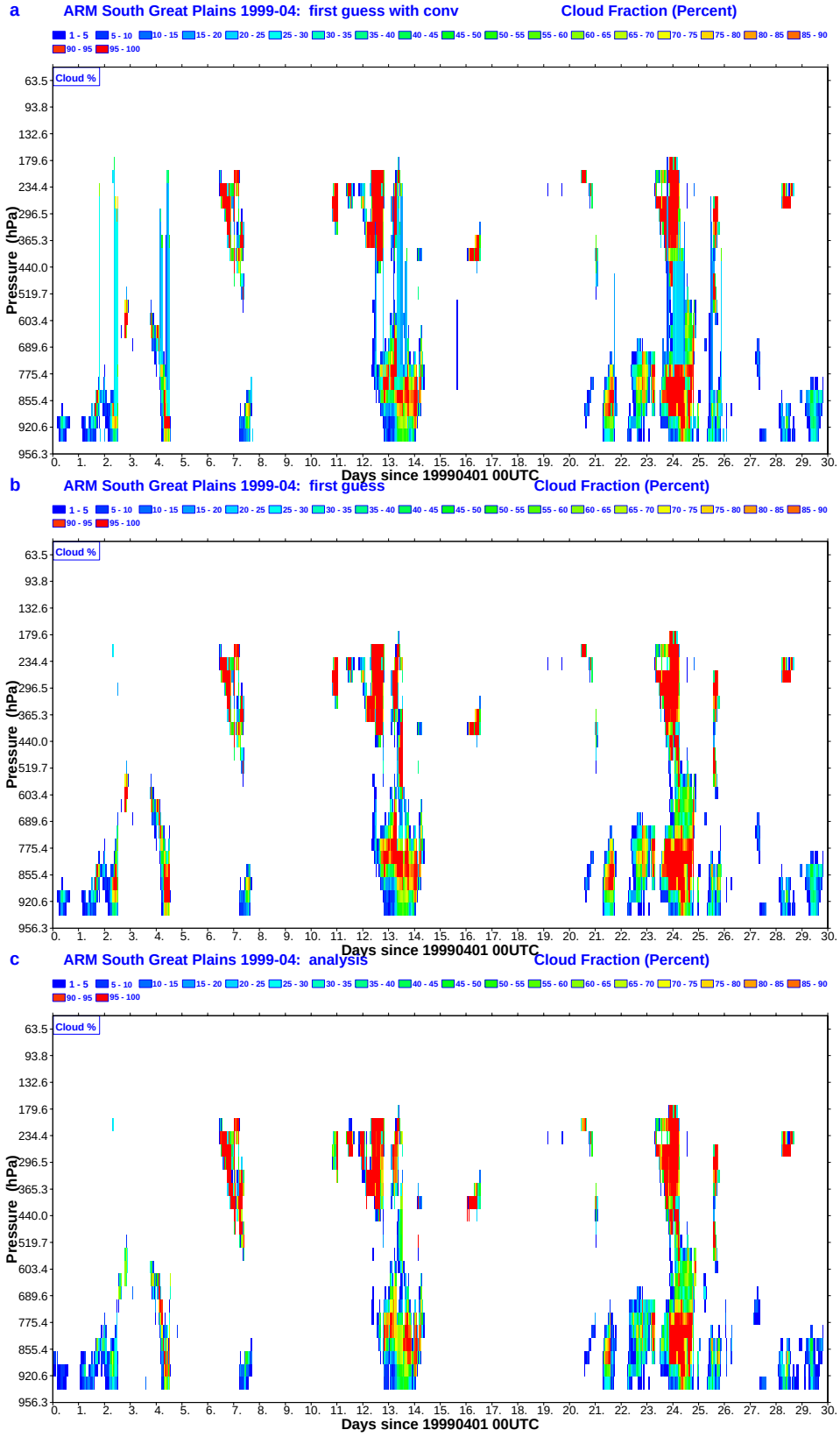

Figure 27: Time series of the cloud cover (%) from the first guess obtained using the diagnostic cloud scheme taking into account convective precipitation (a), from the first guess without convective precipitation in the diagnostic cloud scheme used in 1D-Var experiment (b) and from the analysis (c).

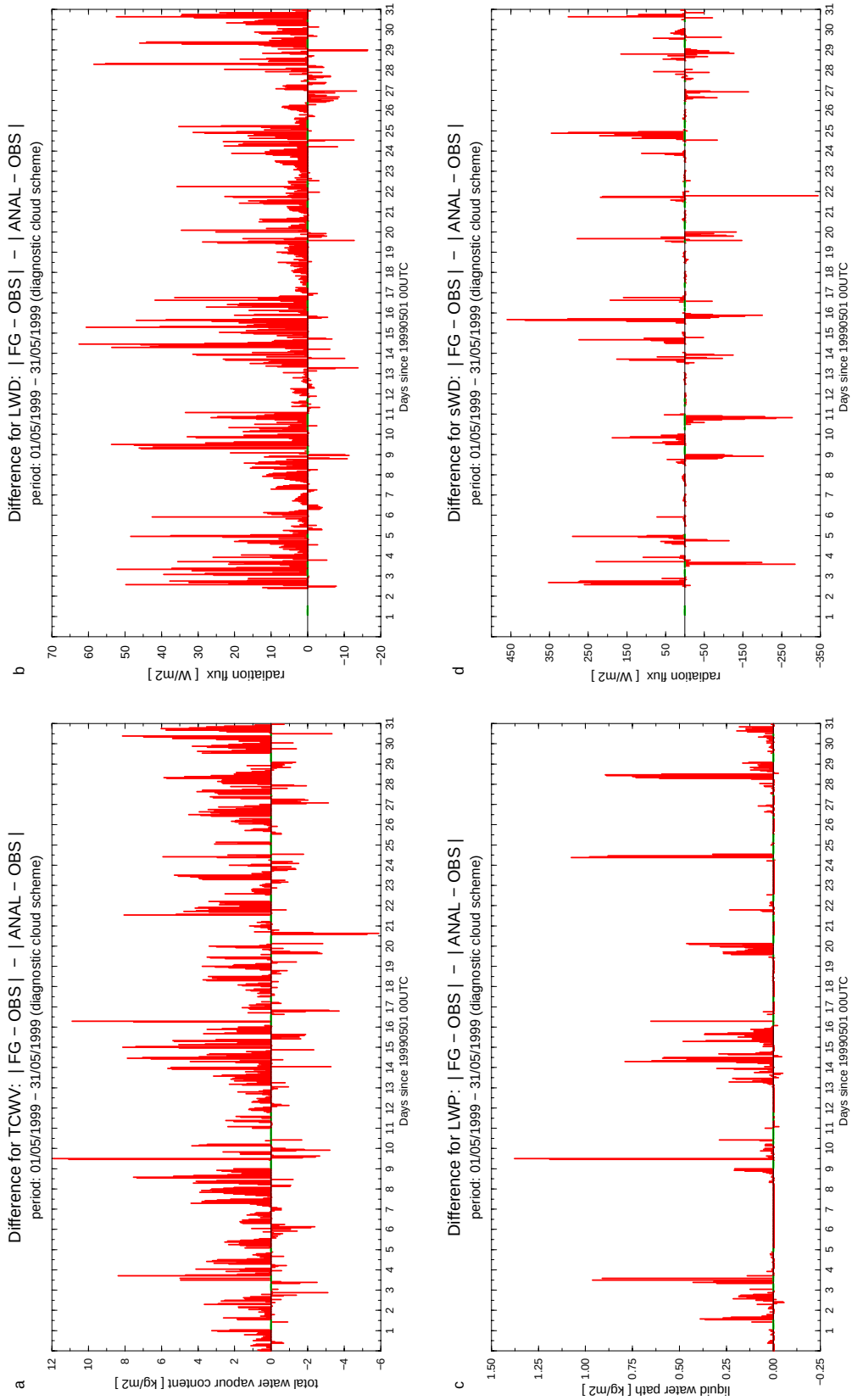

Figure 28: Same as Fig. 25, but for the period of May 1999.

Figure 28:

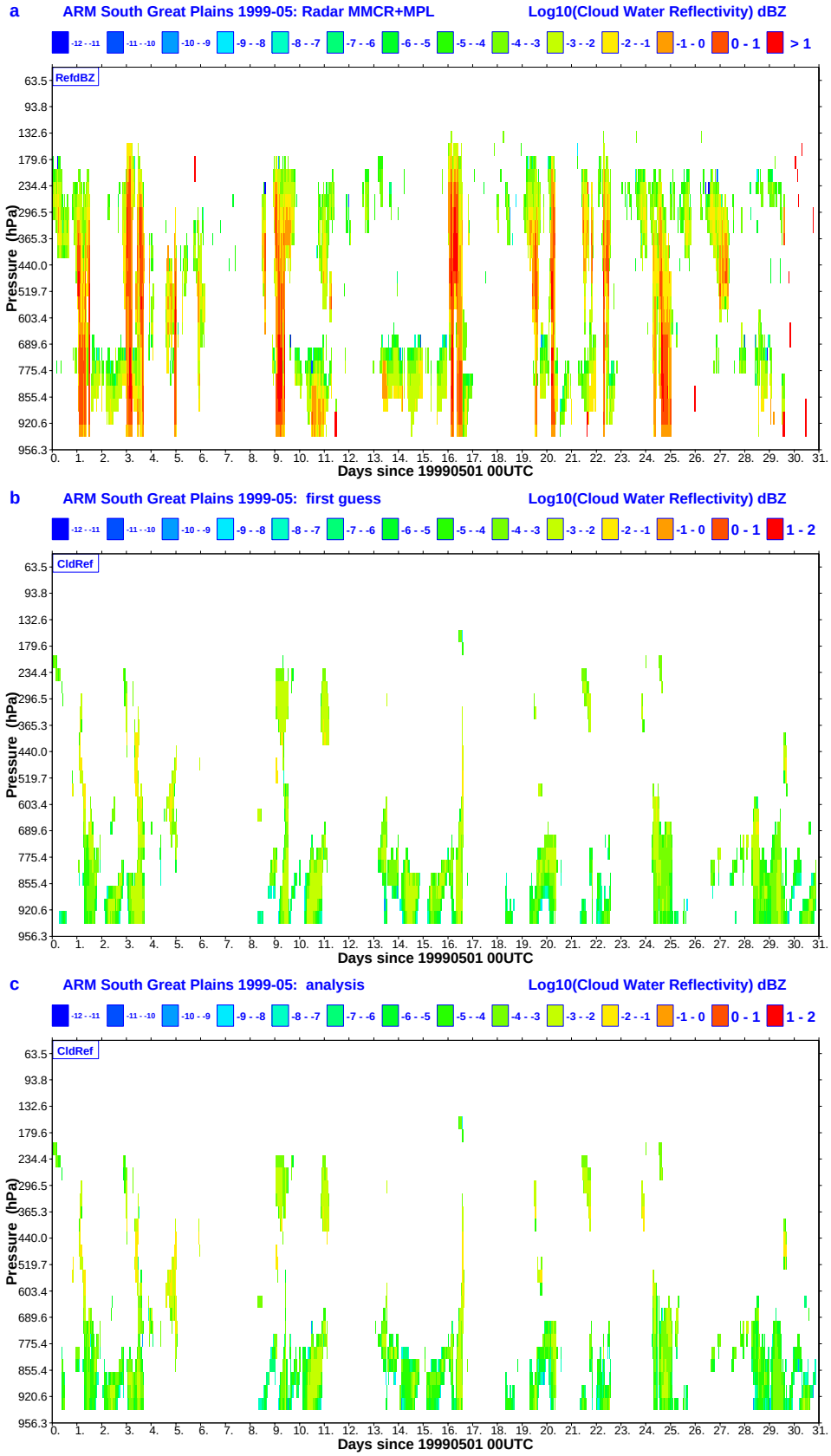

Figure 29: Same as Fig. 26, but for the period of May 1999.

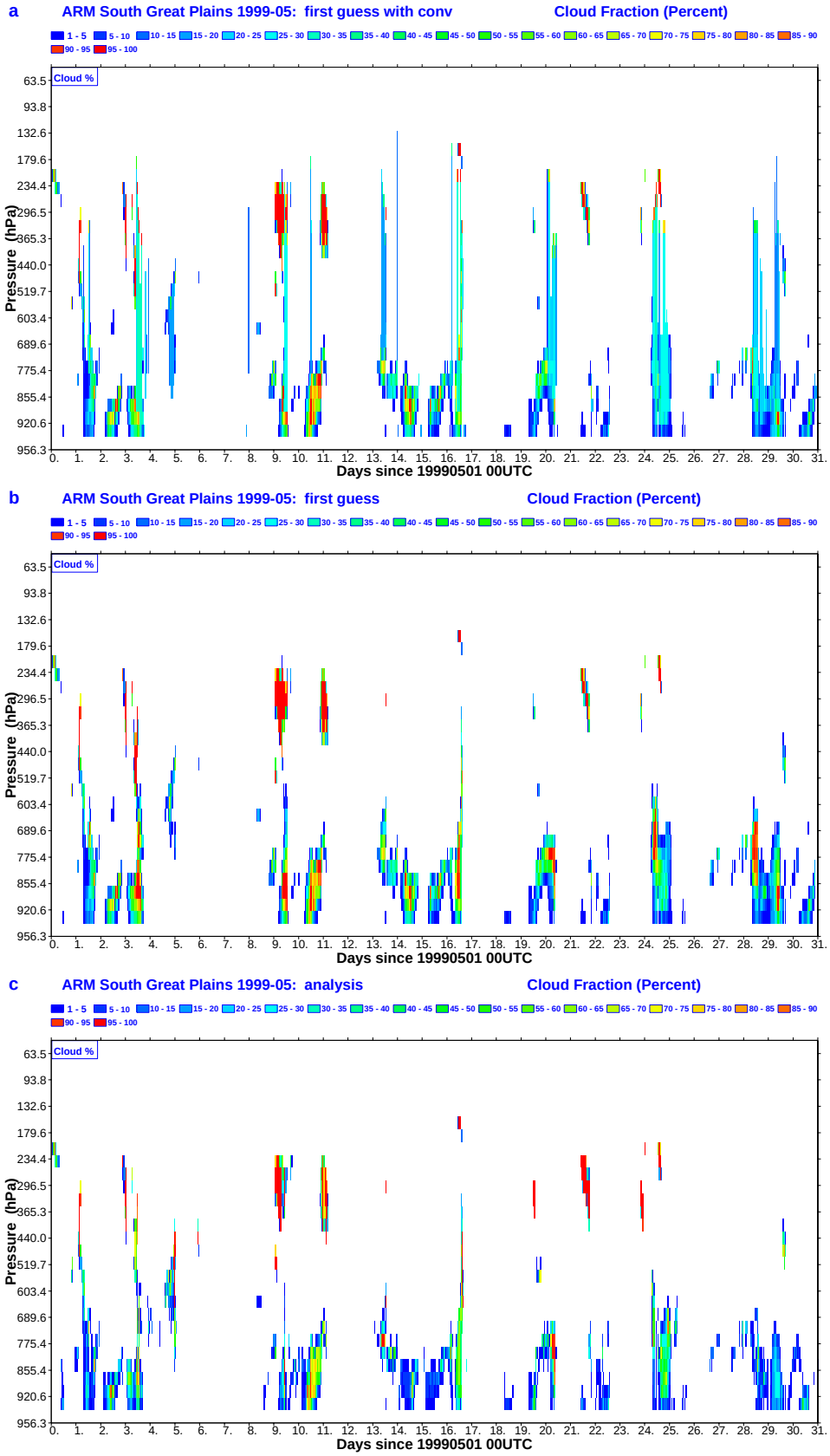

Figure 30: Same as Fig. 27, but for the period of May 1999.

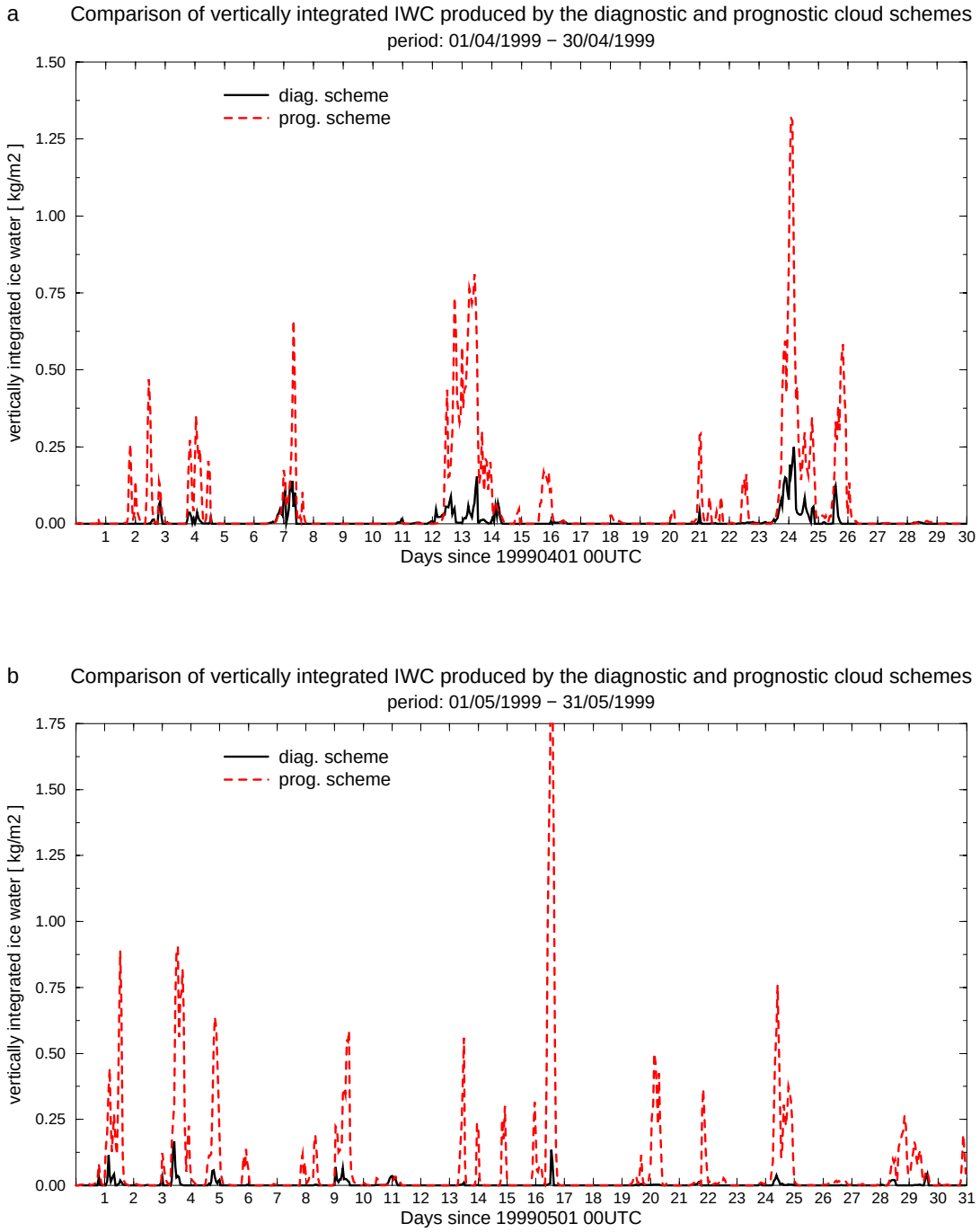

Figure 31: Comparison of the vertically integrated ice water content produced by the diagnostic (solid black line) and the prognostic (red dashed line) cloud schemes. (a) shows the results for April 1999 and (b) for May 1999.

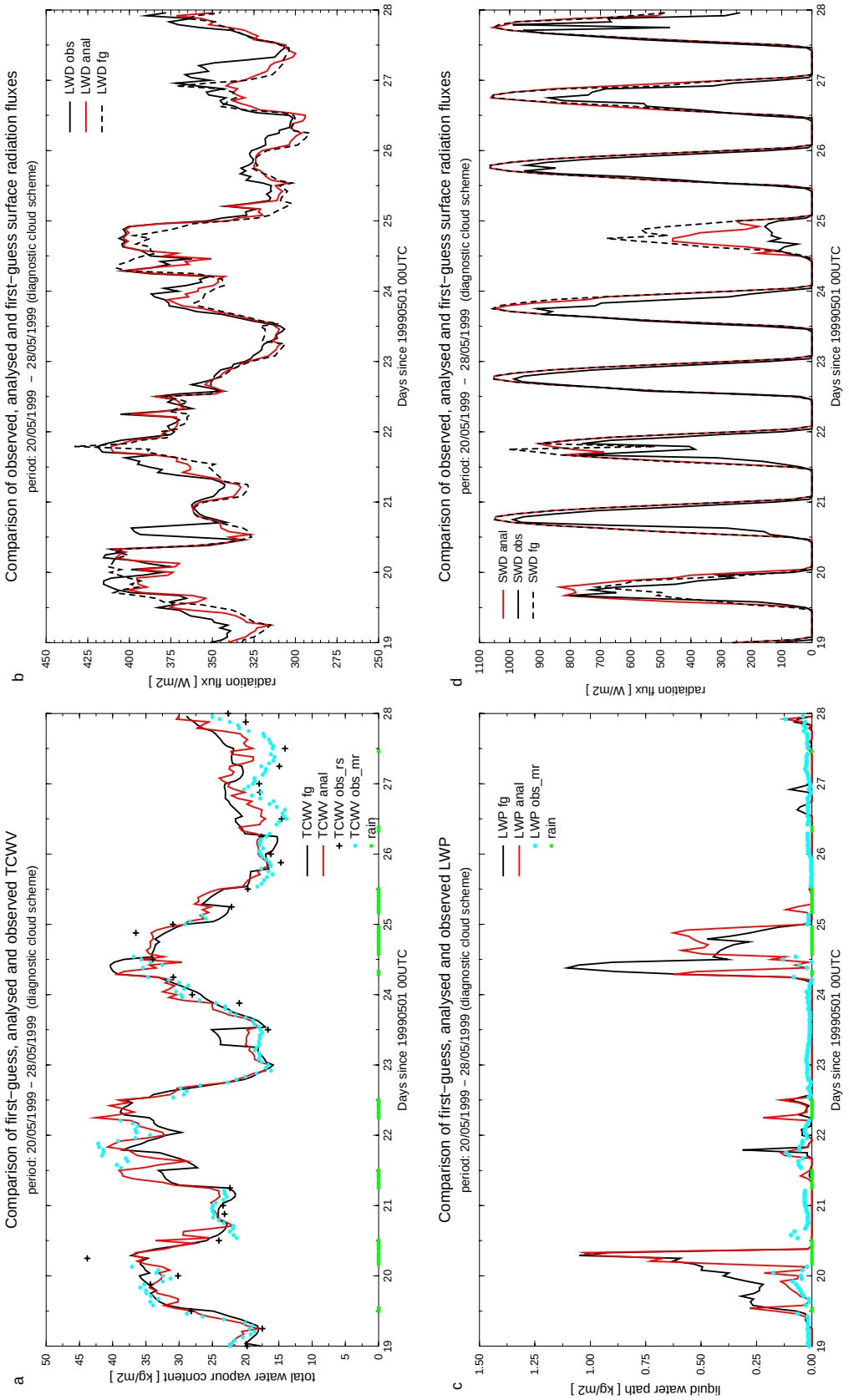

Figure 32: Comparison of the first guess and analysis against the observations for the total column water vapour (a), the downward longwave radiation at the surface (b), the liquid water path (c) and the downward shortwave radiation at the surface (d). Period from 20 to 28 May 1999 at ARM-SGP site.

Figure 32:

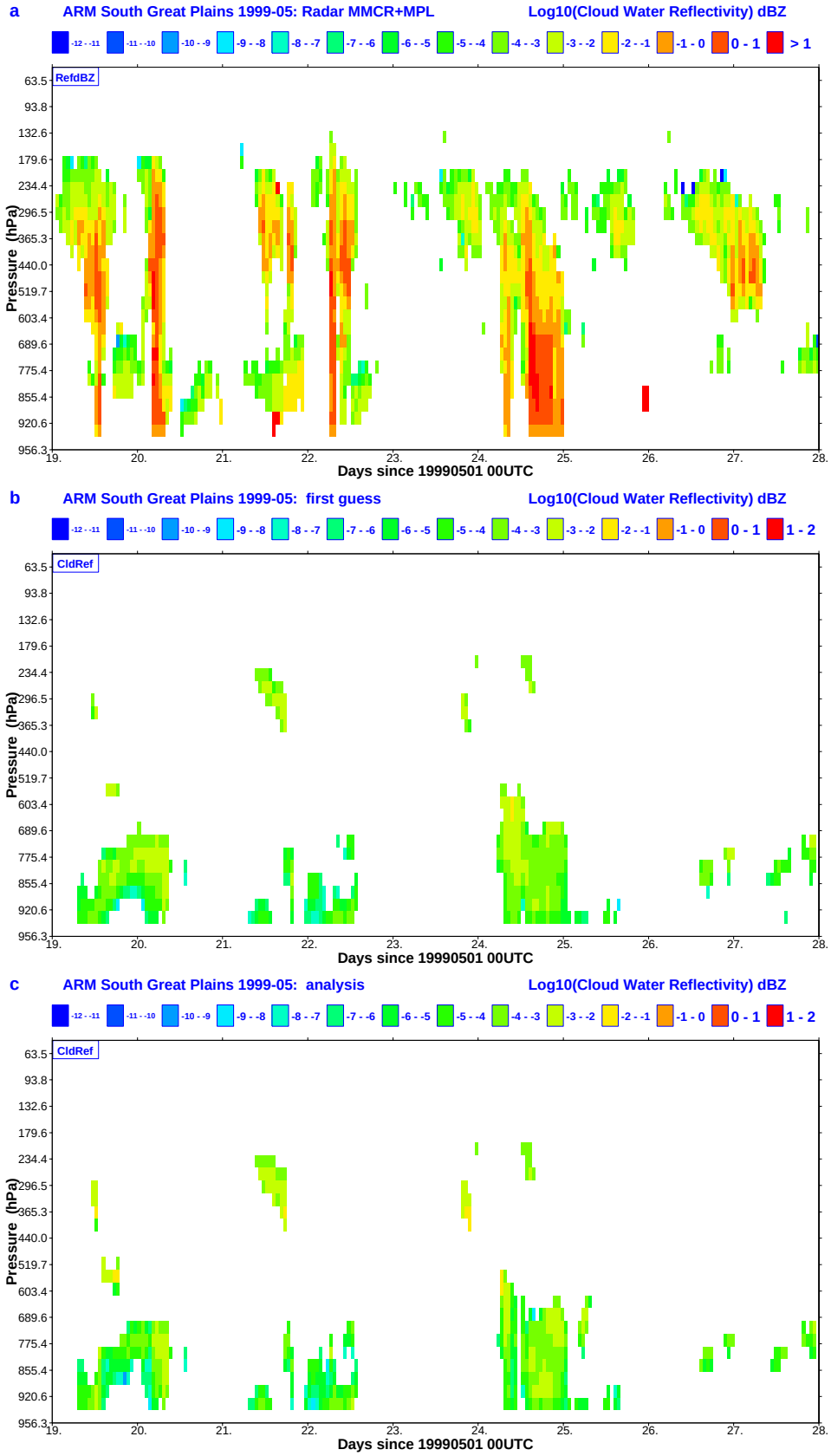

Figure 33: Same as Fig. 26, but for the period from 20 to 28 May 1999.

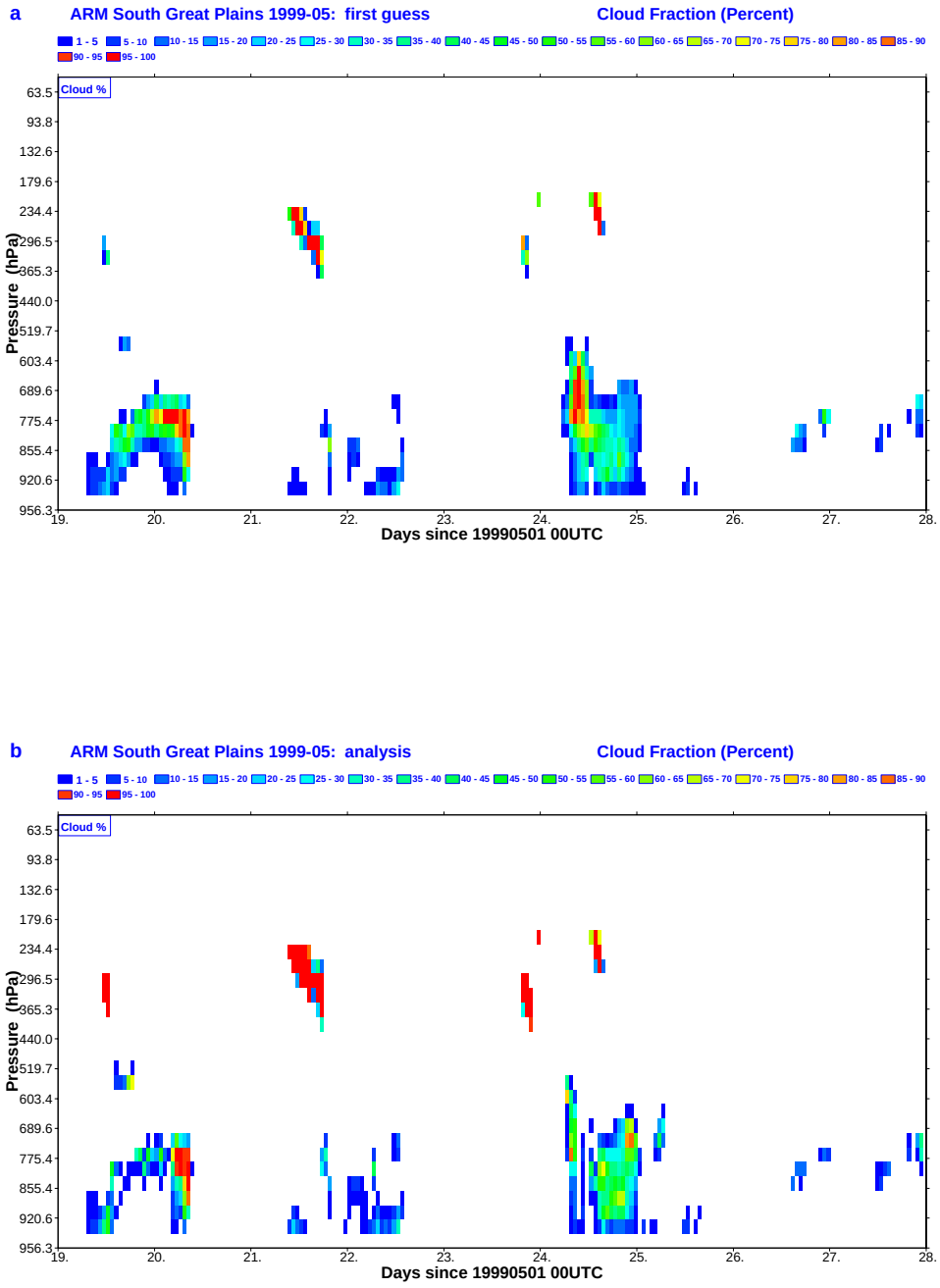

Figure 34: Time-series of the cloud cover (%) from the first guess (a) used for 1D-Var experiment and from the analysis (b) for the period from 20 to 28 May 1999.